Modeling and Simulation of MEMS-based Comb Drive Actuator using Bond Graph Method

Research Scholar:
Abbas Raza
Research Supervisor:
Prof. Dr. Muhammad Afzaal Malik

College of Electrical & Mechanical Engineering, National University of Sciences and Technology, Rawalpindi, Pakistan.

Abstract 4

1 Introduction 6

1.1 MEMS in Pakistan 7
1.2 Gyroscope 8
1.3 Types of Gyroscopes 9
1.3.1 Closed or Open Loop 9
1.3.2 Electro-Statically Suspended Gyroscope 9
1.3.3 Magnetically Suspended Gyroscopes 10
1.3.4 Optical Gyroscopes 10
1.3.5 Ring Laser Gyroscopes 10
1.3.6 Fiber Optic Gyroscope 11
1.3.7 Vibrating Gyroscopes 11
1.3.8 Micro Electro-Mechanical Gyroscope 12

2 Microsystems and MEMS 15

2.1 The promise of technology 15
2.2 What are MEMS—or MST? 18
2.3 What is micromachining? 25
2.4 Applications and markets 25
2.5 Standards 26
2.6 The psychological barrier 26
2.7 Journals, conferences, and Web sites 27
2.7.1 List of journals and magazines 27
2.7.2 List of conferences and meetings 28
2.8 Summary 29

3 Comb Drive and Gyros 30

3.1 Functionality for position sensing 31
3.1.1 Lateral Resonators 32
3.2 Sensing Systems in Comb Drive 36
3.2.1 Basic Sensing Geometry 37
3.3 Comb Drive Based Gyros 38
3.4 Operating Principle of MEMS gyro 39
3.5 Basic Design of MEMS vertical Comb Drive 42
3.6 Microlevel Description of Design 44
3.7 Construction of different types of MEMS gyros 47
3.8 Important Applications of MEMS Gyroscopes Applications 62

4 Modeling methodologies for coupled field domain
THE Bond Graph Method 67

4.1 Introduction to Bond Graph 69
4.2 Foundations of Bond Graphs 70
4.3 Starting points 71
4.4 Energy Modeling and Bond Graphs 72
4.5 Bond Graph theory 73
4.6 Bond Graph Standard Elements 73

4.6.1 Basic 1-Port elements 73
4.6.1.1 R-Elements 74
4.6.1.2 C-Elements 74
4.6.1.3 I-Elements 75
4.6.1.4 Duality and dual domains 76
4.6.1.5 Effort and Flow Sources 76
4.6.2 Basic 2-Port elements 77
4.6.2.1 The Transformer 77
4.6.2.2 The Gyrator 78
4.6.3 The 3-Port junction elements 79
4.7 Dual bond graphs 82
4.8 Intradomain transformers 82
4.9 Power directions on the bonds 82
4.10 Systematic procedure to derive a bond–graph model 84
4.11 Causal analysis 87
4.11.1 Causal Constraints 87
4.11.2 Fixed causality 87
4.11.3 Constrained causality 88
4.11.4 Preferred causality 88
4.11.5 Indifferent causality 89
4.11.6 Causal analysis procedure 89
4.11.7 Model insight via causal analysis 90
4.12 State Equations 93
4.12.1 Order of Set of State Equations 93
4.12.2 Matrix form (linear systems) 94
4.12.3 Generation of equations 94
4.13 Simulation 96
4.14 Review 98
4.15 Advantages of bondgraphic modeling 99
4.16 Discussion of the energy-based formalisms 101
4.17 Conclusions 103

5 Mathematical Model of Comb Drive 106

5.1 Design of a Comb Drive 107
5.2 Mathematical Expressions 108
5.3 Mixed Domain Physical Structure 110
5.4 Bond Graph Development111
5.5 State Space Formulation through Bond Graph Method 113
5.5.1 State Variables 113
5.5.2 Consecutive Equations 113
5.5.3 Mechanical Domain 114
5.5.3.1 I-Junction 114
5.5.3.2 Capacitors 114
5.5.3.3 Spring 114
5.5.3.4 Mass 114
5.5.4 Electrical Domain 114
5.5.4.1 1-Junction 114
5.5.4.2 0-Junction 114
5.5.4.3 1-Junction 115
5.5.4.4 Transformer 115
5.5.5 Equations of the system 115
5.5.6 Developed State Space 116

6 Results and discussions 117

6.1 Bond Graph a Method of Choice 117
6.2 Simulation through Bond Graph 121
6.3 20-SIM Results; Displacement and Electrostatic Force vs. Driving Voltage 123
6.4 ANSYS Results [1]
131
6.4.1 Displacement vs. Driving Voltage 131
6.4.2 Electrostatic Force vs. Driving Voltage 132
6.5 PolyPUMPS Results [2]; Displacement vs. Driving Voltage 132
6.6 Results and discussion 113
6.7 Conclusions 134
6.8 Future Work and Recommendations 135

References 135

Abstract:

A comb drive is an important component of MEMS-based actuators used in many applications such as a dispenser and a fluidic pump, and as a sensor in an accelerometer and in MEMS gyroscope. Such systems are coupled multi-domain energy systems popularly known as mechatronic systems. The modeling and simulation of such systems poses a formidable challenge. Bond Graph Method (BGM) has emerged as a method of choice for the modeling and simulation of coupled multi-domain energy systems. The system is seen as an interplay of power variables and energy variables, thus introducing the immortal concept of cause and effect. The two primary forces, electromechanical and electrostatic, are cast into the cause and effect paradigm whilst expressing power into effort and flow variables.

This research work focuses on investigating the control parameters of lateral electrostatic comb-drive actuators, where the effect of these parameters on the actuation performance is explored using a commercial bond graph package known as 20-SIM. This type of analysis is essential for the design process of system-on-a-chip MEMS applications, where a comb-drive can represent the main source of actuation within the chip system. Of particular interest to this study is the application of the electrostatic comb-drive motor as a fluidic pump in on-a-chip systems used for drug delivery or cooling of microprocessors used in space vehicles. The 20-SIM computer software is used to construct a robust comb-drive model and solve its multi-physics interaction problem using the power of bond graph method. In this model, the driving voltage is taken into account. The calculated comb displacement and the electrostatic force generated are known to be directly proportional to the square of the driving voltage. In this method, a model based on BGM is developed and then directly simulated using 20-SIM. Since a bond graph is a precise mathematical model, it can be used to unfold the state-space equations associated with the physical dynamic system. The bond graph

simulations lead to the desired state space equations, which unfold the dynamic response of the physical system.

1

Introduction

The thirst of miniaturization drives the technology towards microlevel, to think about the sizes in order of microns without any trade-off in terms of performance and reliability. Imagine a machine so small that is imperceptible to the human eye, gears no bigger than a grain of pollen, this all became reality because of the advent of Micro electro-mechanical systems (MEMS) or sometimes called as micro systems technology (MST). It is an emerging technology with lots of application in variety of environments. As the world is focusing on the miniaturization and integration of different functions into one utility, sooner MEMS based products will become essential part of our daily life. Low cost of the MEMS products elevate the standard of living and make it possible for the people of even developing countries to afford and enjoy the benefits of the high tech. gadgets and instruments in their daily life as well as in industry.

MEMS products possess a number of distinctive features. These are miniature embedded systems involving one or many micromachined components or structures. Miniaturization, integration and high volume low cost production reduces the overall cost of the effective systems.

MEMS are the microscopic structures integrated onto silicon that combine mechanical, optical and fluidic elements with electronics with the help of advance infrastructure, materials, design tools and various sensor principles. Silicon has attractive mechanical properties which makes it suitable for batch processing.

In many applications MEMS have great advantages over its predecessors as they are light weight, can occupy a small volume, can handle the microscopic devices with fineness, resistant to shock, vibration and radiation, consume little power, high precision and reproducible fabrication with high reliability.

MEMS are usually divided into two categories, those devices that detect information, called microsensors and those devices that can respond to information or act, called actuators. Microsensors gather local information including for example thermal, biological, chemical, optical and magnetic input. The electronics of the devices can then process the information and may direct actuators to respond and control the environment (e.g. by moving, pumping, and filtering) base on intended design instructions.

1.1 MEMS in Pakistan

Pakistan is a developing country where the growth of higher education and industrial expansion are the most important areas to be addressed. The government is taking keen interest in the field of higher education and also appreciating the plans for industrial development.

Concept of miniaturization is rapidly penetrating not only in the industry but in our daily life. So the area of micro electro-mechanical systems (MEMS) for research work is basically the implementation of miniaturization concepts.

Our country is growing towards many successful projects in the field of power plants, manufacturing, biotechnology, agriculture and communication, and always keen to initiate research projects for our future needs. The work on the micro electro-mechanical systems (MEMS) accelerometer with the aid of MEMS designing and simulation software INTELLISUITE is already been initiated in one of our prestigious institute (Pakistan Institute of Engineering and Applied Sciences, PIEAS). With the collaboration of HEC1 a MEMS chip testing setup will soon be established there. An amount of Rs. 4.05 million has been granted by HEC for the same.

Pakistan is keenly interested to initiate some research projects to adopt this future field for local industry. A proposal is under consideration for approval to develop a research and MEMS based production setup in one of the universities in Pakistan. Dr. Shafaat Bazaz who did his PhD in MEMS and worked in the faculty of University of Waterloo Ontario Canada has been hired to establish a laboratory for MEMS production in Pakistan.

On the basis of above stated facts, I feel that my PhD in this field would enable me to serve my country in a better way. Also I would continue further work in my homeland according to the requirement of my organization.

1.2 Gyroscope:

Long before the advent of satellite global positioning system, the gyroscope was a critical navigational instrument used for maintaining a fixed orientation with great accuracy, regardless of earth rotation.

Thus gyroscope may be defined as follows;

"A device that is used to define a fixed direction in space or to determine the

change in angle or the angular rate of its carrying vehicle with respect to a reference frame is called gyroscope."

Invented in the 19th century, it consisted of a flywheel mounted in gimbals rings.

The large angular momentum of the flywheel counteracts externally applied torques and keeps the orientation of the spin axis unaltered. The demonstration of the ring laser gyroscope in 1963 displaced the mechanical gyroscope in many high-precision applications, including aviation. Inertial navigation systems based on the ring laser gyroscopes are on board virtually all commercial aircrafts. Gyroscopes capable of precise measurement of rotation are very expensive instruments, costing many thousands of dollars.

1.3 Types of Gyroscopes

1.3.1 Closed or Open Loop

Gyros can be operated closed-loop or open-loop. Closed-loop means that a feed
back loop from the gyro output introduces a restoring mechanism either inside the gyro or counter rotating platform motions to maintain the gyro at its null (initial) setting. In open loop operation, the gyro is allowed to operate off its null position as it responds to the input angular rates.

1.3.2 Electro-Statically Suspended Gyroscopes

In the electro statically suspended gyroscope (ESG), a spherical rotor is suspended in a spherical chamber in vacuum by electrostatic forces. External motor windings spin the rotor to the desired speed and are then turned off. The rotor will spin for days before requiring motor excitation. The ESG is

basically a free gyroscope and does not require a torque to keep the rotor and case aligned. ESGs are very accurate and are used for long-term navigation of submarines and aircraft and for land surveying.

1.3.3 Magnetically Suspended Gyroscopes

A magnetically suspended gyro (MSG) uses a magnetic field to suspend the rotor
in vacuum and is similar to the ESG in all other respects.

1.3.4 Optical Gyroscopes

Optical gyros sense phase shifts (the Sagnac effect) between counter propagating beams of light. Optical gyros use the Sagnac effect to detect rotation. The Sagnac effect pertains to the postulate of the theory of relativity that the speed of light is constant, and independent of the motion of the source. If two identical light waves circulate in opposite directions along a closed path undergoing a rotation, then the light beam traveling in the same direction as the rotation takes longer to travel around the path than the other beam, resulting in a changed interference pattern. Optical gyroscopes include the ring laser gyro (RLG) and fiber-optic gyros (FOGs).

1.3.5 Ring Laser Gyroscopes

The ring laser gyro (RLG) is widely used in tactical and navigation systems. It comprises a closed optical cavity (usually a three- or four-sided block of low-expansion-coefficient material), whose light path is defined by mirrors mounted at the corners. The light travels through holes bored in the block containing a low-pressure gas, usually a helium-neon mixture which loses when the anode and cathode are excited. Thus, the RLG is itself actually a laser (that is, it does not require an external light source), and is thus said to

be an active device. The lased light propagates clockwise and counterclockwise so that there are two optical beams, each maintained in resonance (that is, each beam contains an integral number of wavelengths). Under a rotation rate about the gyro input axis, the resonant frequencies of the clockwise and counterclockwise beams change. Some light from both beams is transmitted through one of the mirrors to impinge on a detector. Because the beams have different frequencies, a changing interference pattern (fringes) appears. Measurement of the fringe pattern changes determines the external rotation rate and direction.

1.3.6 Fiber Optic Gyroscope

Fiber-optic gyros use optical fibers, in place of a lasing block, to define the optical path. The light source is external, and its light is split by a beam splitter or optical coupler to produce clockwise and counterclockwise light beams in the fiber-optic coil. FOGs are called passive devices because the optical source (a laser) is external. There are two principal types: interferometric and resonant. The interferometric fiber-optic gyro (IFOG) has up to 1 km (0.6 mi) of optical fiber wound into a coil with both ends brought into a coupler. The resonant fiber-optic gyro (RFOG) maintains the counter propagating light beams in resonance, recirculating them in a short fiber-optic coil.

1.3.7 Vibrating Gyroscopes

Vibrating gyroscopes use an oscillating mass in place of a spinning mass to sense rates. The mass oscillates (sinusoidally) back and forth through a fixed angle; the amplitude of the oscillation is restrained by the elastic (spring) stiffness of the vibrating structure. Nearly all such gyros oscillate at the resonant frequency of the mass-spring system since the gyro output is maximized at this frequency; hence these gyroscopes are also called resonator gyros.

1.3.8 Micro Electro-Mechanical Gyroscope

The mechanical gyroscope derives it precision from the large angular momentum
that is proportional to the heavy mass of the flywheel, its substantial size and its high rate of spin. Thus, in itself, precludes the use of miniature devices for useful gyroscopic action; the angular momentum of a miniature flywheel is miniscule. Instead, micromachined sensors that detect angular rotation utilize the ***Coriolis effect***. There are many types of MEMS Gyro in which different principles are used as we have discussed latterly. In this project we have emphasized in Comb Drive Based MEMS Gyro. It is basically a micromachined angular rate Gyroscope. Fundamentally, the Gyros are strictly angular-rate or yaw-rate sensors, measuring angular velocity.

The Coriolis Effect, named after the French physicist Gaspard Coriolis, manifests itself in numerous weather phenomena, including hurricanes and tornadoes, and is a direct consequence of body's motion in a rotating frame of reference. In general, Coriolis acceleration is the acceleration that must be applied in order to maintain the heading of a body moving on a rotating surface.

All micro-machined angular rate sensors have a vibrating element at their core this is the moving body. In a fixed frame of reference, a point on this element oscillates with a velocity vector $\mathbf{v}$. If the frame of reference begins to rotate at a rate ω, this point is then subjected to a Coriolis force and a corresponding acceleration, equal to ($2\,\omega \times \mathbf{v}$).

The vector cross operation implies that the Coriolis acceleration and the resulting displacement at that point are perpendicular to the oscillation. This, in effect, sets up an energy transfer process from a primary mode of oscillation into a secondary mode that can be measured. It is this excitation of a secondary resonance mode that forms the basis of the detection using the

Coriolis effect. In beam structures, these two frequencies are distinct with orthogonal displacements. But for highly symmetrical elements, such as rings, cylinders or disks, the resonant frequency is degenerate, meaning there are two distinct modes of resonance, sharing the same oscillation frequency. This degeneracy causes the temporal excitation signal (primary mode) to be in phase Quadrature with the sense signal (secondary mode), thus minimizing coupling between these two modes and improving sensitivity and accuracy. Additionally, the degeneracy tends to minimize the device's sensitivity to thermal errors, aging and long-term frequency drifts.

A simple and common implementation is the tuning-fork structure. The two tines of the fork normally vibrate in opposite directions in the plane of the fork (flexural mode). The Coriolis acceleration subjects the tips to describe an elliptical path. Rotation, hence, excites a secondary vibration torsional mode around the stem with energy transferred from the primary flexural vibration of the tines. Quartz tuning-fork uses the piezoelectric properties of the material to excite and sense both vibration modes. The tuning-fork structure is also at the core of micro-machined silicon sensor. Other implementations of angular rate sensors include:

- Simple resonant beams
- Vibrating ring shells
- Tethered accelerometers

Among these all we have worked on Micromachined vibrating angular-rate gyroscope. These types of gyros have received intensive attention since 1990's [1.1]. Among the development of micro gyros the capacitive sensing method frequently used [1.2]. Piezoresistive detection however is seldom reported for its relatively low sensitivity and high temperature coefficient [1.3], 12].Coriolis accelerations and high performance piezoresistive detectors are also used for high resonant frequencies. Some have constructed sensing elements for Coriolis accelerations [1.4].

.

2

Microsystems and MEMS

2.1 The promise of technology

The ambulance sped down the Denver highway carrying Mr. Rosnes Avon to the hospital. The flashing lights illuminated the darkness of the night, and the siren alerted those drivers who braved the icy cold weather. Mrs. Avon's voice was clearly shaking as she placed the emergency telephone call a few minutes earlier. Her husband was complaining of severe heart palpitations and shortness of breath. She sat next to him in the rear of the ambulance and held his hand in silence, but her eyes could not hide her concern and fear. The attending paramedic clipped onto the patient's left arm a small, modern device from which a flexible cable wire led to a digital display that was showing the irregular cardiac waveform. A warning sign in the upper right-hand corner of the display was flashing next to the low blood pressure reading. In a completely mechanical manner reflecting years of experience, the paramedic removed an adhesive patch from a plastic bag and attached it to Mr. Avon's right arm. The label on the discarded plastic package read "sterile microneedles." Then with her right hand, the paramedic inserted into the patch a narrow plastic tube while the fingers of her left hand

proceeded to magically play the soft keys on the horizontal face of an electronic instrument. She dialed in an appropriate dosage of a new drug called Nocilis™. Within minutes, the display was showing a recovering cardiac waveform and the blood pressure warning faded into the dark green color of the screen. The paramedic looked with a smile at Mrs. Avon, who acknowledged her with a deep sigh of relief.

Lying in his hospital bed the next morning, Mr. Avon was slowly recovering from the disturbing events of the previous night. He knew that his youthful days were behind him, but the news from his physician that he needed a pacemaker could only cause him anguish. With an electronic stylus in his hand, he continued to record his thoughts and feelings on what appeared to be a synthetic white pad. The pen recognized the pat-tern of his handwriting and translated it to text for the laptop computer resting on the desk by the window. He drew a sketch of the pacemaker that Dr. Harte showed him in the morning; the computer stored an image of his lifesaving instrument. A little device barely the size of a silver dollar would forever remain in his chest and take control of his heart's rhythm. But a faint smile crossed Mr. Avon's lips when he remembered the doctor saying that the pacemaker would monitor his level of physical activity and correspondingly adjust his heart rate. He might be able to play tennis again, after all. With his remote control he turned on the projection screen television and slowly drifted back into light sleep.

This short fictional story illustrates how technology can touch our daily lives in so many different ways. The role of miniature devices and systems is not immediately apparent here because they are embedded deep within the applications they enable. The circumstances of this story called for such devices on many separate occasions. The miniature yaw-rate sensor in the vehicle stability system ensured that the ambulance would not skid on the icy highway. In the event of an accident, the crash acceleration sensor guaranteed that the airbags would deploy just in time to protect the

passengers. The silicon manifold absolute pressure (MAP) sensor in the engine compartment helped the engine's electronic control unit maintain, at the location's high altitude, the proper proportions in the mixture of air and fuel. As the vehicle was safely traveling, equally advanced technology in the rear of the ambulance saved Mr. Avon's life. The modern blood pressure sensor clipped onto his arm allowed the paramedic to monitor blood pressure and cardiac output. The microneedles in the adhesive patch ensured the immediate delivery of medication to the minute blood vessels under the skin, while a miniature electronic valve guaranteed the exact dosage. The next day, as the patient lay in his bed writing his thoughts in his diary, the microaccelerometer in the electronic quill recognized the motion of his hand and translated his handwriting into text. Another small accelerometer embedded in his pacemaker would enable him to play tennis again. He could also write and draw at will because the storage capacity of his disk drive was enormous, thanks to miniature read and write heads. And finally, as the patient went to sleep, an array of micromirrors projected a pleasant high-definition television image onto a suspended screen.

Many of the miniature devices listed in the above story, particularly the pressure and acceleration microsensors and the micromirror display, already exist as commercial products. Ongoing efforts at many companies and laboratories throughout the world promise to deliver, in the not-too-distant future, new and sophisticated miniature components and microsystems. It is not surprising, then, that there is widespread belief in the technology's future potential to penetrate far-reaching applications and markets.

2.2 What are MEMS—or MST?

In the United States, the technology is known *as microelectromechanical systems* (MEMS); in Europe it is called *microsystems technology* (MST). A question asking for a more specific definition is certain to generate a broad collection of replies, with few common characteristics other than "miniature." But such apparent divergence in the responses merely reflects the diversity of applications this technology enables, rather than a lack of commonality. MEMS is simultaneously a toolbox, a physical product, and a methodology all in one:

1. It is a portfolio of techniques and processes to design and create miniature systems;
2. It is a physical product often specialized and unique to a final application—one can seldom buy a generic MEMS product at the neighborhood electronics store;
3. "MEMS is a way of making things," reports the Microsystems Technology Office of the United States Defense Advanced Research Program Agency (DARPA) [2.1]. These "things" merge the functions of sensing and actuation with computation and communication to locally control physical parameters at the microscale, yet cause effects at much grander scales.

It is an emerging and fast growing field all over the world. The learning curve in *MEMS (Micro-electromechanical Systems)* field does not follow the explosive growth rate. One of the possible explanations resides in the diversity of the MEMS field. MEMS did not culminate into a "dominant technology" in micromachining, unlike MOS circuitry. But as we have seen, sensors and actuators can be considered crucial to the information processing field. Some authors go as far as to state that their greatest power lies in enabling and adding value to Systems [2.2]. In other words, their integration with the modifier unit increases exponentially the value of the overall

system. This view is underlined when refer-ring to MEMS as an *enabling technology.* I would go a bit further, and see ramifications beyond the purely commercial aspects, and beyond the apparent differences. Even the name of the field varies from region to region: Micro electromechanical Systems (MEMS) in USA, Microsystems in Europe, and Micro-mechatronics in Japan. But if we delve under the surface, we find a unifying theme: *microengineering,* as multiple physical domains meet each other in the microscale range. The consequences are large, especially if we realize that different engineering fields developed their unique, custom universe and language. Microengineering opens the door toward a unification of all these various fields. More importantly, a unified view of nature is unveiled, from the cover of different terminologies and analysis methods. An engineer in this context is more than an electrical engineer, a chemical or mechanical engineer. In the long term, the MEMS paradigm might deeply affect the structure of the technical high level education program. A clear trend is noticed, if one integrates over the history of microengineering: complete microsystems merging sensors, actuators and electronics.

To understand the potential of MEMS, one must look to the global context. The two main direction of the present technical society are information technology and micro-miniaturization. A short outlook is presented in Table 2.1.

Table 2.1 Two main trends of the present society

Information era	**Micro-miniaturization**
- Information processing systems	-Distributed information processing
- Physical systems monitoring and control	- High speed, low power, low cost

- Sensor clusters, data fusion systems, smart sensors	- Arrays of programmable sensors and actuators

We have already discussed a couple of aspects regarding the information processing paradigm. The miniaturization gradient lead to the present mature micro-electronic industry, which implicitly boosted the development in the MEMS field. A full infrastructure exists already: Si-foundries, specialized equipment, simulation tools for electronics. The main challenge seems to remain an expansion of the applicability range. As the miniaturization is pushed further toward the borders, new limitations appear. For the analog circuit design, the main constraints appear to be mostly technology-driven. For a given technology, there is a certain constraint upon the maximum gain-bandwidth parameter of an elementary transistor. As the technology is downscaled, the once second-order effects in transistor models (e.g. short-channel effects, leakage currents, sub-threshold conduction, etc.) become significant. It is more and more difficult to rely on hand-computation for designing in the present submicron technologies. The design procedure itself changes, towards a gradually increasing emphasis on simulation tools and accurate submicron models. There is a plethora of specialized transistor models, with increasing number of parameters, very dependent of the technology scale. Because of the new importance of the formerly second order parameters, even the design methodology might suffer dramatic changes, as we see in the field of RF analog design. It is not an easy world for the present-day analog microelectronic designers. There are also fresh directions, in an attempt to change the perspective: translinear circuits, analog neural networks, nano-electronics, but they remained for the moment at the boundary of a large acceptance.

The digital electronics world seems to hit the same obstacles. The performance is mainly technology-driven, and as such, more in the hands of the physicists and chemists as of engineers. Basically the same old

computation models (Von Neumann and Harvard) are used for the last fifty years. There are indeed fresh breaths - asynchronous design, parallel computation, fuzzy logic-based computation, but the main paradigms did not change.

Both analog and digital microelectronics might have therefore some inherent internal limitations. On the other side they foster the development toward micro-systems. An increasing proliferation of the digital computing power creates both demand and opportunity for MEMS-based systems. As for analog electronics, it will always remain on a central path, for a good electrical interface toward the outside physical analog world is of paramount importance.

In this context, MEMS brings a revigorating opening: microscale integrated engineering. In comparison with classic sensor technologies, some of the benefits of MEMS are:

- miniaturization: save materials, power, faster time response, better performance
- integration: integrated with IC and other systems, reduces system size and cost
- batch fabrication: cheap, disposable
- fosters completely new applications

As an example, the price of an optical gyroscope unit is over $1000, while MEMS-based gyroscopes already reached prices of $30 per device.

The idea is that we stand on the verge of a Second Si revolution. The main feature of this paradigm shift will be the integration of new structures, such as micromechanical machines, on silicon, alongside the transistors, creating a whole new generation of integrated microsystems. To evaluate the impact of MEMS on engineering, the following aspects should be considered:

• Orders of magnitude increase in numbers of sensors and actuators. This unleashes the available computational power for advanced signal processing and distributed computation

• Specific VLSI design and synthesis methods for microengineering. It will rather be a unifying perspective, in which the focus is on an integrated, general (not field specific) design and analysis methodology.

- Driver for multiple, mixed technology integration.
- Microscale information systems coupled to physical world.

What about the MEMS market? The distinctive characteristics of MEMS systems generated already a multi-billion market. They take up less space, require less energy and material, and are predestined for cost-savings (batch production and integration with microelectronics) in comparison with their classical, macro-scale counterparts. The annual turnover for microtechnical products (including CD and DVD microdevices and flat displays) was estimated to reach 34 billion US$ in 2000. NEXUS (The Network of Excellence in Multifunctional MicroSystems) market analysis forecasts a 20% annual increase in the MEMS market, to reach $68 billion in 2005. What is even more significant is the remark made by Peripheral Research in one of their market reports: "the average selling price for MEMS will increase 25% over the next 5 years". The price increase is justified by the increasing complexity of the MEMS-based systems. The direction is therefore in sight for some time. It remains to be seen what is the optimum integration between various subsystems of a complex microsystem.

How far can this integration go? If one looks to Fig. 1.1, should a clear interface between the modification unit and the interface units be maintained, or is it more advantageous to distribute the intelligence among the modules'? As we

have seen, the decoupling between the energetic and informational features of a signal has resulted in a very fast evolution of the digital computing.

A loose coupling between separate modules allows a faster development cycle for each individual subsystem, a clear division of tasks among the components, and an incremental refinement, in the spirit of an object-oriented approach. This flexibility in design and reuse is a powerful argument in the favour of keeping separate functional modules, optimized for specific tasks.

When is then a tight coupling between subsystems preferable? As this thesis will try to argue, having a tight coupling sometimes generates added functionality, which cannot be directly inferred from the functions that each component can perform separately. The value of the tightly coupled system is that the strong interaction between its constituent parts gives a value beyond the sum of the values of the individual components. The interactions define the system.

Down-scaling of the dimensions has huge potential in this respect, because it allows an energetic coupling at the microscale level between the electrical domain and the various interface domains (mechanical, thermal, etc.) towards the real world. This coupling could be much stronger than at the macroscale level. The modifier unit is normally in the electrical domain while the physical interaction with the environment, as far as this thesis is concerned, is of mechanical nature. The strong microscale coupling may give access to parameters that have been immeasurable or uncontrollable so far.

The objective of the work presented in this thesis is to exemplify these aspects for the particular case of an accelerometer. This is among the best known microsensors, and yet there is new potential to be explored. A promising one is to exploit a feedback loop between the mechanical and the electrical field. It is

also a plea for the concept of ***smart sensors,*** as a functional integration between sensors and processing electronic circuitry, in a tight coupled system configuration.

This thesis is written within the context of two aspects relevant to MEMS. The first is the challenge brought by the development of MEMS field. However, developing its potential also brought new problems, as the design and analysis tools commonly employed in microelectronics have shown not sufficient. By its nature, MEMS encompasses several energy domains. To build systems combining mechanical and electrical components requires a unitary modeling and analysis approach. This aspect is elaborated in several places in the thesis. The unified perspective helps in enlarging the range of information-processing systems from inside the electrical domain to a larger, interdisciplinary universe.

A second issue is the need for structuring. If the emphasis in MEMS is to be put on the interaction across the border between domains, then we need a reason-able way to discern between different orders of complexity of a system, and to account for the added features introduced by intercoupling. Such a general principle was already proposed for digital electronics, and it is based on the concept of feedback [2.3]. Gheorghe Stefan observed that the introduction of a feedback path between digital systems could generate new behavioral patterns, while connecting them in series or in parallel will not produce qualitatively different behavior. For instance, two combinational circuits interconnected in series can generate only a new combinational circuit, in which the output is a strict function of the present input. A different qualitative behavior is a logical circuit with an internal state (with memory), in which the output will depend on both the actual and past inputs. To go from simpler combinational circuits to components with internal state is necessary to create a feedback loop in the interconnection topology.

Based on this, Gheorghc Stefan classified the digital systems in a hierarchical manner, depending on the number of feedback paths included. Thus if the combinational circuits are systems of zero order (no feedback path), then the memory cells are systems of order one. Finite state machines are of order two, the processors of order three, etc. The essence of this "principle of structured growth" *is* the remarkable ability of a feedback connection to change the qualitative behavior of a system.

2.3 What is micromachining?

Micromachining is the set of design and fabrication tools that precisely machine and form structures and elements at a scale well below the limits of our human perceptive faculties—the microscale. Micromachining is the underlying foundation of MEMS fabrication; it is the toolbox of MEMS.

Arguably, the birth of the first micromachined components dates back many decades, but it was the well-established integrated circuit industry that indirectly played an indispensable role in fostering an environment suitable for the development and growth of micromachining technologies. As the following chapters will show, many tools used in the design and manufacturing of MEMS products are “borrowed” from the integrated circuit industry. It should not then be surprising that micromachining relies on silicon as a primary material, even though the technology was certainly demonstrated using other materials.

2.4 Applications and markets

Present markets are primarily in pressure and inertial sensors and inkjet print heads, with the latter dominated by Hewlett Packard Company of Palo Alto, California. Future and emerging applications include high-resolution displays, high-density data storage devices, valves, and fluid management

and processing devices for chemical microanalysis, medical diagnostics, and drug delivery. While estimates for MEMS markets vary considerably, they all show significant present and future growth, reaching aggregate volumes in the many billions of dollars by the year 2004. The expected growth is driven by technical innovations and acceptance of the technology by an increasing number of end users and customers.

2.5 Standards

Few disagree that the burgeoning MEMS industry traces many of its roots to the integrated circuit industry. However, the two market dynamics differ greatly with severe implications, one of which is the lack of standards in MEMS. Complementary metal-oxide semiconductor (CMOS) technology has proven itself over the years to be a universally accepted manufacturing process for integrated circuits, driven primarily by the insatiable consumer demand for computers and digital electronics. In contrast, the lack of a dominant MEMS high-volume product, or family of products, combined with the unique technical requirements of
each application have resulted in the emergence of multiple fabrication and assembly processes. The following chapters will introduce these processes. Standards are generally driven by the needs of high-volume applications, which are few in MEMS. In turn, the lack of standards feeds into the diverging demands of the emerging applications.

2.6 The psychological barrier

It is human nature to cautiously approach what is new because it is foreign and untested. Even for the technologically savvy or the fortunate individual living in high-tech regions, there is a need to overcome the comfort zone of the present before engaging the technologies of the future. This cautious behavior translates to slow acceptance of new technologies and derivative

products as they are introduced into society. MEMS acceptance is no exception. For example, demonstration of the first micromachined accelerometer took place in 1979 at Stanford University. Yet it took nearly fifteen years before it became accepted as a device of choice for automotive airbag safety systems. Naturally, in the process, it was designed and redesigned, tested and qualified in the laboratory and the field before it gained the confidence of automotive suppliers. The process can be lengthy, especially for embedded systems.

Today, MEMS and associated product concepts generate plenty of excitement, but not without skepticism. Companies exploring for the first time the incorporation of MEMS solutions into their systems do so with trepidation, until an internal "MEMS technology champion" emerges to educate the company and raise the confidence level. With many micromachined silicon sensors embedded in every car and in numerous critical medical instruments, and with additional MEMS products finding their way into our daily lives, the height of this hidden psychological barrier appears to be declining.

2.7 Journals, conferences, and Web sites

The list of journals and conferences focusing on micromachining and MEMS continues to grow every year. There is also a growing list of on-line Web sites, most notably the MEMS Clearinghouse hosted by the Information Sciences Institute (ISI), Marina del Rye, California, and the European Microsystems Technology On-line (EMSTO), Berlin, Ger-many, sponsored by the ESPRIT program of the European Commission. The sites provide convenient links and maintain relevant information directories

2.7.1 List of journals and magazines

Several journals and trade magazines published in the U.S. and Europe cover research and advances in the field. Some examples are:

- Sensors and Actuators (A, B & C): a peer-reviewed scientific journal published by Elsevier Science, Amsterdam, The Netherlands.
- Journal of Micromechanical Systems (JMEMS): a peer-reviewed scientific journal published by the Institute of Electrical and Electronic Engineers (IEEE), Piscataway, New Jersey, in collaboration with the American Society of Mechanical Engineers (ASME), New York, New York.
- Journal of Micromechanics and Microengineering (JMM): a peer-reviewed scientific journal published by the Institute of Physics, Bristol, United Kingdom
- Sensors Magazine: a trade journal with an emphasis on practical and commercial applications published by Helmers Publishing Inc., Peterborough, New Hampshire.
- MST news: an international newsletter on microsystems and MEMS published by VDI/VDE Technologiezentrum Informationstechnik GmbH, Teltow, Germany.
- Micromachine Devices: a publication companion to R&D Magazine with news and updates on MEMS technology published by Cahners Business Information, Des Plaines, Illinois.

2.7.2 List of conferences and meetings

Several conferences cover advances in MEMS or incorporate program sessions on micromachined sensors and actuators. The following list gives a few examples:

- International Conference on Solid-State Sensors and Actuators (Transducers): held on odd years and rotates sequentially between North America, Asia, and Europe.

- Solid-State Sensor and Actuator Workshop (Hilton Head): held on even years in Hilton Head Island, South Carolina, and sponsored by the Transducers Research Foundation, Cleveland, Ohio.
- MicroElectroMechanical Systems Workshop (MEMS): an international meeting held annually and sponsored by the Institute of Electrical and Electronics Engineers (IEEE), Piscataway, New Jersey.
- International Society for Optical Engineering (SPIE): regular conferences held in the United States and sponsored by SPIE, Bellingham, Washington.
- MicroTotalAnalysis Systems (MTAS): a conference focusing on microanalytical and chemical systems. This conference was held on alternating years, but will become annual beginning in the year 2000. It alternates between North America and Europe.

2.8 Summary

Microelectromechanical structures and systems are miniature devices that enable the operation of complex systems. They exist today in many environments, especially automotive, medical, consumer, industrial, and aerospace. Their potential for future penetration into a broad range of applications is real, supported by strong developmental activities at many companies and institutions. The technology consists of a large portfolio of design and fabrication processes (a toolbox), many borrowed from the integrated circuit industry. The development of MEMS is inherently interdisciplinary, necessitating an understanding of the toolbox as well as the end application.

3

Comb Drive Gyros

*Comb Drive is a Micro Device through which w*e can measure acceleration with the help of Displacement (Δx) of comb fingers. It senses acceleration by sensing the change in position. Sensitivity dictated by mass (m) and nature of spring (k: material dependent)

It can be used as sensor and actuator in MEMS. As an actuator a high force and displacement can be achieved from comb drive by applying voltage. As sensor generated voltage can be sensed due to the displacement of combs. Comb Drive accelerometer is a basic part for a gyroscope and can be converted into gyro by sensing the rate in all three dimensions. *So the Comb Drive can be called a one dimensional Gyro.*

Its working principle is based on an electrostatic force generated between biased conductor plates as one moves relative to the other it sense this movement with the help of any sensing geometry and gives the exact information about the amount of motion of that object as shown in figure 3.1.

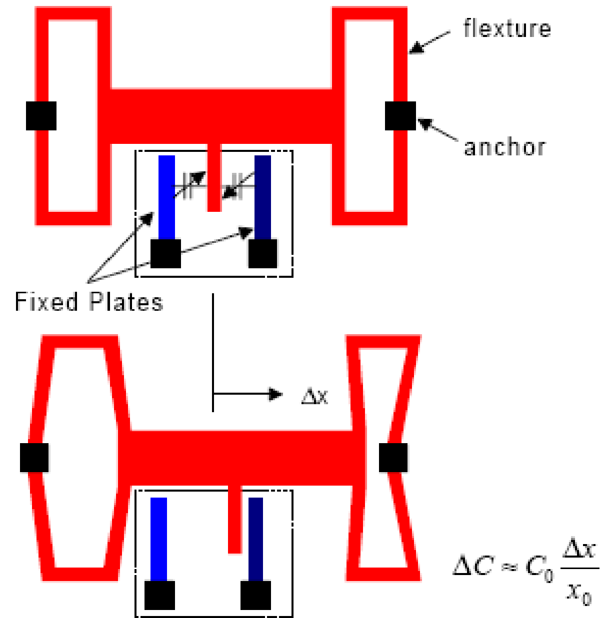

Figure 3.1. Basic concept of Comb Drive Gyro

3.1 Functionality for Position Sensing:

On the basis of dynamic functionality, comb drive resonators, can be classified into two types as shown in figure 3.2.

1. Lateral resonators
2. Vertical resonators

Figure 3.2. Comb Drive resonators

The lateral resonator, based on inter digitated electrodes, has weak drive and sense but the drive or vibration amplitudes of this kind of comb drive are much higher. A variety of actuation mechanisms with high gain can be designed through this resonator.

Vertical resonator also called **parallel resonator** has good drive and sense. But high gain value for this design is not possible because the amplitude of resonance is limited to <1/3rd of the gap between the plates. Mechanical coupling of this kind of resonator is much more difficult so limitised the design verity.

3.1.1 Lateral Resonator:

Laterally-resonant electrostatic comb-drive microactuators are well established components. Single-axis devices have been fabricated by surface micromachining of polysilicon [3.1–5] and single-crystal silicon [3.6, 7], bulk micromachining of doped silicon [3.8, 9], combined surface and bulk micromachining [3.10] and electroplating of metals [3.11, 12]. Applications have been found in lateral tunneling units [3.11], vibromotors [3.13, 14], microengines [3.15], external cavities for laser diodes [3.16], scanning mirrors [3.14, 17], gyroscopes [3.18] and pressure sensors [3.19]. Linearly-coupled devices have been used as electromechanical filters [3.20] and orthogonally coupled devices have been used as *x*–*y* stages for atomic force microscopy (AFM) applications [3.21–24]. Early devices were formed from thin (2–10 _m) mechanical layers; more robust components are now being developed [3.25, 26], based either on bonded silicon-on-insulator [3.27, 28], deep dry etching using an inductively coupled plasma [3.29, 30] or on metals electroplated in deep molds [3.31]. The dynamics of single-axis devices are well understood [3.1] and have been visualized in stroboscopic experiments [3.32]. They consist of a single dominant mass—the moving half of the electrode and its supporting shuttle—suspended on elastic flexures and constrained to move along a single axis. Due to the span of the electrode, its mass is distributed, but the shuttle is designed to be sufficiently rigid so that the assembly can be considered a point like mass for in-plane motion. The suspension is often small enough, compared with the shuttle, that it can be considered mass less,

although the Rayleigh method can be used to estimate its effect on resonant frequency [3.1, 2]. Although elastic nonlinearities have been observed [3.33, 34], the effects may be neglected for small deflections. Moreover, electromechanical linearization is being developed [3.35, 36]. Single-axis devices are therefore one-degree-of-freedom (1DOF) systems, and their dynamics

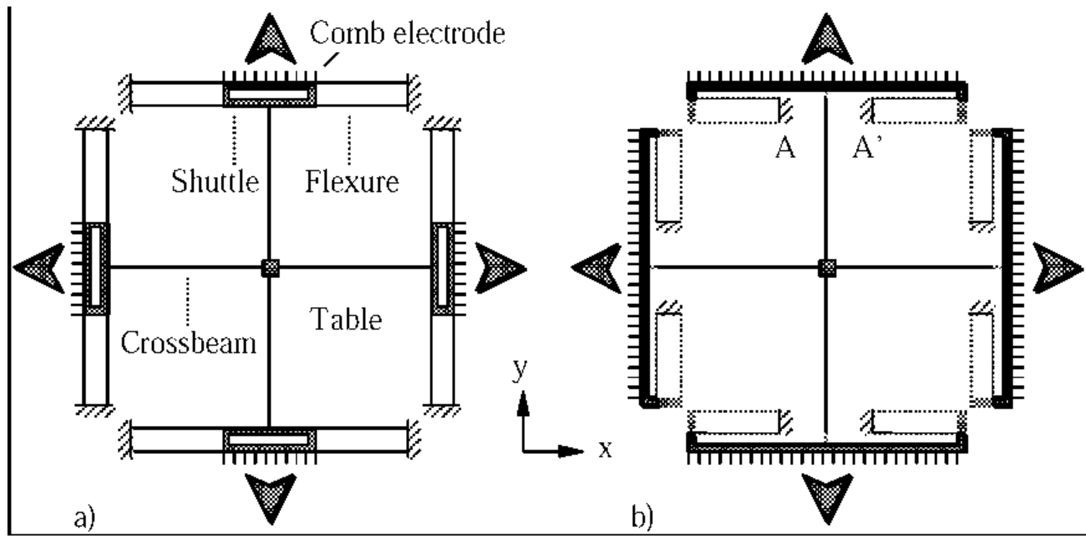

Figure 3.3. Dual-axis electrostatic comb-drive actuators with (a) hammock and (b) folded suspension.

can be described by linear, lumped-element and mass-spring damper models [3.1].Refinements have generally concerned secondary effects, such as the accurate modeling of damping [3.37–39], electrostatic levitation caused by the substrate [3.40] or fringing fields in the drive [3.41]. More complicated behavior is expected in multi axis stages, since these contain several masses that are independently suspended but linked by coupling beams. Consequently they are multi-DOF systems, even for in-plane motion. For example, figure 3.3(a) shows an *x*–*y* stage similar to that used in [3.23, 24]. Here, a table is suspended between four electrostatic drives by two flexible crossbeams. The moving part of each drive consists of a shuttle carrying a comb electrode which is suspended from a 'hammock' flexure formed by four beams [3.22]. The fixed part of each drive is omitted for simplicity. The majority of the system mass lies in the shuttle assemblies. Each is

constrained to translate in one direction, and an additional constraint is provided by the crossbeams, which force the masses to move in pairs. Consequently, this is a 2DOF system. With this design, the electrode can only occupy a small part of the overall device span. Figure 3.3(b) shows an alternative, where the hammock is replaced by a folded suspension. Here, the electrode covers the entire span, minimizing the drive voltage, and maximizing the current obtained in the capacitative readout. Either a single or a double flexure may be used at each end of each comb. However, care must be taken to design the suspension to prevent rotation of the electrode spars, because linear translation of the table will cause this rotation to be excited by the crossbeam. The consequence will be unnecessary energy dissipation, and the existence of four unwanted vibrational modes, since the device is now a 6DOF system. Figure 3.4 illustrates the layout of an *x*–*y* stage with a single-flexure suspension.

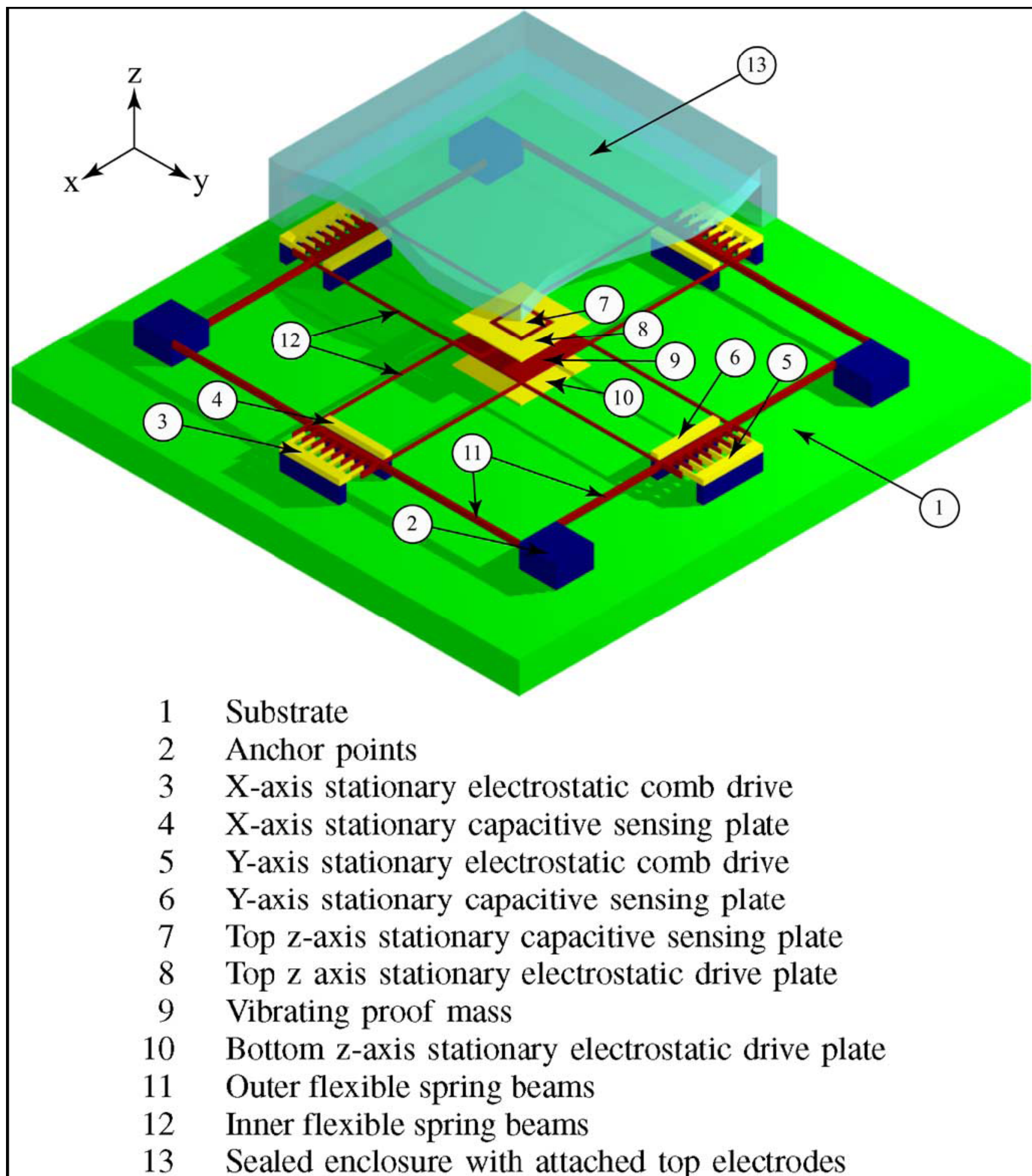

Figure 3.4. Experimental layout of an *x*–*y* stage with a single-flexure suspension.

3.2 Sensing Systems in Comb Drive

The sensing system used in comb drive can be capacitive, figure 3.5(a) and piezo-resistive, figure 3.5(b). In capacitive sensing, drive reads the change in position of combs which creates difference in comb finger capacitance. The value of capacitance can be noted as voltage. This type of sensing is not much temperature sensitive and also has low power dissipation. Current designs of comb drive generally use capacitive sensing system. In piezo-resistive sensing the deflection of comb structure produces strain in the flexure and deform it. Resistivity of the structure varies due to this strain and sensor reads the difference of resistance. This type of comb drive has high sensitivity against temperature and its power dissipation is also high.

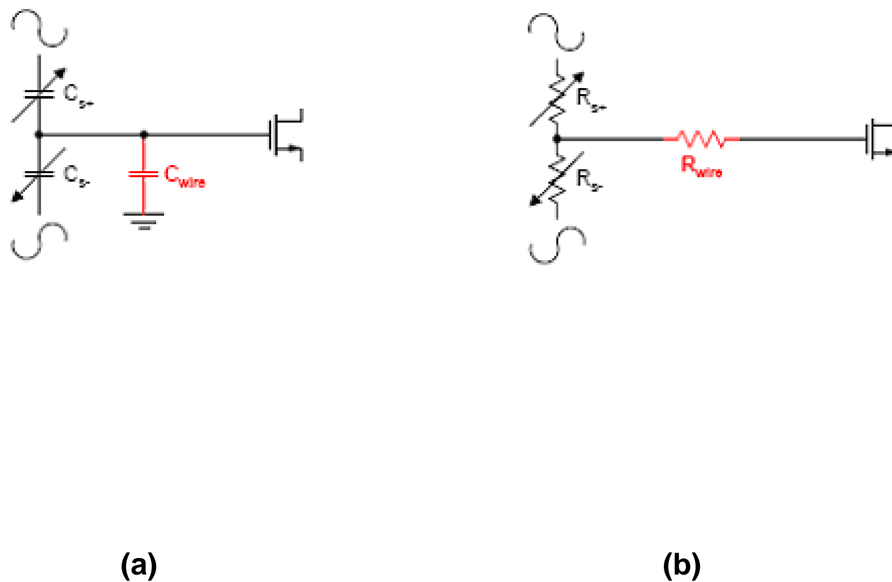

(a) **(b)**

Figure 3.5. Sensing system of comb drive

(a) Capacitive sensing and (b) Piezo-resistive sensing.

3.2.1 Basic Sensing Geometry

Figure.3.6 depicts the schematic view of the device. The device consists of a glass / silicon/glass triple stack structure. Stator electrodes are symmetrically arranged around the ring-shaped rotor to form capacitor for capacitive detection and electrostatic actuation

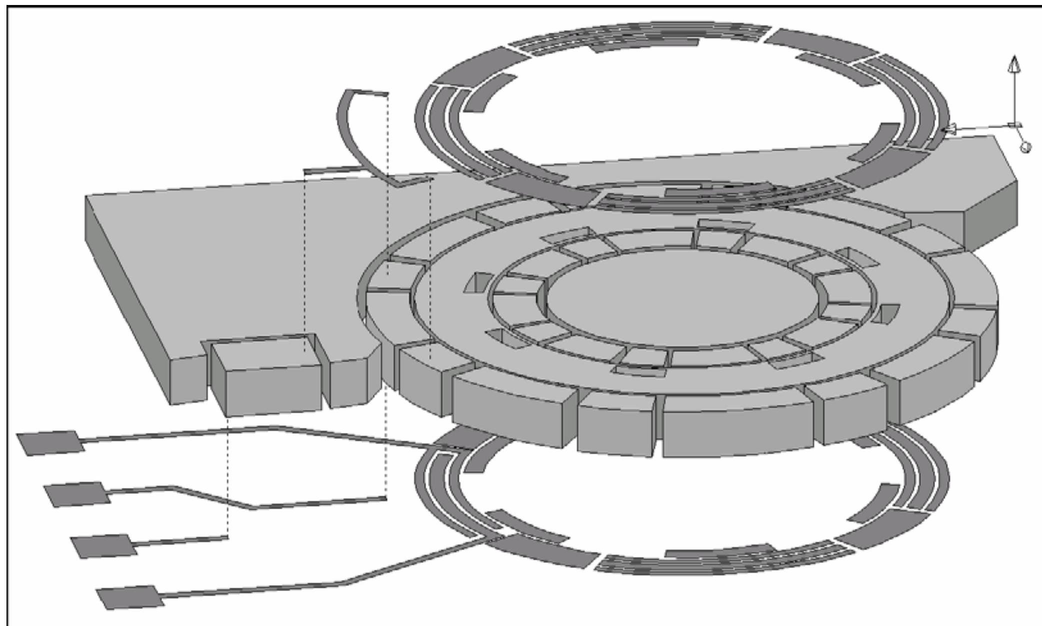

Figure 3.6 Schematic view of the sensor

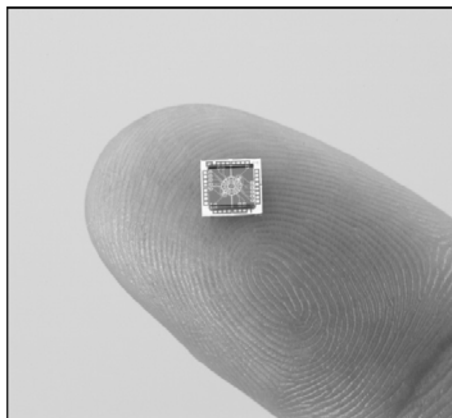

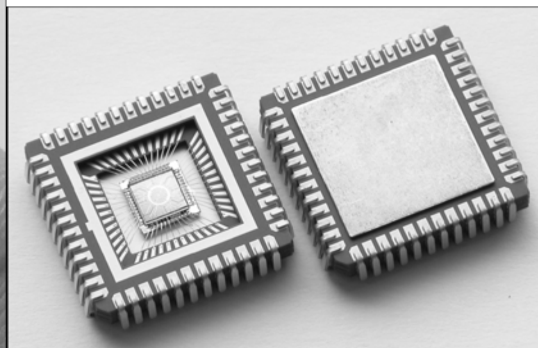

Figure 3.7 Sensor Chip **Figure 3.8** Packaged Sensor

Silicon layer forms a rotor, electrodes for radial position control and common electrodes for output. Radial gaps between the rotor and electrodes are

formed by deep RIE using ICP. This ring-shaped structure can provide 1) variable gap capacitors with narrow gaps to reduce voltages for levitation in radial direct ions and to increase sense capacitance and 2) large enough diameter of the rotor, i.e. large moment of inertia of the rotor about the spinning axis, to achieve high performance. The rotor has a diameter of 1.5mm, 150μm wide, 50μm thick and a radial gap of 2.2μm. Electrodes for axial position control, rotation control and common electrodes are placed on top and bottom glass plates and 3μm axial gaps are formed. The sensor chip as shown in figure 3.7 is mounted in a 48- pin ceramic package and bonded with Au wire. The package is then sealed in figure 3.8.

3.3 <u>Comb Drive Based Gyros</u>

Figure 3.9 shows the schematic of the fabricated micro-gyroscope. The outer and inner masses are driven together in the x direction at the driving mode resonant frequency. When an angular rate is applied in the z direction, the inner mass moves in the y direction. Note that there are different masses and different springs for the driving mode and the sensing mode. In a more conventional coupled-mode gyroscope with only one set of springs and one mass for driving and sensing, an induced Coriolis force makes the oscillation motion elliptical. This elliptical motion reduces the mechanical stability and becomes a source of a mechanical noise. The elliptical motion becomes more pronounced as the resonant frequency mismatch of the driving and sensing mode decreases. In the remainder of this paper, gyroscopes with one set of suspensions are called “coupled” gyroscopes, and gyroscopes with separate sets of suspensions for the driving and sensing mode are called “decoupled” gyroscope. It is well known that the resolution of a coupled gyroscope is relatively lower than that of a decoupled gyroscope, because of the strong mode coupling

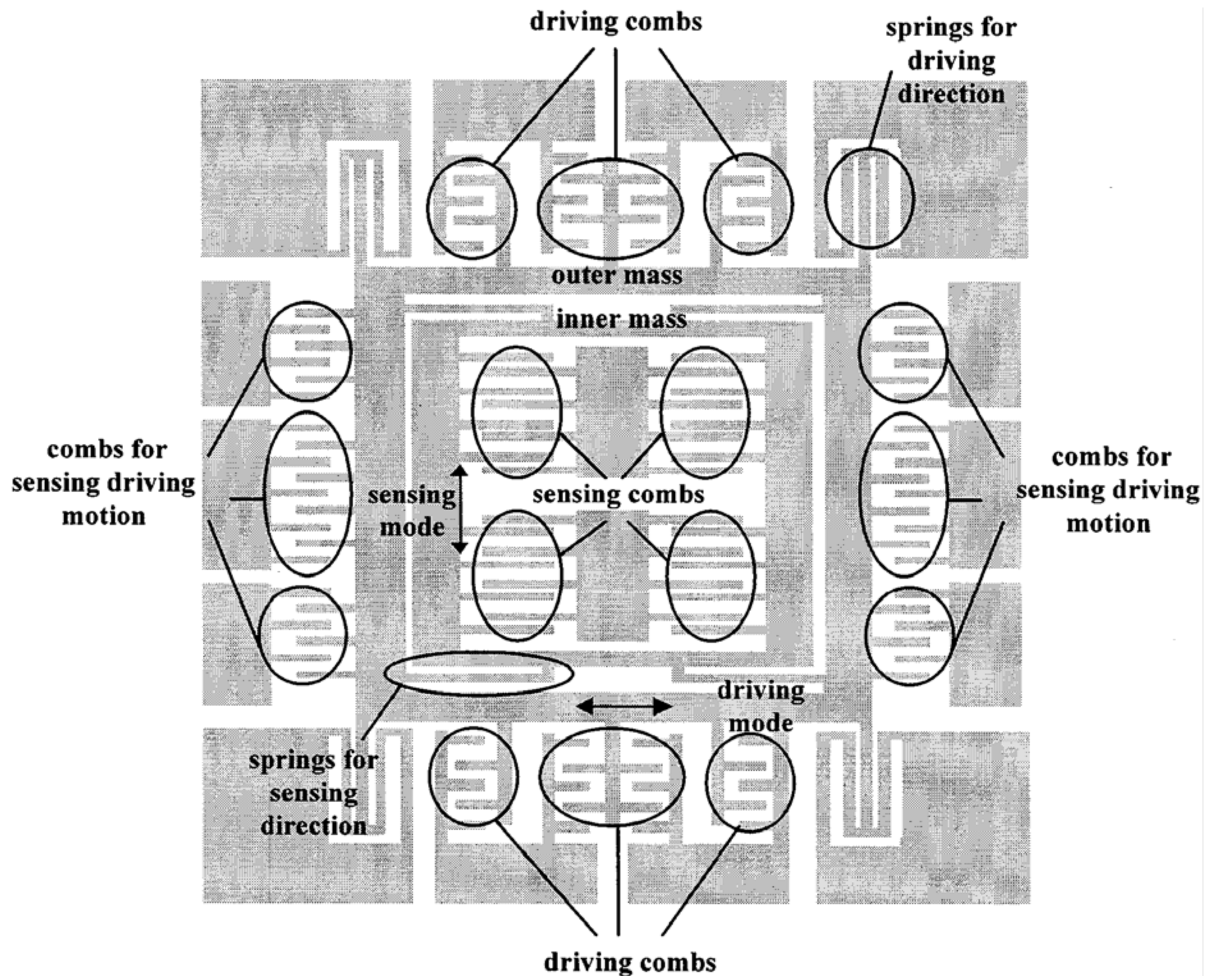

Figure 3.**9:** Schematic of the designed micro-gyroscope.

3.4 Operating Principle of MEMS Gyro:

Almost all reported micromachined gyroscopes use vibrating mechanical elements to sense rotation. They have no rotating parts that require bearings, and hence they can be easily miniaturized and batch fabricated using micromachining techniques. All vibratory gyroscopes are based on the transfer of energy between two vibration modes of a structure caused by Coriolis acceleration. Coriolis acceleration, named after the French scientist and engineer

G. G. de Coriolis (1792–1843), is an apparent acceleration

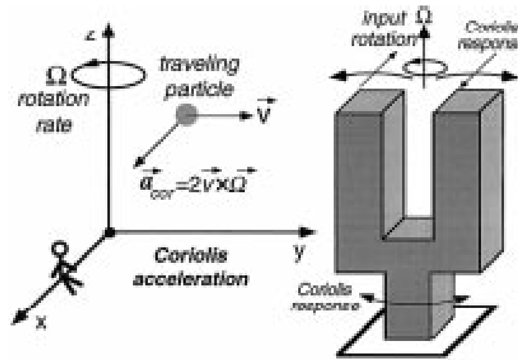

Figure 3.10: (a) The Coriolis effect. (b) Tuning-fork vibratory gyroscope. The tines are differentially driven to a fixed amplitude.

Coriolis force is detected either as differential bending of the tuning-fork tines or as a torsional vibration of the tuning-fork stem. This arises in a rotating reference frame and is proportional to the rate of rotation. To understand the Coriolis Effect, imagine a particle traveling in space with a velocity vector v. An observer sitting on the -axis of the xyz coordinate system, shown in figure 3.10 (a) and (b), is watching this particle. If the coordinate system along with the observer starts rotating around the -axis with an angular velocity Ω, the observer thinks that the particle is changing its trajectory toward the x-axis with an acceleration equal to 2v x Ω. Although no real force has been exerted on the particle, to an observer, attached to the rotating reference frame an apparent force has resulted that is directly proportional to the rate of rotation. This effect is the basic operating principle underlying all vibratory structure gyroscopes. Resolutions, drift, zero-rate output (ZRO) and scale factor are important factors that determine the performance of a gyroscope. In the absence of rotation, the output signal of a gyroscope is a random function that is the sum of white noise and a slowly varying function [3.42]. The white noise defines the resolution of the sensor and is expressed in terms of the standard deviation of equivalent rotation rate per square root of bandwidth of detection [(/s)/ Hz or (/h)/ Hz]. The so-called "angle random walk" in $^{o}/\sqrt{h}$ may be used instead. The peak-to-peak value of the slowly varying function defines the short- or long-term drift of the gyroscope and is usually expressed in /s or /h

[3.42]. Scale factor is defined as the amount of change in the output signal per unit change of rotation rate and is expressed in V/ (ω/s). Last, an important factor for any gyroscope that is primarily defined by device imbalances is the ZRO, which represents the output of the device in the absence of a rotation rate.

In general, gyroscopes can be classified into three different categories based on their performance: inertial-grade, tactical-grade, and rate-grade devices. Table 1 summarizes the requirements for each of these categories [3.42], [3.43]. Over the past few years, much of the effort in developing micromachined silicon gyroscopes has concentrated on “rate-grade” devices, primarily because of their use in automotive applications. This application requires a full scale range of at

Parameter	*Rate Grade*	*Tactical Grade*	*Inertial Grade*
Angle Random Walk, °/√h	>0.5	0.5-0.05	<0.001
Bias Drift, °/h	10-1000	0.1-10	<0.01
Scale Factor Accuracy, %	0.1-1	0.01-0.1	<0.001
Full Scale Range (°/sec)	50-1000	>500	>400
Max. Shock in 1msec, g's	10^3	10^3-10^4	10^3
Bandwidth, Hz	>70	–100	–100

Table 1 Performance Requirements for Different Classes of Gyroscopes

least 50 /s and a resolution of about 0.1 /s in a bandwidth of 50 Hz, all at a cost of $10–20 [3.44]. The operating temperature is in the range from -40 to 85 C. There are also several other applications that require improved performance, including inertial navigation, guidance, robotics, and some consumer electronics.

Today, optical gyroscopes are the most accurate gyroscopes available in the market. Among these, ring laser gyroscopes have demonstrated inertial-grade performance, while fiber-optic gyroscopes are mainly used in tactical-grade applications.

Delco's hemispherical resonator gyroscope (HRG) is a vibratory gyroscope that has achieved impressive inertial-grade performance [3.45]. Although highly accurate, these devices are too expensive and bulky for many low-cost applications. Achieving "tactical- and inertial-grade" performance levels has proven to be a tough challenge for micromachined gyroscopes, and new technologies and approaches are being developed. Because of their greater compatibility with batch fabrication technologies, this paper will only review silicon micromachined vibratory gyroscopes.

3.5 Basic Design of MEMS Vertical Comb Drive Gyro:

The mechanism of vertical offset between the fixed comb and the movable comb is based on thermal residual stress. As illustrated in figure 3.11, the fixed combs are anchored to bimorph cantilevers made of two materials with dissimilar thermal coefficients of expansion (TCE), i.e., silicon dioxide and single crystal silicon. The bimorph cantilevers are deflected by residual stress generated within TCE mismatch layers in cooling down from the oxidation temperature to room temperature and the anchored fixed combs are bent down so the vertical offset between the fixed combs and the movable combs is generated.

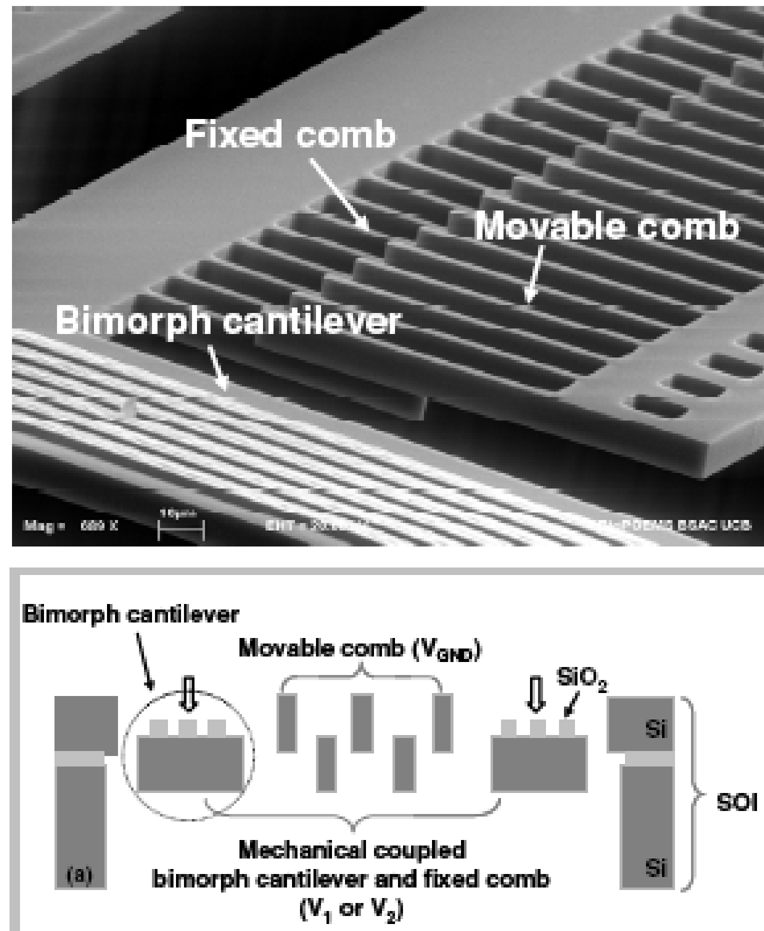

Figure 3.11: SEM image and schematic of self aligned comb drive

The vertical comb drive consists of one movable comb above two anchored combs on either side as shown in figure 3.12(*a*). The movable comb structure incorporates a micromirror, pinhole, microlens ring holder, or diffraction grating as shown in figures 3.12(*c*) and (*d*). The device consists of three electrodes connected to each comb structure. It can be operated in torsional by generating the electrostatic force between the upper movable comb (*V*GND) and one lower fixed comb (*V*1 or *V*2) or in piston motion between the upper movable combs (*V*GND) and two lower fixed combs (*V*1 and *V*2). The design of this self-aligned vertical comb drive requires the approximation of the deflection of a bimorph cantilever that provides the initial engagement between a movable comb and fixed combs. Even though the residual stress

arises from either intrinsically or extrinsically stress causing factors, the deflection was calculated using the analysis presented in previous work, under the assumption that TCE mismatch is the dominant contributor to the deflection of the bimorph cantilever, especially made of single crystal silicon and silicon dioxide with the small thickness ratio [3.46]

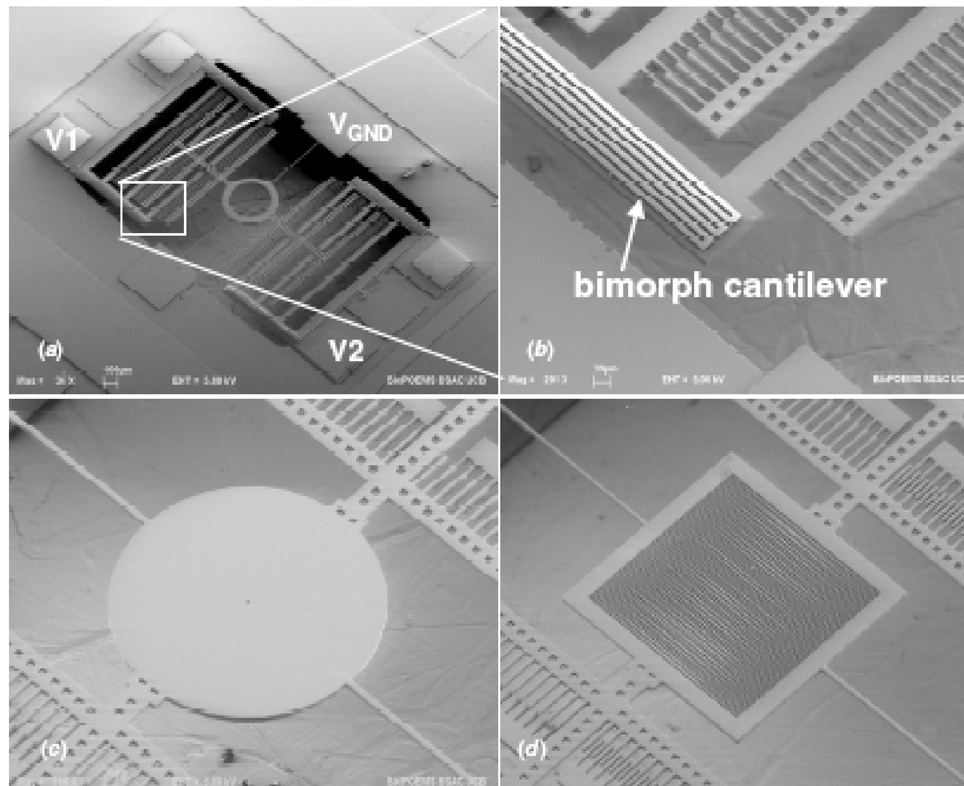

Figure 3.12: (a) Self aligned comb drive with microlens holder. (b) bimorph cantilever anchoring fixed combs. (c) tunable pinhole of 5 μm, and (d) reconfigurable diffraction grating with 4 μm slit width.

3.6 Microlevel Description of Comb Drive Gyro Design

Figure 3.13 is the microscopic picture of the physical device. The mechanical gyro consists of few functional parts, the two proof masses, the flexures, the base beam, the inner and outer motor combs, and the sense plates. figure 3.13 shows these subunits

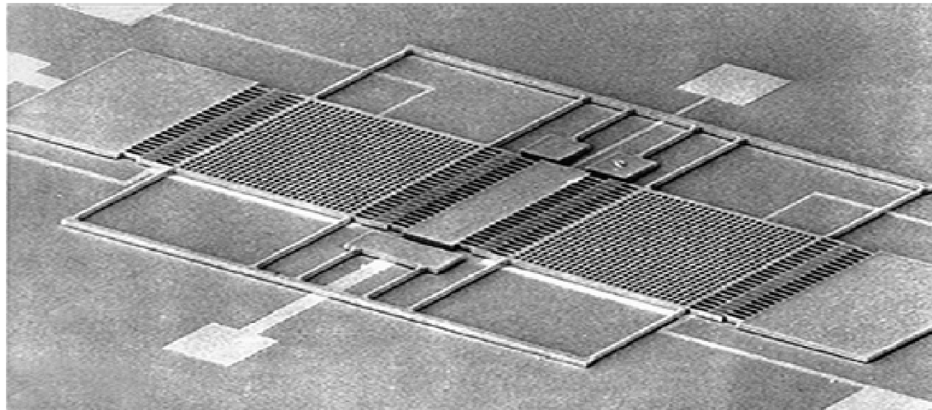

Figure 3.13: Microscope picture of the MEMS gyro

All of the structure lies in a single plane which will be referred to as plane of the device. Motion is possible both in plane and perpendicular to the plane. figure 3.14 and 15 gives diagram illustrating the major functional parts of the gyro. The figure also labels the three orthogonal directions as input, motor and sense.

The two proof masses are plates of silicon through which many square holes have been machined. The masses are physically driven by the gyro system and create the physics needed to sense rate. The holes exist to allow fluid (usually air) to flow through the proof masses, helping to reduce thin film damping effects. Each proof mass has a mass of approximately $3.6\ 10^{-8}$ kg.

Both proof masses are constrained by flexures, which are beams machined by the silicon wafer. The beams act as springs, bending to allow the proof mass to move both in the plane of the device and out of plane. The beam dimension determine their stiffness.

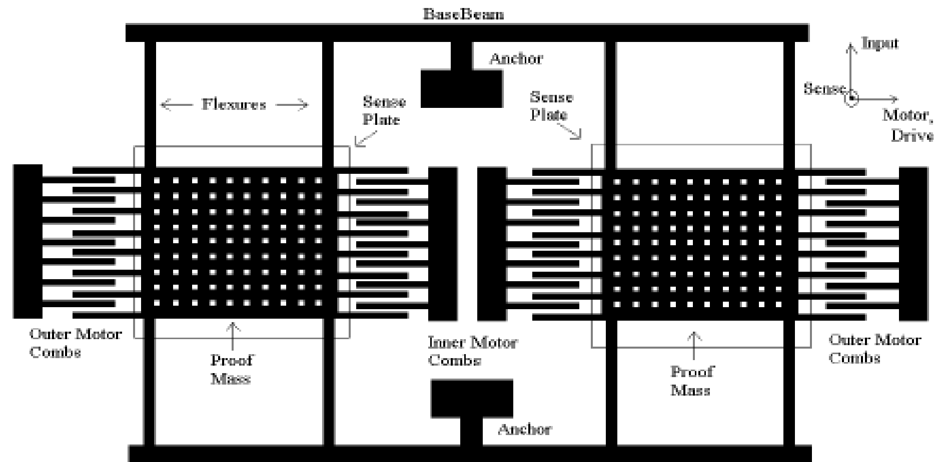

Figure 3.14: Functional units in the Gyro (Looking down on the plane of the device)

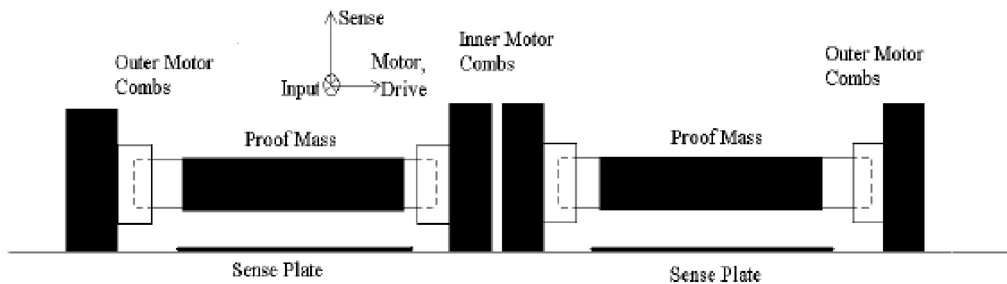

Figure 3.15: Functional units in the Gyro. (View in the plane of the device)

Instead of connecting directly to anchors, the flexures connect to a much larger, and thus stiffer, base beam. The base beam connects to the substrate at an anchor point, and provides the main support for the gyro structure.
For driving and sensing the motion in the plane of the device, the inner and outer motor comb structures are utilized. These structures are anchored directly to the substrate. They consists of the long slender fingers which mesh with identical fingers connected to the proof mass. Each side of the proof mass has a set of fingers. Thus there are 4 sets of interdigitated fingers, two

between the masse and two outsides. The interdigitated fingers form capacitors which allow the gyro sense and drive motion in the plane.
Below the proof masses there are large, fixed conducting plates which form a parallel plate capacitor with the proof masses themselves (two capacitors, one for each proof mass). These capacitors are used to sense motion out of plane. [3.47].

3.7 Construction of Different types of MEMS Gyro

The drive for miniaturization propelled technology towards smaller devices. Though each move, brought equipment whose compromise for size did not mean a trade-off in terms of performance. Today the world is thinking small, the units have been scaled down to micro and nano levels, thus emerged machines that operate and execute functions while scaled at one millionth of a centimeter. These are devices for whom a razor edge is like a platform, thus exhausting the idioms of our every day lexicon. Micro Electro Mechanical Systems (MEMS) or the more European term Micro Systems Technology (MST), are devices whose applications are being discovered. While technology can advance at supersonic speed, the ability of the human mind to grasp its true implications lag behind. Radio was invented in 1895. it took fifty years for some one to realize that it can be used for one to many communication rather than only one-to-one. Although a universal definition is lacking, MEMS products possess a number of distinctive features. They are miniature embedded systems involving one or many micromachined components or structures. They enable higher level functions, although in and of themselves their utility may be limited—a micromachined pressure sensor in one’s hand is use-less, but under the hood it controls the fuel-air mixture of the car engine. They often integrate smaller functions into one package for greater utility—for example, merging an acceleration sensor with electronic circuits for self-diagnostics. They can also bring cost benefits, directly through low unit pricing, or indirectly by cutting service and maintenance costs.

Although the vast majority of today's MEMS products are best categorized as components or subsystems, the emphasis in MEMS technology is on the "systems" aspect.

The comb-drive actuator is one of the main building blocks of micro-electromechanical systems (MEMS). Its working principle is based on an electrostatic force that is generated between biased conductor plates as one move relative to the other. Because of its capability of force generation, it finds wide application in micro-mechanical systems. Sample applications include polysilicon microgrippers [3.48], scanning probe devices [3.49], force-balanced accelerometers [3.50], actuation mechanisms for rotating devices [3.51], laterally oscillating gyroscopes [3.52] and RF filters [3.53]. Consequently, any improvement to this basic actuator could have far-reaching effects.

Specifically, we are interested in comb finger designs which would generate force-deflection profiles that have linear shapes. These linear relationships could partially compensate for the mechanical restoring force due to the action of a linear suspension spring. This electrostatic weakening or stiffening of the mechanical spring can decrease the drive voltage of actuators or change the resonant frequency of resonators.

Several previous researchers have investigated various comb shapes. Hirano et al. [3.54] reported techniques for fabricating fingers which could dramatically reduce the separation gap after only a short motion. These fingers were designed for maximum possible force output at a nearly constant rate. Rosa et al. [3.55] continued this search for high-force actuators

The product life cycle of MEMS is made cumbersome by the modeling and simulation using IntelliCAD, and FEM packages, such as Intellisuite and ANSYS. This research work is aimed at cutting down the length of the whole effort by employing the power of Bond Graph Method. The multi-physics

approach and cross-domain reach of bond graph method rids us of the need to use coupled domains and work under the supposition that the domains have been decoupled under some assumed approximation. Such approximations have usually made the model deviate from the specifications leading to unexpected behavior in physical conditions. It is expected that theoretically the Bond Graph approach shall bring the model closer to empirical results. Though the methodology has been in use since the last three decades, its power has been fully realized recently, while its object oriented modeling capabilities and marrying of genetic programming has been exploited to the greatest benefit.

Bond graph method has been applied to RF MEMS comb drive switches by Dr. Rosenberg et al. the same has been tried on vertical comb drive actuator in this research. The initial effort has been focused on formulating the bond graph while tuning it to have a system approach of the model available for further results to be extracted by specifying the various parameters in the state space of the bond graph method. The work has been done in the way that it can be expended to Micro Electro-Mechanical Gyro in future.

The designing an accelerometer-based gyroscope-free inertial navigation system (INS) that uses only comb drive as accelerometers to compute the linear and angular motions of a rigid body is more reliable, precise, accurate and cost effective method to apply in navigation systems Feasibility of a Gyroscope-free Inertial Navigation System for Tracking Rigid Body Motion, Chin-Woo Tan, Kirill Mostov, Pravin Varaiya, Paper UCB-ITS-PRR-2000-9]

A number of vibratory gyroscopes have been demonstrated, including tuning forks [3.56],[3.57]–[3.59], vibrating beams [3.60], and vibrating shells [3.44]. Tuning forks are a classical example of vibratory gyroscopes. The tuning fork, as illustrated in figure 3.10 (b), consists of two tines that are connected to a junction bar. In operation, the tines are differentially resonated to a fixed amplitude, and when rotated, Coriolis force causes a differential sinusoidal

force to develop on the individual tines, orthogonal to the main vibration. This force is detected either as differential bending of the tuning fork tines or as a torsional vibration of the tuning fork stem. The actuation mechanisms used for driving the vibrating structure into resonance are primarily electrostatic, electromagnetic, or piezoelectric. To sense the Coriolis-induced vibrations in the second mode, capacitive, piezoresistive, or piezoelectric detection mechanisms can be used. Optical detection is also feasible, but it is too expensive to implement. In general, silicon micromachining processes for fabrication of vibratory gyroscopes fall into one of four categories:

1) silicon bulk micromachining and wafer bonding;

2) polysilicon surface micromachining;

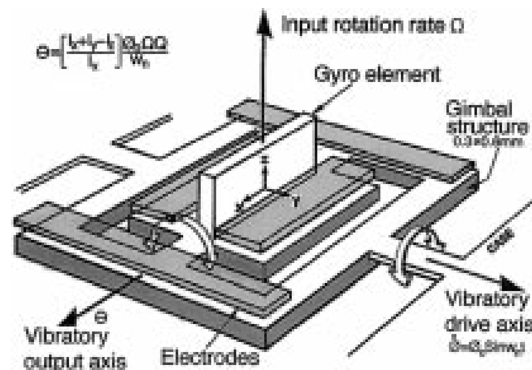

Figure 3.16: *Draper's first silicon micromachined double-gimbal vibratory gyroscope (1991)*

3) metal electroforming and LIGA; and

4) combined bulk-surface micromachining or so-called mixed processes.

Piezoelectric vibratory gyroscopes were demonstrated in the early 1980's. Examples of these devices are fusedquartz HRG by Delco [3.45], quartz tuning forks [3.61] like the Quartz Rate Sensor by Systron Donner [3.62],

[3.63], and a piezoelectric vibrating disc gyro [3.99]. Although quartz vibratory gyroscopes can yield very high quality factors at atmospheric pressure with improved level of performance, their batch processing is not compatible with IC fabrication technology. In the late 1980's, after successful demonstration of batch-fabricated silicon accelerometers, some efforts were initiated to replace quartz with silicon in micromachined vibratory gyroscopes. The Charles Stark Draper Laboratory demonstrated one of the first batchfabricated silicon micromachined rate gyroscopes in 1991. This bulk silicon device was a double gimbal vibratory gyroscope supported by torsional flexures, with the vibrating mechanical element made from p++ silicon [3.64].

As illustrated in figure 3.16, the outer gimbal was electrostatically driven at a constant amplitude using the drive electrodes, and this oscillatory motion was transferred to the inner gimbal along the stiff axis of the inner flexures.

When exposed to a rotation normal to the plane of the device, Coriolis force causes the inner gimbal to oscillate about its weak axis with a frequency equal to the drive frequency. Therefore, maximum resolution is obtained when the outer gimbal is driven at the resonant frequency of the inner gimbal, causing the sensitivity to be amplified by the mechanical quality factor of the sense resonance mode of the structure. A rotation rate resolution of 4 /s in a 1 Hz bandwidth was realized using this structure.

Later in 1993, Draper reported an improved 1 mm^2 silicon-on-glass tuning fork gyroscope [3.57] fabricated through the dissolved wafer process [3.65]. This gyroscope was electrostatically vibrated in its plane using a set of interdigitated comb drives [3.66] to achieve large amplitude of motion (10 m). Any rotation in the plane of the substrate perpendicular to the drive mode will then excite the out-of-plane rocking mode of the structure,

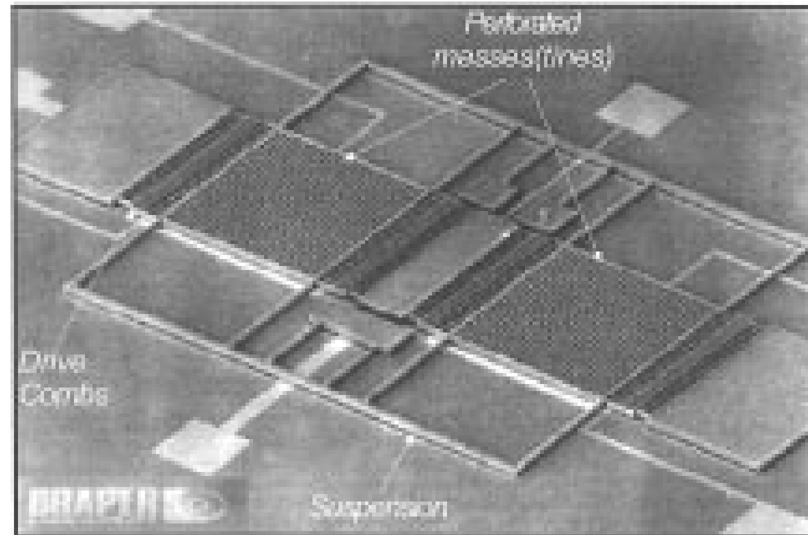

Figure 3.17: SEM view of Draper's single-crystal silicon-on-glass tuning-fork gyroscope [3.67].

which is capacitively monitored. Figure 3.17 shows an SEM view of the device with a perforated mass to minimize damping. The in-plane motion of the structure is lightly damped by air, while out-of-plane motion is strongly damped due to squeeze film effects. Therefore, for out of-plane modes Q, rises rapidly as pressure is reduced, in contrast to the in-plane Q , which shows a small increase
as the pressure drops. At pressures of 100 mTorr, a Q of 40 000 was observed for the drive mode and 5000 for the sense mode. The silicon-on-glass technology used in this device has the advantage of low stray capacitance.

The noise equivalent rate observed by this structure was 470 /h in a 60 Hz bandwidth, equivalent to 0.02 /s in a 1 Hz bandwidth or angle random walk of 0.72 $^{o}/\sqrt{h}$ [3.67]. The scale-factor accuracy was better than 0.1%, and bias stability was 55 /h overnight. The projected performance was 10–100 /h for bias stability and resolution in a 60 Hz bandwidth.

If the sense and drive resonant modes of a tuning fork have equal frequencies, the output signal will be amplified by the quality factor Q of the sense mode, resulting in much higher sensitivity. However, this involves extreme control of device dimensions and may lead to temperature drift problems if these natural frequencies do not track with temperature. Because of these difficulties, most tuning fork designs are not based on matched vibration mode frequencies.

Other tuning-fork designs have used electromagnetic excitation to obtain large amplitude of motion [3.58], [3.59], [3.68]. Bosch's silicon yaw rate sensor [3.59] achieves vibration amplitudes as large as 50 m using a permanent magnet mounted inside a metal package. This device was fabricated through a combination of bulk- and surface micromachining processes, and it consists of two bulk micromachined oscillating masses, each of which supports two surface-micromachined accelerometers for detection of Coriolis force. The sensor chip is anodically bonded to a supporting glass wafer and is covered by another silicon cap wafer. Operating at atmospheric pressure, the device has shown a resolution of 0.3 /s in a 100 Hz bandwidth, thanks to its large amplitude of vibration. Although such a large amplitude of oscillation (50 m) can increase the output signal level, it increases the total power consumption and may cause fatigue problems over long-term operation.

Cross talk between the sense and drive modes was minimized through mechanical decoupling of these modes by separating the oscillator and sense proof masses, resulting in a stable ZRO.

Piezoresistive detection has also been used in some gyroscope designs. Daimler Benz has demonstrated a tuning fork angular rate sensor for automotive applications that piezoresistively measures the rotation-induced shear stress in the stem of the tuning-fork device [3.56]. In this device, a piezoelectric actuation mechanism was used by depositing a piezoelectric aluminum nitride (AlN) thin film layer on one of the tines. The use of

piezoelectric thin films such as AlN and ZnO on silicon degrades and causes large temperature variation of offset and sensitivity [3.69]. This device was fabricated through a combination of bulk micromachining and bonding of SOI wafers. Researchers at the University of Neuchatel, Switzerland, have demonstrated a tuning-fork design based on two isolated vibrating proof masses, each supported by a four beam bridge-type suspension [3.68]. These proof masses are electromagnetically vibrated in plane and anti-phase, and the rotation-induced out-of-plane motion is then detected by means of four piezoresistors connected in a Wheatsone bridge configuration, showing a sensitivity of 4 nV/ /s with excellent linearity up to 750 /s. This device was fabricated through silicon bulk micromachining and was wafer-level vacuum packaged by anodic bonding of the silicon wafer to encapsulating glass wafers. In general, package-induced stress on the sensor structure can be lowered by low-temperature anodic bonding of glass wafers with silicon [3.69]. Although piezoresistive devices are easier to fabricate and require a simpler electronic interface due to their lower output impedance compared to capacitive devices, they have large temperature sensitivity and poor resolution.

Also reported in the literature are capacitive bulk micromachined silicon-on-glass vibrating beams [3.70], vibrating membranes [3.71], and double-gimbaled structures [3.72]. Since the Young's modulus of single-crystal silicon changes with crystallographic orientation, symmetric vibrating structures made of single-crystal silicon may show excessive mechanical coupling between drive and sense modes (due to this anisotropy), resulting in a large ZRO with unacceptable drift characteristics [3.70].

Surface-micromachined vibratory gyroscopes have also been demonstrated. Some have been integrated with the readout electronic circuitry on a single silicon chip, reducing parasitic capacitances and hence increasing the signal-to-noise ratio. In addition, the vibrating structure is made of polysilicon, which has a high quality factor and an orientation-independent Young's modulus.

Single and dual-axis polysilicon surface-micromachined gyroscopes have been realized by researchers at Berkeley [3.73], [3.74] and Samsung [3.75]–[3.77]. Berkeley's z-axis vibratory rate gyroscope [3.73] resembles a vibrating beam design and consists of an oscillating mass that is electrostatically driven into resonance using comb

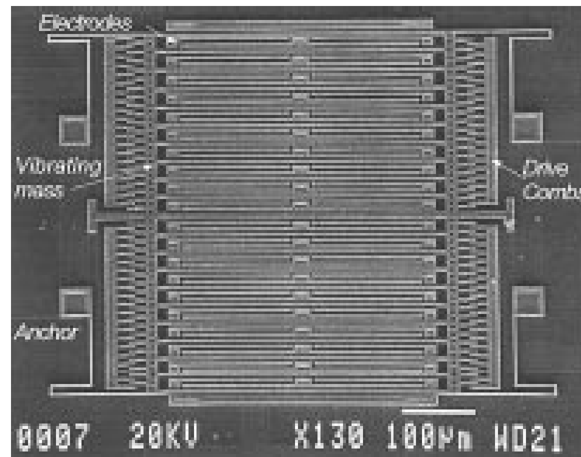

Figure 3.18: SEM view of a comb-driven polysilicon surface micromachined z-axis vibratory gyroscope [3.76].

drive. Any deflections that result from Coriolis acceleration are detected differentially in the sense mode using interdigitated comb fingers. This device, 1 mm across, was integrated with a transresistance amplifier on a single die using the Analog Devices BiMEMS process. The remaining control and signal-processing electronics were implemented off chip. Quadrature error nulling and sense-mode resonant frequency tuning can be accomplished in this design by applying a control dc bias voltage to the position sense fingers. The dc bias voltage generates an electrostatic negative stiffness, which reduces the resonant frequency of the sense mode. By slightly changing this dc bias voltage on the differential comb fingers (±ΔV), a lateral electrostatic field arises that can be used to align the drive mode oscillations and reduce the quadrature error. This device demonstrated a resolution of 1 /s/ Hz with performance projected to improve to 0.1/s/Hz in a second-generation device.

Samsung has also reported a very similar surface micromachined x-axis device, shown in figure 3.18, with a 7- m-thick polysilicon resonating mass supported by four fishhook-shaped springs [3.76]. This device, though not integrated with electronics, has demonstrated a resolution of 0.1 /s at 2 Hz, an operating bandwidth of 100 Hz, and a linearity of 1% full scale in a range of 90 /s. Hybrid attachment of the sensor chip to a CMOS application specific integrated circuit (ASIC) chip used for readout and closed-loop operation of the gyro was done in a vacuum-packaged ceramic case.

Murata has presented a surface-micromachined polysilicon gyroscope that is sensitive to lateral (xy- or x-axis) angular rate [3.78]. The sense electrode was made underneath the perforated polysilicon resonator by diffusing phosphorous into the silicon substrate (junction isolation). This device showed an open-loop noise-equivalent rate of 2 /s/ Hz. The junction-isolation scheme used in this device, although simple, has the disadvantage of relatively large parasitic capacitance and large amount of shot noise associated with the existing pn junction, which in

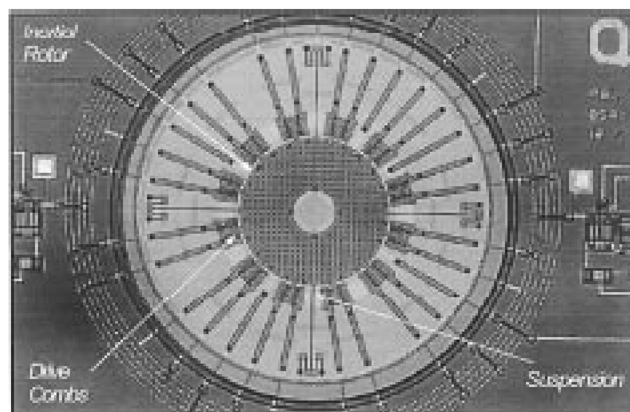

Figure 3.19: Close-up die shot of Berkeley's dual-axis rate gyroscope, integrated with sense and drive electronics using Analog Devices, Inc., surface-micromachining process [3.79].

turn degrade the resolution. Later in 1997, Samsung reported a similar device that used a 3000-A° -thick polysilicon sense electrode underneath a 7.5- m-thick low-pressure chemical vapor deposition (LPCVD) polysilicon resonating mass [3.73]. Since the detection mode is highly damped by squeeze film damping, these devices have to operate under vacuum. Samsung's device, vacuum packaged in an Al_2O_3 case, showed an improved open-loop noise-equivalent rate of 0.1 /s/ Hz with a good linearity up to 100 /s.

Berkeley has reported a surface-micromachined dual-axis gyroscope based on rotational resonance of a 2- m-thick polysilicon rotor disk, as shown in [3.79] (figure 3.19). Since the disk is symmetric in two orthogonal axes, the sensor can sense rotation equally about these two axes. This device, integrated with electronics, yielded a random walk as low as 10 $^{o}/\sqrt{h}$ with cross-axis sensitivity ranging 3–16%. Resolution can be further improved to 2 $^{o}/\sqrt{}$ h by frequency matching at the cost of excessive cross-axis sensitivity. Also reported in the literature is a cross-shaped nickel-on-glass two-axis micromachined gyroscope [3.80], which has shown a rate sensitivity of 0.1 mV/ /s. The JPL, in collaboration with the University of California, Los Angeles, has demonstrated a bulk-micromachined, precision silicon MEMS vibratory gyroscope for space applications [3.81], [3.82]. This clover-leaf-shaped gyroscope consists of three major components: a silicon clover-leaf vibrating structure; a silicon base plate, which is bonded to the clover-leaf structure; and a metal post, which is epoxied inside a hole on the silicon resonator. A hermetically sealed package, 1 x 1 x 0.7 in, houses the microgyroscope and most of its control electronics. This packaged gyroscope has a 7 Hz split between its drive and sense mode (1.44 kHz), a scale factor of 24 mV/ /s, a bias stability of 70 /h, and an angle random walk of 6.3 $^{o}/\sqrt{}$ h. Recently, researchers at HSG-IMIT, Germany, have demonstrated and reported a surface-micromachined precision x-axis vibratory gyroscope (MARS-RR) with a very small ZRO achieved by mechanical decoupling of the drive and sense vibration modes [3.83]. This device (6 mm), shown in figure 3.20, was fabricated through the

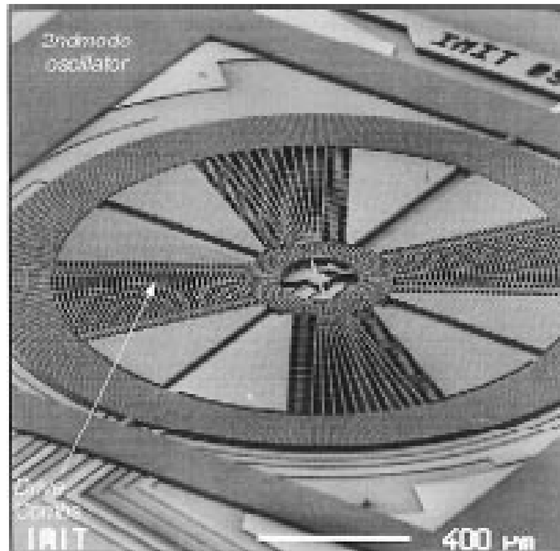

Figure 3.20: SEM of HSG-IMIT's surface-micromachined x-axis vibratory gyroscope (MARS-RR) fabricated through Bosch's process with a 10μm thick structural polysilicon layer [3.83].

standard Bosch foundry process featuring a 10μthick structural polysilicon layer in addition to the buried polysilicon layer, which defines the sense electrodes. The reported performance of this device is quite impressive: a random angle walk of 0.27 $^o/\sqrt{h}$, a bias stability of 65° /h, and a scale-factor nonlinearity of <0.2%. Researchers at General Motors and the University of Michigan have developed a vibrating ring gyroscope [3.44], schematically shown in figure 3.21. This device consists of a ring, semicircular support springs, and drive, sense, and balance electrodes, which are located around the structure.

Symmetry considerations require at least eight springs to result in a balanced device with two identical flexural modes that have equal natural frequencies [3.84]. The ring is electrostatically vibrated into an in-plane elliptically shaped primary flexural mode with a fixed amplitude. When it is subjected to rotation around its normal axis, Coriolis force causes energy to be transferred from the primary mode to the secondary flexural mode, which is located 45° apart from

the primary mode, causing amplitude to build up proportionally in the latter mode; this buildup is capacitively monitored. The vibrating ring structure has some important features compared to other types of vibratory gyroscopes. First, the inherent symmetry of the structure makes it less sensitive to spurious vibrations.

Only when the ring has mass or stiffness asymmetries can environmental vibrations induce a spurious response. Second, since two identical flexural modes of the structure “with nominally equal resonant frequencies” are used to sense rotation, the sensitivity of the sensor is amplified by the quality factor of the structure, resulting in higher sensitivity. Third, the vibrating ring is less temperature sensitive since the vibration modes are affected equally by temperature. Last, electronic balancing of the structure is possible. Any frequency mismatch due to mass or stiffness asymmetries that occurs during the fabrication

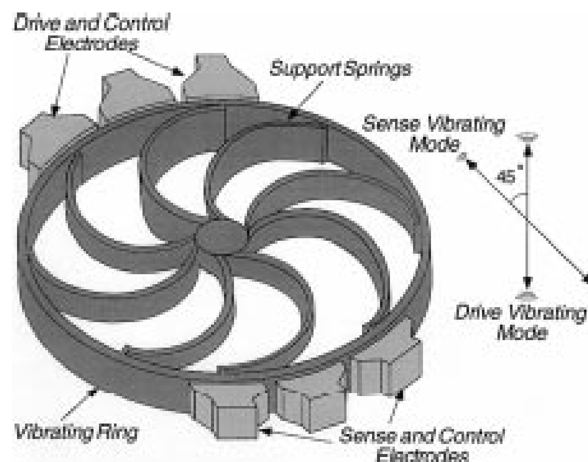

Figure 3.21: Structure of a vibrating ring gyroscope.

process can be electronically compensated by use of the balancing electrodes that are located around the structure. The first micromachined version of the vibrating ring gyroscope was fabricated by electroforming nickel into a thick polyimide (or photoresist) mold on a silicon substrate in a post circuit process

[3.44], [3.84], [3.85]. The gyroscope demonstrated a resolution of ~0.5^{o} /s in a 25 Hz bandwidth limited by the readout electronic noise. The sensor was integrated with a low-input capacitance source-follower buffer and the amplifier on a silicon chip. The zero bias drift was <10° /s over the temperature range -40 to 85° C, and the sensitivity of the device varied by less than 3% over the same temperature range. Scale-factor nonlinearity in a ±100^{0} /s rate range was <0.2% [3.85]. To improve performance further, a new polysilicon ring gyroscope (PRG) [3.86] was recently fabricated through a single-wafer, all-silicon, high-aspect-ratio p++ /polysilicon trench-refill technology [3.87] at the University of Michigan.

In this new process, the vibrating ring and support springs are created by refilling deep dry-etched trenches with polysilicon deposited over a sacrificial LPCVD oxide layer. Each sense electrode is made from a p++ silicon island (12μm deep) hanging over an ethylenediamine-pyrocatechol (EDP)-etched pit. Figure3.22 shows a SEM picture of a 1.7x 1.7 mm^2 PRG. This device provides several important features required for high-performance gyroscopes, including small ring-to-electrode gap spacing (<1 μm) for increasing the sense capacitance; large structural height for increasing the radius and sense capacitance and reducing the resonant frequency; and a better structural material (polysilicon) for increasing with an orientation-independent Young's modulus. By taking advantage of these features, a tactical-grade ring microgyroscope with projected random walk as small as 0.05 $^{o}/\sqrt{h}$ can be potentially realized, providing orders of magnitude improvement in performance. British Aerospace Systems and Equipment, in collaboration with Sumitomo Precision Products, has also developed a micromachined single-crystalline silicon ring gyroscope

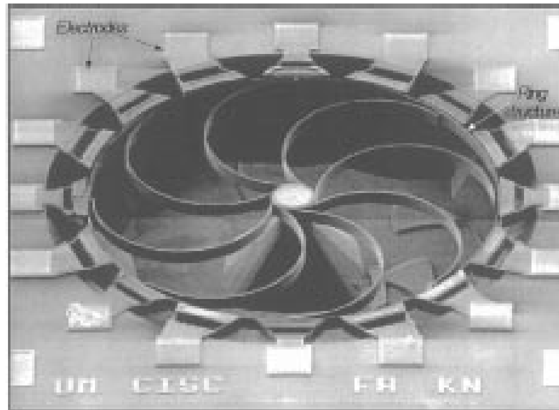

Figure3.22: SEM view of a PRG [3.86]. The polysilicon ring is 1mm in diameter, 3 μm wide, and 35 μm tall.

with a reported root-mean-square noise floor of 0.15° /s in a 30 Hz bandwidth and an in-run drift of approximately 0.05° /s [3.88]. This device was fabricated through deep dry etching of a 100- μm-thick silicon wafer, which was then anodically bonded to a glass support wafer. Levitated micromachined spinning-disc gyroscopes have also been investigated [3.89], [3.90]. The concept was based on a rotor disc, levitated using electromagnetic or electrostatic means and spun at a very high rate by means of a motor to produce angular momentum. With additional electrostatic fields, the rotor can be held in equilibrium even if the sensor is tilted or inverted. It is predicted that spinning microgyroscopes can yield a lower drift than a vibrating structure gyroscope [3.90]. The performance of these devices is yet to be demonstrated.

2.8 Important Applications Of MEMS Gyroscope:

Comb based vibratory gyroscopes are projected to become a potential alternative to expensive and bulky conventional inertial sensors in the near future. High-performance gyroscopic sensors including precision fiber-optic gyroscopes, ring laser gyroscopes, and conventional rotating wheel gyroscopes are too expensive and to o large for use in most emerging applications. With micromachining processes allowing mass-production of micro-mechanical systems on a chip together with their control and signal conditioning electronics, low-cost and micro-sized gyroscopes will provide high accuracy rotation measurements. Moreover, advances in the fabrication techniques allow the detection and control electronics to be integrated on the same silicon chip together with the mechanical sensor elements. Thus, miniaturization of vibratory gyroscopes with innovative micro-fabrication processes and gyroscope designs is expected to become an attractive solution to current inertial sensing market needs, as well as open new market opportunities.

With their dramatically reduced cost, size, and weight, MEMS gyroscopes potentially have a wide application spectrum in the aerospace industry, military, automotive industry and consumer electronics market. The automotive industry applications are diverse, including high performance navigation and guidance systems, ride stabilization, advanced automotive safety systems like yaw and tilt control, roll-over detection and prevention, and next generation airbag and anti-lo ck brake systems. A very wide range of consumer electronics applications include image stabilization in video cameras, virtual reality products, inertial pointing devices, and computer gaming industry. Miniaturization of Gyroscopes also enables higher-end applications including micro-satellites, micro-robotics, and even implantable devices to cure vestibular disorders.

Among the presently uses of MEMS or those under study are;

Inertial navigation system: includes gyroscope and accelerometer with high precision, high performance, shock absorbing capabilities.

Biomedical: includes various research projects to develop bio-chips for detection of hazardous chemicals, biological agents and microsystems for high- throughput drug screening and selection.

Communication: high frequency circuits based on RF-MEMS technology giving considerable benefits in the field of communication, in addition to this Analog and Mix Signal (AMS) integrated systems are the application areas in telecommunication.

Electronics: MEMS devices are finding application in high frequency electronics, currently the main areas of interest are MEMS switches capable of giving 100 billion switching cycles, high quality MEMS resonators and mechanically tuned capacitors.

Microfluidic systems: cheap disposable microfluidic devices such as blood pressure sensor are rugged enough for application outside research laboratories.

Aviation industry: the aviation industry is experimenting with “active surfaces” based on MEMS technology which maintaining aerodynamic drag on aircraft, same technology being applied to impeller blades in compressor or to the internal surface of transmission pipelines.

Robotics: development of smart products, augmenting the computational ability of microelectronics with precision and control capabilities of micro actuators, enable to use it in robotics surgery.

Optical switching devices: that can switch light signals over different paths at 20 nanoseconds switching speed.

Sensing devices: embedded sensors for buildings, sensor driven heating and cooling systems are some examples of sensing devices.

The comb drive finds numerous other applications in latest fields of technology like Optical shutter for tunable lasers [3.91], Microelectromechanical Filters for Signal

Defense	Medical	Electronics	Communications	Automotive
Munitions guidance	Blood pressure sensor	Disk drive heads	Optical or Photonic switches and cross-connects in broadband networks	Internal navigation sensors
Surveillance	Muscle stimulators and drug delivery systems	Inkjet printer heads	RF relays, switches, and filters	Air conditioning compressor sensor
Arming systems	Implanted pressure sensors	Projection Screen Televisions	Projection displays in portable communications devices and instrumentation	Brake force sensors and suspension control accelerometers
Embedded sensors	Prosthetics	Earthquake sensors	Voltage controlled oscillators (VCOs)	Fuel level and vapour pressure sensors
Data storage	Miniature analytical instruments	Avionics pressure sensors	Splitters and couplers	Airbag sensors
Aircraft control	Pacemakers	Mass data storage systems	Tunable lasers	“Intelligent” tires

Table 2

Processing [3.92], 1-D and 2-D resonant microscanners for display and imaging applications [3.93,94], multiprobe scanners for Scanning probe microscopy (SPM) [3.95], micromechanical resonant electrostatic field sensor [3.96], for calculating Fluid Effects in Vibrating Micromachined Structures [3.97], microactuator in HD Drive suspension [3.98], Stepped actuator for microtweezer application [3.99], Electrostatic Microactuator System for Application in High-Speed Jet flows [3.100].

Today high volume MEMS can be found in diverse systems ranging across defense, medical, electronics, communication and automotive applications, Table 2 [3.101], they can function individually or as a part of an array to sense the need for and then control and trigger actions or events.

DARPA (Defense advanced Research Project Agency, USA) conducted research on the market growth and concluded that the segments listed in Table3 outpace the collective MEMS market growth [3.102]

Technology Area	Typical Devices / Applications
Inertial Measurement	Accelerometers, Rate Sensors, Vibration Sensors
Microfluidics and Chemical Testing/Processing	Gene Chip, Lab on Chip, Chemical Sensors, Flow Controllers, Micronozzles, Microvalves
Optical MEMS (MOEMS)	Displays, Optical Switches, Adaptive Optics
Pressure Measurement	Pressure Sensors for Automotive, Medical, and Industrial Applications
RF Technology	RF switches, Filters, Capacitors, Inductors, Antennas, Phase Shifters, Scanned Apertures
Other	Actuators, Microrelays, Humidity Sensors, Data Storage, Strain Sensors, Microsatellite Components

Table 3

The work on the applications of MEMS stated above is in progress almost all world ranking universities of the world. Pakistan is trying to be the part of this emerging technology by setting up the facilities for the designing, modeling and testing of MEMS as this technology will soon capture the industry due to

its low cost and small size. PhD level work on this field has already been initiated in several universities of Pakistan proving its importance however lack of in-house fabrication facilities because of advance, highly sophisticated and very expensive equipment. Cost of each equipment may start from some hundred of thousand and can go to some tens of million dollars.

At this stage we can't afford any kind of expensive setup so we have successfully modeled a MEMS Comb-Drive with Bond Graph technique which is an emerging and reliable method to model different kind of multi-domain system with domain independency.

The most needed and active research field in the world of MEMS is Gyroscope. We have modeled a Comb Drive which can be extended into Gyro and other actuators and sensors etc.

4

Modeling methodologies for coupled field domain: The Bond Graph Method

The purpose of this chapter is to present the general methodologies used for the analysis and synthesis of systems covering several energy fields. When dealing with micro electromechanical *systems (MEMS),* the interaction between the mechanical, electrical, thermal, etc. domains becomes an essential ingredient in the functioning of the whole system as a unit. In micro-accelerometers, for instance, the movement of the inertial mass is usually detected either as a change in capacitance, or as a change in resistance. In both cases, the energy source is the mechanical acceleration field, while the readout is performed in the electrical domain. For high resolution measurements and for getting a better linearity of the response, a negative feedback loop is used to counteract the displacement from the zero position induced by acceleration action. This actuation is commonly done through electrostatic forces. In such a case there is an inverse energy path flow, from the electrical domain toward the mechanical one. Consequently, the analysis and design of such an accelerometer requires a broader, multidisciplinary view at the system level. A high-level perspective is needed, with unifying concepts, which allows analytical or/and numerical modeling of system dynamics based on coupled energy domains. In case of coupled mechanical and electrical domains, a common description is required for similar terms used in either domain. The common framework is

to use energy as a state variable of a system, together with the energy conservation principle. The discipline focusing on such unifying methodologies is called system dynamics[4.1]. It could be defined as the study of unified methods of analyzing and modeling multidisciplinary engineering systems. The main concern in this field is the operation of a complete system, rather than just the operation of the components. This "system viewpoint" is essential, because it forces a common language and symbols, abstracted away from any particular physical mechanisms. The fundamental processes underlying a system's dynamic behavior are *the storage, transmission and transformation of power and energy among system components and between a system and its surroundings.* Depending on this behavior, a classification scheme for physical components and their interconnections can be made in a systematic fashion. The basis for a unified modeling methodology to deal with multidisciplinary fields was put by the pioneering works of Firestone[4.2], dating back in 1933, Trent[4.3] and later on Paynter [4.4], in 1961. The key idea is that pairs of variables (constrained by the requirement that their product has the unit of power) are used throughout for describing the system dynamics. These variables are called either *through-* and across-variable, as in the *linear digraph formalism,* or *effort* and *flow* variable, as in *bond-graph method.* Examples of such power variables are branch currents and potentials for electrical circuits, or velocities and forces in the mechanical domain. Because power variables form inseparable couples (if the energy balance is to be taken automatically into account), one always deals with n-ports as basic system components, interconnected to define system's function. This description language allows models of electrical, mechanical, hydraulic, thermal, magnetic or any other nature, using only a rather small set of ideal elements. The dynamics of the entire system can be analyzed at a general, abstract level, independent of the physical domain where the energy processes take place. In some contexts, the transmission or processing of information is more important than the energy carrier components. Then the perspective in abstraction changes

and the direction (causality) in the information flow chain becomes more important than the energy inter-coupling mechanisms.

4.1 Introduction to Bond Graph

Bond graph is an explicit graphical tool for capturing the common energy structure of systems. It increases one's insight into systems behavior. In the vector form, they give concise description of complex systems. Moreover, the notations of causality provides a tool not only for formulation of system equations, but also for intuition based discussion of system behavior, viz. controllability, observability, fault diagnosis, etc.

In 1959, Prof. H.M.Paynter gave the revolutionary idea of portraying systems in terms of power bonds, connecting the elements of the physical system to the so called junction structures which were manifestations of the constraints. This power exchange portray of a system is called Bond Graph (some refer it as Bondgraph), which can be both power and information oriented. Later on, Bond Graph theory has been further developed by many researchers like Karnopp, Rosenberg, Thoma, Breedveld (1968, 1975, 1983, 1990), etc. who have worked on extending this modeling technique to power hydraulics, mechatronics, general thermodynamic systems and recently to electronics and non-energetic systems like economics and queuing theory. They developed it such that it could be used in practice (Thoma, 1975; Van Dixhoorn, 1982). By means of the formulation by Breedveld (1984, 1985) of a framework based on thermodynamics, bond-graph model description evolved to a systems theory.

By this approach, a physical system can be represented by symbols and lines, identifying the power flow paths. The lumped parameter elements of resistance, capacitance and inductance are interconnected in an energy conserving way by bonds and junctions resulting in a network structure. From

the pictorial representation of the bond graph, the derivation of system equations is so systematic that it can be algorithmized. The whole procedure of modeling and simulation of the system may be performed by some of the existing software
e.g., ENPORT, Camp-G, SYMBOLS, COSMO, LorSim

4.2 Foundations Of Bond Graph

Analogies between different systems were shown in the previous section: Different systems can be represented by the same set of differential equations. These analogies have a physical foundation: the underlying physical concepts are analogous, and consequently, the resulting differential equations are analogous. The physical concepts are based on energy and energy exchange. Behavior with respect to energy is domain independent. It is the same in all engineering disciplines, as an be concluded when comparing the RLC circuit with the damped mass spring system. This leads to identical bond graphs. It aspires to express general class physical systems through power interactions. The factors of power i.e., Effort and Flow, have different interpretations in different physical domains. Yet, power can always be used as a generalized co-ordinate to model coupled systems residing in several energy domains. One such system may be an electrical motor driving a hydraulic pump or an thermal engine connected with a muffler where the form of energy varies within the system. Power variables of bond graph may not be always realizable (viz. in bond graphs for economic systems); such factual power is encountered mostly in non-physical domains and pseudo bond graphs.

In the following table, effort and flow variables in some physical domains are listed.

Systems	Effort (e)	Flow (f)
Mechanical	Force (F)	Velocity (v)
	Torque (τ)	Angular velocity (ω)
Electrical	Voltage (V)	Current (i)
Hydraulic	Pressure (P)	Volume flow rate (dQ/dt)
Thermal	Temperature (T)	Entropy change rate (ds/dt)
	Pressure (P)	Volume change rate (dV/dt)
Chemical	Chemical potential (μ)	Mole flow rate (dN/dt)
	Enthalpy (h)	Mass flow rate (dm/dt)
Magnetic	Magneto-motive force (e_m)	Magnetic flux (ϕ)

4.3 Starting points

Before discussing the specific properties of bond graphs and the elementary physical concepts, we first recall the assumptions general for network like descriptions of physical systems, like electrical networks, mechanical or hydraulic diagrams:

- The conservation law of energy is applicable.
- . It is possible to use a *lumped approach*

This implies that it is possible to separate system properties from each other and to denote them distinctly, while the connections between these submodels are ideal. *Separate system properties* mean physical concepts and the *ideal connections* represent the energy flow, i.e. the bonds between the submodels. This *idealness* property of the connections means that in these connections no energy can be generated or dissipated. This is called *power continuity*. This structure of connections is a *conceptual structure*, which does *not* necessary have a size. This concept is called *reticulation* (Paynter, 1961) or *tearing* (Kron, 1963).

The system's submodels are *concepts*, idealized descriptions of physical phenomena, which are recognized as the dominating behavior in *components* (i.e. real–life, tangible system parts). This implies that a model of a concrete part is not necessary only *one* concept, but can consist of a set of interconnected concepts.

4.4 Energy Modeling and Bond Graphs

For a long time mechanical engineers have used the Lagrange or Hamiltonian equations to model mechanical systems i.e. the modeling is based on the total energy contained in a mechanical system. However the approach has two major drawbacks (I) If non conservative forces are present the Lagrange and Hamiltonian equations are no longer useful (II) The equations are based on the total energy of the complete system i.e. it is not possible to use the energy of subsystems and then connect these subsystems together in a modular fashion. Similar problems occur in other engineering fields if modeling is based on energy method.

To overcome these two deficiencies Henry Paynter invented in the early1960s the bond graph .Paynter by computing the time derivative of the energy and using the power P instead of the energy E for modeling both of the aforementioned difficulties vanish. In this new approach power continuity equations are formulated instead of energy conservation laws. It turns out that in any physical system the power balance is a local property i.e. the modeler can express power balance equations for each subsystem separately and then connect all the subsystems as long as it is made sure that the power is also balanced at all the interfaces between submodels.
This very same property also makes it possible to use power balance equations to describe dissipative systems Resistors simply become two-port elements where free energy drops out and decides to henceforth be called heat.

4.5 Bond Graph theory

As a bonus power in any physical system can be written as the product of two conjugate variables called the effort and the flow in bond graph terminology. In a bond graph energy flow from one point of a system to another is denoted by a harpoon a semi arrow.

The orientation of a bond, i.e. the direction of the half arrow, denotes the direction of positive power. An element with an incoming bond consumes power when the product of effort and flow is positive. For R, C and I-elements an incoming bond is the standard orientation. For sources the standard orientation is outgoing, because a source supplies power to the rest of the system. For the TF and GY-element the standard orientation is one incoming bond and one outgoing bond, since this reflects the natural flow of power. For the other bonds in a model, as much as possible an orientation from source to load is applied.

4.6 Bond Graph Standard Elements

In bond graphs, one needs to recognize only four groups of basic symbols, i.e., three basic one port passive elements, two basic active elements, two basic two port elements and two basic junctions. The basic variables are effort (e), flow (f), time integral of effort (P) and the time integral of flow (Q).

4.6.1 Basic 1-Port elements

A 1-port element is addressed through a single power port, and at the port a single pair of effort and flow variables exists. Ports are classified as passive ports and active ports.

The passive ports are idealized elements because they contain no sources of power. The inertia or inductor, compliance or capacitor, and resistor or dashpot are classified as passive elements.

4.6.1.1 R-Elements :

The 1-port resistor is an element in which the effort and flow variables at the single port are related by a static function. Usually, resistors dissipate energy. This must be true for simple electrical resistors, mechanical dampers or dashpots, porous plugs in fluid lines, and other analogous passive elements. The bond graph symbol for the resistive element is shown below.

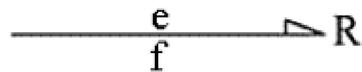

The half arrow pointing towards **R** means that the power i.e., product of F and V (or $e * f$) is positive and flowing into **R**, where e, represents effort or force, and f, represents flow or velocity. The constitutive relationship between e, f and R is given by :

$$e = R * f$$

$$\text{Power} = e * f = R * f2$$

4.6.1.2 C-Elements :

Consider a 1-port device in which a static constitutive relation exists between an effort and a displacement. Such a device stores and gives up energy without loss. In bond graph terminology, an element that relates effort to the generalized displacement (or time integral of flow) is called a one port capacitor. In the physical terms, a capacitor is an idealization of devices like springs, torsion bars, electrical capacitors, gravity tanks, and accumulators, etc.

The bondgraphic symbol, defining constitutive relation for a C-element are shown below.

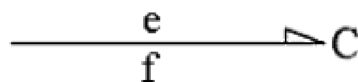

In a spring, the deformation (Q) and the effort (e) at any moment is given by,

$$Q = \int_{-\infty}^{t} f\,dt, \qquad e = K\int_{-\infty}^{t} f\,dt.$$

Here, flow is the cause and deformation (and hence effort) is the consequence. In a capacitor, the charge accumulated on the plates (Q) or voltage (e) is given by,

$$Q = \int_{-\infty}^{t} i\,dt, \qquad e = C^{-1}\int_{-\infty}^{t} i\,dt.$$

Here, the current is the cause and the total charge (and hence voltage) is the consequence.

4.6.1.3 I-Elements:

A second energy storing 1-port arises if the momentum, *P*, is related by a static constitutive law to the flow, *f*. Such an element is called an inertial element in bond graph terminology.

The inertial element is used to model inductance effects in electrical systems and mass or inertia effects in mechanical or fluid systems. The bond graph symbol for an inertial element is depicted in the figure given below.

If the mechanics of mass point is examined by considering the impulse-momentum equation, then we have;

$$P = \int_{-\infty}^{t} e\,dt, \qquad f = m^{-1}\int_{-\infty}^{t} e\,dt.$$

Here, effort is the cause and velocity (and hence momentum) is the consequence. Similarly the current in an inductor is given by;

$$i = L^{-1}\int_{-\infty}^{t} e\,dt.$$

4.6.1.4 Duality and dual domains:

As indicated in section 4.1, the two storage elements are each other's dual form. The role of effort and flow in a C–element and I–element are exchanged. Leaving one of the storage elements (and also one of the sources) out of the list of bond graph elements, to make this list as small as possible, can be useful from a mathematical viewpoint, but does not enhance the insight in physics.

Decomposing an I–element into a GY and a C, though, gives more insight. The only storage element now is the C–element. The flow is only a time derivative of a conserved quantity, and the effort determines the equilibrium. This implies that the physical domains are actually pairs of two dual domains: in mechanics, we have *potential* and *kinetic* domains for both rotation and translation), in electrical networks, we have the *electrical* and *magnetic* domains. However, in the thermodynamic domain, no such dual form exists (Breedveld, 1982). This is consistent with the fact that no thermal I–type storage exists (as a consequence of the second law of thermodynamics: in a thermally isolated system, the entropy never decreases).

4.6.1.5 Effort and Flow Sources :

The active ports are those, which give reaction to the source. For, example if we step on a rigid body, our feet reacts with a force or source. For this reason, sources are called active ports. Force is considered as an effort source and the surface of a rigid body gives a velocity source. They are represented as an half arrow pointing away from the source symbol. The effort source is represented by

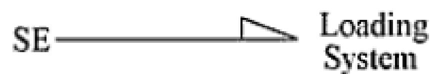

and the flow source is represented as shown below.

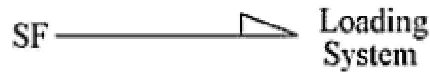

In electrical domain, an ideal shell would be represented as an effort source. Similarities can be drawn for source representations in other domains.

4.6.2 Basic 2-Port elements

There are only two kinds of two port elements, namely ``**Transformer**" and ``**Gyrator**". The bond graph symbols for these elements are **TF** and **GY**, respectively. As the name suggests, two bonds are attached to these elements.

4.6.2.1 The Transformer

The bondgraphic transformer can represent an ideal electrical transformer, a mass less lever, etc. The transformer does not create, store or destroy energy. It conserves power and transmits the factors of power with proper scaling as defined by the transformer modulus (discussed afterwards).

The meaning of a transformer may be better understood if we consider an example given here. In this example, a mass less ideal lever is considered. Standard and bondgraphic nomenclature of a lever are shown in the figure below. It is also assumed that the lever is rigid, which means a linear relationship can be established between power variables at both the ends of the lever.

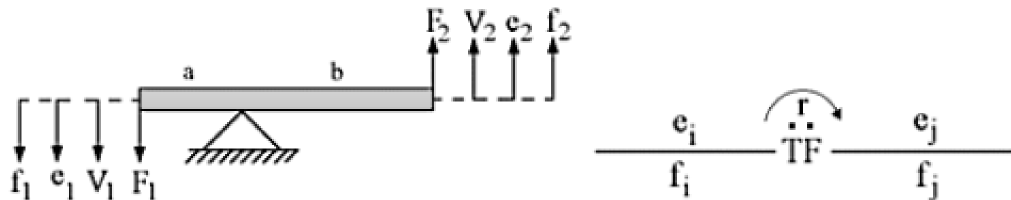

From the geometry, we have,

$V_2 = (b/a)\ V_1$

The power transmission implies

$F_2 = (a/b)\ F_1$, so that $V_2\ F_2 = V_1\ F_1$.

In bondgraphs, such a situation may be represented as shown in the above figure.

The '**r**' above the transformer denotes the modulus of the transformer, which may be a constant or any expression (like 'b/a'). The small arrow represents the sense in which this modulus is to be used.

$f_j = r\ f_i$, and $e_j = (1/r)\ e_i$.

Thus the following expression establishes the conservation of power,

$e_j\ f_j = e_i\ f_i$.

4.6.2.2 The Gyrator:

A transformer relates flow-to-flow and effort-to-effort. Conversely, a gyrator establishes relationship between flow to effort and effort to flow, again keeping the power on the ports same. The simplest gyrator is a mechanical gyroscope, shown in the figure below.

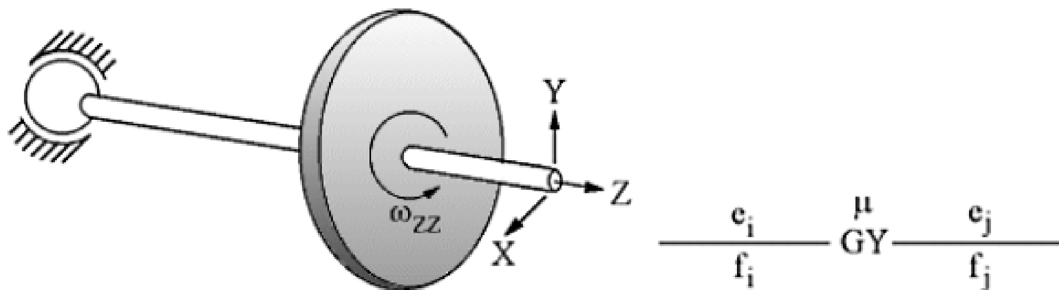

A vertical force creates additional motion in horizontal direction and to maintain a vertical motion, a horizontal force is needed. So the force is

transformed into flow and flow is transformed into force with some constant of proportionality. In this example, I_{zz} stands for moment of inertia about z axis. w_x , w_y and w_z stand for angular velocities about respective axes; T_x , T_y and T_z represent torque acting about the corresponding axis.

$$T_x = I_{zz}\, w_z w_y\, .$$

The power transmission implies

$$T_y = I_{zz}\, w_z\, w_x\, , \text{ so that } T_x w_x = T_y\, w_y\, .$$

Such relationship can be established by use of a **Gyrator** as shown in the figure above.

The μ above the gyrator denotes the gyrator modulus, where $\mu = I_{zz}\, w_z$. This modulus does not have a direction sense associated with it. This modulus is always defined from flow to effort.

$$e_j = \mu\, f_i\, ,\ e_i = \mu\, f_j\, .$$

Thus the following expression establishes conservation of power,

$$e_i\, f_i = e_j\, f_j\, .$$

In the electrical domain, an ideal DC motor is represented as an gyrator, where the output torque is proportional to the input current and the back emf is proportional to the motor angular speed. In general, gyrators are used in most of the cases where power from one energy domain is transferred to another, viz. electrical to rotational, electrical to magnetic, and hydraulic to rotational.

4.6.3 The 3-Port junction elements:

The name 3-port used for junctions is a misnomer. In fact, junctions can connect two or more bonds. There are only two kinds of junctions, the **1** and

the **0** junction. They conserve power and are reversible. They simply represent system topology and hence the underlying layer of junctions and two-port elements in a complete model (also termed the J unction Structure) is power conserving.

1-junctions have equality of flows and the efforts sum up to zero with the same power orientation. They are also designated by the letter **S** in some older literature. Such a junction represents a common mass point in a mechanical system, a series connection (with same current flowing in all elements) in an electrical network and a hydraulic pipeline representing flow continuity, etc. Two such junctions with four bonds are shown in the figure below.

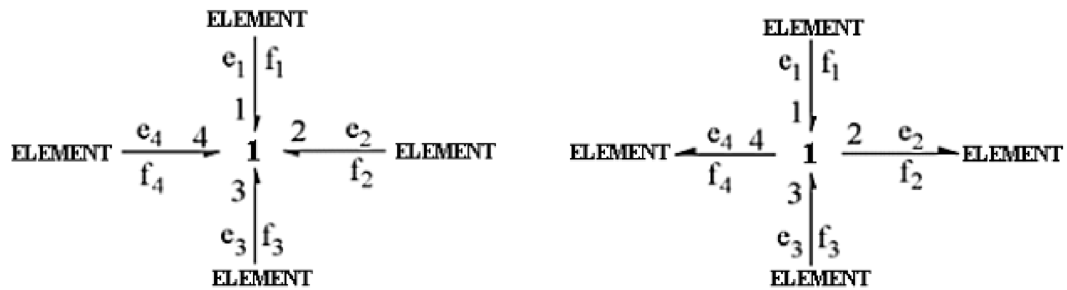

Using the inward power sign convention, the constitutive relation (for power conservation at the junctions) for the figure in the left may be written as follows;

$$e_1 f_1 + e_2 f_2 + e_3 f_3 + e_4 f_4 = 0.$$

As 1 junction is a flow equalizing junction,

$$f_1 = f_2 = f_3 = f_4 .$$

This leads to,

$$e_1 + e_2 + e_3 + e_4 = 0.$$

Now consider the above bond graph shown on the right. In this case, the constitutive relation becomes,

$$e_1 f_1 - e_2 f_2 + e_3 f_3 - e_4 f_4 = 0 ,$$

and,

$$f_1 = f_2 = f_3 = f_4 .$$

Thus,

$$e_1 - e_2 + e_3 - e_4 = 0.$$

So, a 1**-** junction is governed by the following rules:

The flows on the bonds attached to a 1-junction are equal and the algebraic sum of the efforts is zero.

The signs in the algebraic sum are determined by the half-arrow directions in a bond graph.

0-junctions have equality of efforts while the flows sum up to zero, if power orientations are taken positive toward the junction. The junction can also be designated by the letter **P**. This junction represents a mechanical series, electrical node point and hydraulic pressure distribution point or pascalian point.

4.7 Dual bond graphs

Above model's gyrator with m = 1 is a special case. Such a gyrator is called symplectic gyrator and actually denoted with SGY. As mentioned before, the choice which variable of the pair to take as effort is arbitrary and can be modified. A bond graph using i as effort and u as flow variable is the dualized variant of the standard electric bond graph and also capable to model electric circuits. In such a dual bond graph inductances change to capacitances, resistors change to conductors, 0- junction change to 1-junctions and everything vice versa. A symplectic gyrator is the tool to couple dualized variants and therefore partially dualized bond graphs are possible.

You may now conclude from the example in figure discussed above that a magnetic bond graph is nothing else than a dualized electric bond graph.

4.8 Intradomain transformers

Of course the usage of transformer elements is not limited to interdomain modeling. Transformers can as well model processes within a single domain. A simple voltage transformer or a mechanic lever are classical examples for this. Gyrators appear mostly in interdomain modeling.

4.9 Power directions on the bonds:

When one analyses a simple problem of mechanics, say, the problem of a single mass and spring system as shown in the figure below, one initially fixes a co-ordinate system.

One may take positive displacement, x, towards right and all its time derivatives are then taken positive towards right. The force acting on the mass may also be taken positive towards right. The system, however, in the course

of motion may attain such a state that when it is displaced towards the right, the force on the mass happens to be towards the left.

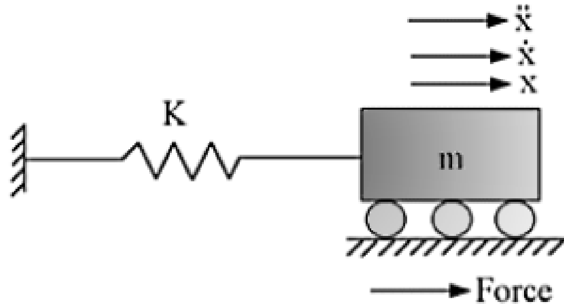

This phenomenon may be interpreted from the results obtained by solving the system of equation(s) when a positive value of displacement and a negative value of force are seen.

So, the initial fixing of positivity is arbitrary. However, further analysis is related to this fixation. In practice, bond graphs are drawn for general systems. Thus left and right, up and down, clockwise or counter-clockwise, etc., may not be of general relevance. One has to then create a view point which is general and any particular system interpretation should be easily derivable. This is done by assigning the bonds with **Power directions**. This may be as arbitrary as fixing co-ordinate systems in classical analysis. Say in a bond graph, the power is directed as shown in figure below, where

J : junction,

E : element,

half arrow : direction of power.

This assignment means, such variables are chosen for effort and flow, so that whenever both these variables acquire positive values, then the power goes from J to E. However, for mixed signs of the variables, the power direction is reversed.

As has been discussed earlier, the interpretation of the relative orientation of positive effort and flow may be subjective depending on whether the analysis

is carried out from the stand point of J or E. For instance, we can say the downward motion is positive for a particular mass and the upward motion is positive for another mass according to our co-ordinate system; but for a spring, upward and downward motion do not convey any meaning. In such cases, either the compression or the tension of the spring must be identified as a coordinate.

4.10 Systematic procedure to derive a bond–graph model

To generate a bond–graph model starting from an *ideal–physical model*, a *systematic method* exist, which we will present here as a procedure. This procedure consists roughly of the identification of the domains and basic elements, the generation of the connection structure (called the *junction structure*), the placement of the elements, and possibly simplifying the graph. The procedure is different for the mechanical domain compared to the other domains. These differences are indicated between parentheses. The reason is that elements need to be connected to *difference variables* or *across variables*. The efforts in the non–mechanical domains and the velocities (flows) in the mechanical domains are the across variables we need.

Step 1 and 2 concern the identification of the domains and elements.

1. Determine which physical domains exist in the system and identify all basic elements like C, I,R, Se, Sf, TF and GY. Give every element a unique name to distinguish them from each other.

2. Indicate in the ideal–physical model per domain a reference effort (reference velocity with positive direction for the mechanical domains).
Note that only the references in the mechanical domains have a direction.

Steps 3 through 6 describe the generation of the connection structure (called the *junction structure*).

3. Identify all *other* efforts (mechanical domains: velocities) and give them unique names.

4. Draw these efforts (mechanical: velocities), and *not* the references, graphically by 0–junctions (mechanical: 1–junctions). Keep if possible, the same layout as the IPM.

5. Identify all effort differences (mechanical: velocity (= flow) differences) needed to connect the ports of all elements enumerated in step 1 to the junction structure.

Give these differences a unique name, preferably showing the difference nature. The difference between e1 and e2 can be indicated by e12.

6. Construct the effort differences using a 1–junction (mechanical: flow differences with a 0–junction) according to Figure below and draw them as such in the graph.

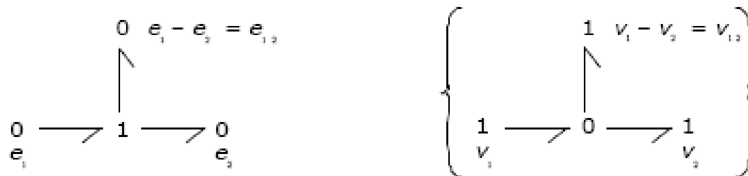

Construction of effort differences (velocity differences)

The junction structure is now ready and the elements can be connected.

7. Connect the port of all elements found at step 1 with the 0–junctions of the corresponding efforts or effort differences (mechanical: 1–junctions of the corresponding flows or flow differences).

8. Simplify the resulting graph by applying the following simplification rules (Figure 18):

- A junction between two bonds can be left out, if the bonds have a 'through' power direction (one bond incoming, the other outgoing).
- A bond between two the same junctions can be left out, and the junctions can join into one junction.
- Two separately constructed identical effort or flow differences can join into one effort or flow difference.

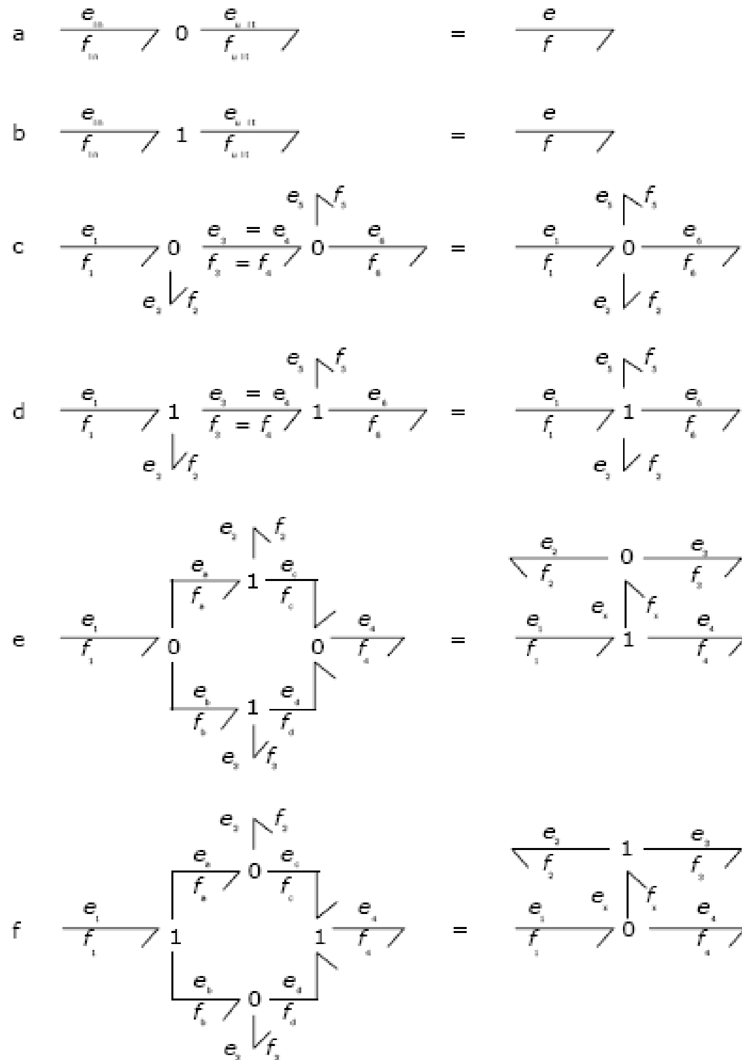

Figure 18: Simplification rules for the junction structure. (a, b) Elimination of a junction between bonds. (c, d) Contraction of two the same junctions. (e, f) Two separately constructed identical differences fuse to one difference.

4.11 Causal analysis:

Causal analysis is the determination of the signal direction of the bonds. The energetic connection (bond) is now interpreted as a bi-directional signal flow. The result is a *causal bond graph*, which can be seen as a compact block diagram. Causal analysis is in general completely covered by modeling and simulation software packages that support bond graphs like Enport (Rosenberg, 1974), MS1
(Lorenz, 1997), CAMP (Granda, 1985) and 20- SIM (Broenink, 1990, 1995, 1997, 1999b; Broenink and Kleijn, 1999). Therefore, in practice, causal analysis need not be done by hand. Besides derivation of equations, causal analysis can give insight in the correctness and competency of the model. This last reason especially motivates the discussion of causal analysis in this chapter.

Dependent on the kind of equations of the elements, the element ports can impose constraints on the connected bonds. There are four different constraints, which will be treated before a systematic procedure for causal analysis of bond graphs is discussed.

4.11.1 Causal Constraints:

4.11.2 Fixed causality:

Fixed causality is the case, when the equations only allow one of the two port variables to be the outgoing variable. This occurs at sources: an effort source (Se) has by definition always its effort variable as signal output, and has the

causal stroke outwards. This causality is called *effort-out causality* or *effort causality*. A flow source (Sf) clearly has a *flow-out causality* or *flow causality*.

Another situation where fixed causality occurs is at nonlinear elements, where the equations for that port cannot be inverted (for example, division by zero). This is possible at R, GY, TF, C and I elements. Thus, there are two reasons to impose a fixed causality:

1. There is no relation between the port variables.

2. The equations are not invertable ('singular').

4.11.3 Constrained causality:

At TF, GY, 0– and 1–junction, relations exist between the causalities of the different ports of the element. These relations are *causal constraints*, since the causality of a particular port imposes the causality of the other ports. At a TF, one of the ports has effort-out causality and the other has flow out causality. At a GY, both ports have either effort-out causality or flow-out causality. At a 0–junction, where all efforts are the same, *exactly one* bond must bring in the effort. This implies that 0–junctions always have exactly one causal stroke at the side of the junction. The causal condition at a 1–junction is the dual form of the 0-junction. All flows are equal, thus *exactly one* bond will bring in the flow, implying that *exactly one* bond has the causal stroke away from the 1–junction.

4.11.4 Preferred causality:

At the storage elements, the causality determines whether an integration or differentiation with respect to time will be the case. Integration has preference above a differentiation. At the integrating form, an initial condition must be specified. Besides, integration with respect to time is a process, which can be

realized physically. Numerical differentiation is not physically realizable, since information at future time points is needed. Another drawback of differentiation occurs when the input contains a step function: the output will then become infinite. Therefore, integrating causality is seen as the *preferred causality*. This implies that a C–element has effort-out causality and an I–element has flow-out causality at its preference.

4.11.5 Indifferent causality:

Indifferent causality is used, when there are no causal constraints! At a linear R, it does not matter which of the port variables is the output. Consider an electrical resistor. Imposing a current (flow) yields:

$$V \doteq i\,R$$

It is also possible to impose a voltage (effort) on the linear resistor:

$$i \doteq V / R$$

There is no difference choosing the current as incoming variable and the voltage as outgoing variable, or the other way around.

4.11.6 Causal analysis procedure:

The procedure for assigning causality on a bond graph starts with those elements that have the strongest causality constraint namely fixed causality (deviation of the causality condition cannot be granted by rewriting the equations, since rewriting is not possible). Via the bonds (i.e. connections) in the graph, one causality assignment can cause other causalities to be assigned. This effect is called *causality propagation*: after one assignment, the causality propagates through the bond graph due to the causal constraints.

The causality assignment algorithm is as follows:

1a. Chose a fixed causality of a *source* element, assign its causality, and propagate this assignment through the graph using the causal constraints. Go on until all sources have their causalities assigned.

1b. Chose a not yet causal port with *fixed* causality (non-invertable equations), assign its causality, and propagate this assignment through the graph using the causal constraints. Go on until all ports with fixed causality have their causalities assigned.

2. Chose a not yet causal port with *preferred* causality (storage elements), assign its causality, and propagate this assignment through the graph using the causal constraints. Go on until all ports with preferred causality have their causalities assigned.

3. Chose a not yet causal port with *indifferent* causality, assign its causality, and propagate this assignment through the graph using the causal constraints. Go on until all ports with indifferent causality have their causalities assigned.

Often, the bond graph is completely causal after step 2, without any causal conflict (all causal conditions are satisfied). If this is *not* the case, then the moment in the procedure where a conflict occurs or where the graph becomes completely causal, can give insight in the correctness and competence of the model. Before discussing these issues, first an example will be treated.

4.11.7 Model insight via causal analysis

We discuss here those situations whereby conflicts occur in the causal analysis procedure or when step 3 of the algorithm appears to be necessary. The place in procedure where a conflict appears or the bond graph becomes

completely causally augmented, can give insight in the correctness of the model.

Often, the bond graph is completely causal after *step 2*, *without* any causal conflict (all causal conditions are satisfied). Each storage element represents a state variable, and the set of equations is an explicit set of ordinary differential equations (not necessarily linear or time invariant).

When the bond graph is completely causal after *step 1a*, the model does *not* have any dynamics. The behaviour of all variables now is determined by the fixed causalities of the sources. Arises a causal conflict at *step 1a* or at *step 1b*, then the problem is ill posed. The model must be changed, by adding some elements. An example of a causal conflict at *step 1a* is two effort sources connected to one 0-junction. Both sources 'want' to determine the one effort variable.

At a conflict at *step 1b*, a possible adjustment is changing the equations of the fixed–causality element such that these equations become *invertable*, and thus the *fixed*ness of the constraint disappears. An example is a diode or a valve having zero current resp. flow while blocking. Allowing a small resistance during blocking, the equations become invertable.

When a conflict arises at *step 2*, a storage element receives a *non*-–preferred causality. This means that this storage element does *not* represent a *state variable*. The initial value of this storage element cannot be chosen freely. Such a storage element often is called a *dependent storage element*. This indicates that a storage element was *not* taken into account during modeling, which should be there from physical systems viewpoint. It can be deliberately omitted, or it might be forgotten. At the hoisting device example, the load of the hoist (I—element) is such a dependent storage element.

Elasticity in the cable was *not* modeled. If it had been modeled, a C-storage element connected to a 0—junction between the cable drum and load would appear.

When *step 3* of the causality algorithm is necessary, a so—called *algebraic loop* is present in the graph. This loop causes the resulting set differential equations to be *implicit*. Often this is an indication that a storage element was not modeled, which should be there from a physical systems viewpoint.

In general, different ways to handle the causal conflicts arising at step 2 or step 3 are possible:

1. Add elements.
For example, you can withdraw the decision to neglect certain elements. The added elements can be parasitic, for example, to add elasticity (C—element) in a mechanical connection, which was modeled as rigid. Additionally adding a damping element (R) reduces the simulation time considerably, which is being advised.

2. Change the bond graph such that the conflict disappears.

For a step 2 conflict, the dependent storage element is taken together with an independent storage element, having integral causality. For a step 3 conflict, sometimes resistive elements can be taken together to eliminate the conflict. This can be performed via transformations in the graph. The complexity of this operation depends on the size and kind of submodels along the route between the storage elements or resistors under concern.

3. The bond graph is *not* changed and during simulation, a special (implicit) integration routine is needed. The implicit equations are solved by means of the iteration schemes present in the implicit integration methods. In 20-SIM, only the BDF method can handle this situation. Also, the loop can be '*cut*' by

adding a one-time step delay, which is a rather pragmatic solution, but can be useful when no implicit integration methods are available. The accuracy might get too low. Note that the amplification of all elements in the loop must be smaller than one to obtain a stable solution.

Algebraic loops and loops between a dependent and an independent storage element are called *zero–order causal paths* (*ZCPs*). Besides these two kinds, there are three other kinds, having an increasing complexity and resulting in more complex equations. These occur for instance in rigid–body mechanical systems (van Dijk and Breedveld, 1991).

By interpreting the result of causal analysis, several properties of the model can be recognized, which could *otherwise* only be done after deriving equations.

4.12 State Equations:

4.12.1 Order Of Set Of State Equations:

The causal analysis also gives information on the order of the set equations. The number of *initial conditions* equals the number of storage elements with integral causality, which was also the preference during causality assignment. This number is called the *order of the system.*

The *order of the set state equations* is smaller than or equal to the order of the system, because storage elements can depend on each other. These kind of dependent storage elements each have their own initial value, but they together represent *one* state variable. Their input signals are equal, or have a factor in between.

4.12.2 Matrix form (linear systems):

If the system is linear, we can write the resulting set of state equations in the standard form, namely,

$$dx/dt = Ax + Bu$$

where **A** is the *system matrix*, and **B** is the *input matrix*. The order of the system is the dimension of the square matrix **A** and the order of the set of state equations is the *rank* of **A**.

When dependent states or algebraic loops are present, the matrix description is as follows:

$$E\, dx/dt = Ax + Bu$$

where **E** is a square matrix of size equal to the amount of storage elements plus the amount of algebraic loops. For each differential storage element and for each algebraic loop, **E** contains one row of zeros. The state vector **x** is extended with the algebraic loop variables, to enable implicit integration methods to solve these kinds of systems. The hoisting device gives such a set of equations.

4.12.3 Generation of equations

A causal bond graph contains all information to derive the set of state equations. It is either a set of *ordinary first–order differential equations, ODEs*, when the model is explicit (*no* causal conflicts), or a set of *differential and algebraic equations, DAE*s, when the model is implicit (a causal conflict in step 2 of the procedure or step 3 is necessary, cf. section 6.2).

The procedure to derive the equations is covered by bond–graph software like Enport (Rosenberg, 1974), MS1 (Lorenz, 1997), CAMP (Granda, 1985) and

20-SIM (Broenink, 1990, 1995, 1997, 1999b; Broenink and Kleijn, 1999). Therefore, in practice, generation of equations need not be done by hand.

However, we *do* discuss the generation of equations on the one hand to be complete and on the other hand to indicate what exactly has to be done.

We use the following procedure to generate equations:

1. We first write the *set of mixed differential and algebraic equations*. These are the constitutive relations of all elements in computational form, or *causal form*. This comprises of 2*n* equations of a bond graph having *n* bonds. *n* equations compute an effort and *n* equations compute a flow, or derivatives of them.

2. We then eliminate the algebraic equations. We can organize this elimination process by first eliminate the identities coming from the sources and junctions. Thereafter, we substitute the multiplications with a parameter, stemming from resistors and transducers (TF, GY). At last, we substitute the summation equations of the junctions into the differential equations of the storage elements. Within this process, it is efficient to *first* mark the state variables. In principle, the state variables are the contents of the storage elements (*p* or *q* type variables). However, if we write the constitutive relations of storage elements as one differential equation, we can also use the *efforts* at C-elements and *flows* at I-elements.

If we are going to generate the equations by hand, we can take the first elimination step into account while formulating the equations by, at the sources, directly use the signal function at the bond.

Furthermore, we can write the variable determining the junction along all bonds connected to that junction. The *variable determining the junction* is that variable, which gets assigned to bond variables of all the other bonds

connected to that junction via the identities of the junction equations. At a 0–junction, this is the effort of the only bond with its causal stroke *towards* the 0-junction. At a 1– junction, this is the flow of the only bond with its causal stroke *away from* the 1-junction.

In case of dependent storage elements, we have to take care that the accompanying state variable gets
not eliminated. These are the so–called *semi state variables*. When we mark the state variables, including the semi state variables in this situation, on beforehand, we can prevent the wrong variable from being eliminated. In case of algebraic loops, implicit equations will be encountered. We choose one of the variables in these loops as *algebraic loop breaker* and that variable becomes a *semi state variable*. See also section 6.5. The equation consisting of the semi state variable of a storage element gets eliminated at the second elimination step: it is a multiplication. The semi state variable itself must *not* be substituted.

4.13 Simulation:

The resulting set of equations coming from a bond–graph model is called the *simulation model*. It consists of first–order ordinary differential equations (ODEs), possibly extended with algebraic constraint equations (DAEs). Hence, it can be simulated using standard numerical integration methods. However, because numerical integration is an *approximation* of the actual integration process, it is useful to check the simulation model on aspects significant for simulation. As a result, an appropriate integration method can be chosen: the computational work is minimal and the results stay within a specified error margin.

Since at causal analysis, one can decide whether or not to change the bond–graph model to obtain an explicit simulation model, it is useful to know about

the consequences for simulation of relevant characteristics of the simulation model. The following 4 aspects of simulation models are relevant for choosing an numerical integration method:

1. Presence of implicit equations.

Implicit models (DAEs) can only be simulated with *implicit* integration methods. The iteration procedure of the implicit integration method is also used to calculate the implicit model. Explicit models (ODEs) can be simulated with both explicit as implicit integration methods. Sometimes, implicit integration methods need more computation time than explicit integration methods.

During causal analysis, one can see whether a simulation model will be explicit or implicit.

2. Presence of discontinuities.

Integration methods with special provisions for events will perform best. If that is not available, variable step methods can be used. Multistep methods become less accurate, since they need information from the past, which is useless after a discontinuity. While constructing the model, presence of discontinuities can be marked.

3. Numerical stiffness.

S(t), the *stiffness ratio* , is a measure for the distance between real parts of eigenvalues. The time step is now determined by the stability instead of the accuracy (namely, eigenvalues are now used to determine the step size). When the high frequency parts are faded out, they do not influence the step size anymore. Hence, the step size can grow to limits determined by the lower frequencies.

4. Oscillatory parts.

When a model has *no* damping, it should not be simulated with a stiff method. Stiff methods perform badly for eigenvalues on the imaginary axis (i.e. no damping) of the complex eigenvalue plane.

Eigenvalues can be localized in a causal bond graph, especially when *all* elements are linear. There is a bond graph version of *Mason's Loop rule* to determine the transfer function from a bond graph (Brown, 1972). As a side effect, the eigenvalues can be calculated. We will not discuss the procedure to obtain eigenvalues from a causal bond graph by hand.

4.14 Review:

In this chapter, we have introduced bond graphs to model physical systems in a *domain independent* way. Only *macroscopic* systems are treated, thus *quantum effects* do *not* play a significant role.

Domain independence has its basics in the fact that *physical* concepts are analogous for the different physical domains. 6 different elementary concepts exist: storage of energy, dissipation, transduction to other domains, distribution, transport, input or output of energy.

Another starting point is that it is possible to write models as *directed graphs*: parts are interconnected by bonds, along which exchange of energy occurs. A bond represents the energy flow between the two connected submodels. This energy flow can be described as the product of 2 variables (effort and flow), letting a bond be conceived as a *bilateral signal* connection. During modeling, the first interpretation is used, while during analysis and equations generation the second interpretation is used.

Furthermore, we presented a method to systematically build a bond graph starting from an ideal physical model. Causal analysis gives, besides the computational direction of the signals at the bonds, also information about the correctness of the model. We presented methods to derive the causality of a bond graph. In addition, procedures to generate equations and block diagrams out of a causal bond graph are presented.

This chapter is only an introduction to bond graphs. Sometimes, procedures are just presented, without a deep motivation and possible alternatives. It was also *not* the incentive to elaborate on physical systems modeling. We did *not* discuss multiple connections (arrays of bonds written as one multibond) and multiport elements (to describe transducers), neither different causal analysis algorithms. Those different causality algorithms give slightly different sets of DAEs especially when applied to certain classes of models (for instance multibody systems with kinematics loops).

4.15 Advantages of bondgraphic modeling:

Bond graphs are a modeling tool like any other, but compared to equations bond graphs are less general, because there are certain intrinsic assumptions that the bondgraphic concept is based on:

- The systems can be described by a finite set of elements.
- The state of the system can be described by a finite set of continuous state variables.
- There is an energy function for the system and all its subparts that satisfies the first law of thermodynamics
- There are no relativistic effects and time is a global variable.
- The second law of thermodynamics holds.
- The exchange of power happens continuously.

These intrinsic assumptions limit the applicability to physical systems, but give bond graphs also their strength. Concerning the modeling of complex physical systems they find the right balance between specificity and generality.

The interdisciplinary concept of energy and power flows creates a semantic level for each bond graph, even by unawareness of the modeling domain. Thus strong beliefs in physics like the first rule of thermodynamics can always be verified in a bond graph, independent of its application.

This semantic level helps the modeler to avoid errors and to find an appropriate solution for his task. Modeling by equations is far more general and therefore leaves more room for mistakes or errors.

The usage of causal bonds helps to understand the computational side of the model and to foresee structural problems. Another advantage of bond graphs is the graphical way of modeling. Relations can be expressed more naturally by two dimensional drawings than in 1-dimensional code. Also the limitations of the screen (or drawing board) force the modeler to split his model into simple, understandable elements. “Spaghetti code”-like models are therefore avoided.

Compared to equations bond graphs are less general, because there are certain intrinsic assumptions that the bond graphic concept is based on:

• The systems can be described by a finite set of elements.
• The state of the system can be described by a finite set of continuous state variables.
• There are no relativistic effects and time is a global variable.
• The exchange of power happens continuously.

These intrinsic assumptions limit the applicability to physical systems, but give bond graphs also

- Their strength. Concerning the modeling of complex physical systems they find the right balance between specificity and generality.
- The interdisciplinary concept of energy and power flows creates a semantic level for each bond graph, even by unawareness of the modeling domain. Thus strong beliefs in physics like the first rule of thermodynamics can always be verified in a bond graph, independent of its application.
- The usage of causal bonds helps to understand the computational side of the model and to foresee structural problems.
- Another advantage of bond graphs is the graphical way of modeling.
- The most important feature of a bond graph is that it operates on energy rather than on individual signals. There by it is guaranteed that no component and no interface will ever generate or lose energy in an uncontrolled fashion.
- very important feature of bond graphs is that they are modular and hierarchical [Cellier 1992] This makes it possible to construct bond graphs of sub models and connect them topologically to more complex bond graph elements that can then be connected further in a hierarchical manner. Since the interface points between bond graph submodels can be restricted to be always 0 junctions, power continuity at the interface between submodels is automatically guaranteed.

4.16 Discussion of the energy-based formalisms:

The modern approaches to physical system modeling use energy-based method, in the same way that modem physics uses Hamiltonian or Lagrangian mechanics rather than Newtonian one, when it comes to more complex systems [4.5, 4.6]. The reason clearly results from the explorations made in the previous sections: the possibility of a systematic, unified treatment, which scales up from simple to very complex interactions, including nonlinear one.

The starting ideas for system modeling in this fashion is to enable the use of interconnected lumped elements. It should be noted that the number of elements in the model does not necessarily coincide with the number of identifiable physical parts in the system.

The primary advantages of discrete lumped element modeling are:

- well developed models already exists (circuit models, linear graphs, bond graph models). This means that the knowledge accumulated into one field is easily transported to any other. There are real "templates" for design and analysis.

- finite order of the differential equations describing the system

- the treatment of the intercoupling between domains is done uniformly, starting from a single scalar function (forces as spatial derivatives of potential energy), rather than defining local expressions for the interactions

- the resulting models have given a good fit with the experimental results in many cases

Of course, the simplifications made along the path brought disadvantages as well:

- restricted validity of the model (discrete elements are used to model a physical continuum, where the physical laws are rather in terms of partial differential equations). This means that the most lumped element models are generally accurate only for the relatively low-frequency range.

- there are structures in which the continuous nature of the medium plays a major role in determining system's behavior (e.g., SAW filters). In consequence, their structure is not well modelled by interconnecting primitive lumped elements blocks

Choosing whether a lumped-element representation is suitable or not depends than on the context. Verification with finite analysis simulations or experimental results is a required step. Nevertheless, the strong physical insight which results from such a modeling approach is an important benefit to be exploited in the design phase.

4.17 Conclusions:

Microelectronics and MEMS fields, even if both deal with systems at the microscale level, present different features which sometimes lead to different modeling methodologies. A short comparative list is given below:

Microelectronics

- few elementary structures
- complex system topologies and topographies
- huge number of interconnected simple electrical components
- electrical signal dominant

MEMS

- growing number of elementary structures
- generally simple topologies
- few components, but of high individual complexity
- different energy domains, with no dominance

As a result of these differences, MEMS modeling techniques should concentrate on an unified perspective over the representation of various systems, regard-less of the energy-domain to which they belong. The coupling between energy-domains becomes more and more important as the dimensions are scaled-down.

An energetic coupling modeling offers several formalisms. The main goal is to show that by applying the energetic modeling approach, based on the use

of complementary power variables, one bridges the gap between system modeling, analysis and design in both microelectronics and MEMS, and borrow successful techniques from one field to the other. For an electrical engineer, a Spice-like representation of a mechanical system can immediately give a qualitative/ quantitative insight over the functioning and the main control parameters. Efficient techniques for signal processing developed in the electrical domain can be mapped immediately to other domains, by just making a different correspondence between the electrical scheme representation and the physical field to be considered. Alternatively, borrowing the techniques from the mechanical domain related to Lagrangian/Hamiltonian characterization of constrained motions could prove very successful when applied in the electrical domain, especially in the case of nonlinear systems. Of course, the challenge remains to go smoothly between different levels of abstractions, where each level takes different types of details into account:

• information processing level - representation by means of block or state-flow diagrams, or directly as abstract mathematical equations (methods used in programming languages as Matlab/Simulink, Mathematica, Macsy-ma, etc.)

• network topology representations - like in Spice, MAST(SABER), or more recently, in VHDL-AMS and Modelica languages

• geometry level - used for instance when a finite element analysis is per-formed (Ansys, Nastran, etc.)

The purpose of this thesis is not to tackle these aspects, but rather to use the methodologies in a consistent manner for deriving qualitative or/and quantitative analytical models and compare them with numerical models and experimental results. The advantage of having an analytical model at hand is essential for a designer in MEMS field. Even if it is imperfect, a

qualitative analytical model can offer directions of improvements and explorations in a more direct manner than pure FEM analysis. The problem with numerical modeling is the huge dimension of the parameters exploration space. This high dimensionality of the problem often hides the essential aspects and control parameters - "one cannot see the forest because of the trees". This is mainly the role of an analytical model, even at the conceptual level. It reduces the number of essential parameters to a small number, and offers a prototype device in the design phase. The FEM analysis comes in a second step, when already the hints about the main degrees of freedom were already given by the analytical model. The numerical, detailed modeling, at the geometry level, has the role to confirm the conceptual model, and to refine it by taking into account second-order effects, or to perform optimizations in a reduced-order space

5

Mathematical Model of Comb Drive

Developing a bond graph model and thus state space of a comb drive actuator with large static displacement and continuous motion capability has always been a hub of research interests in micro domain.

There are many MEMS simulation tools available in the literature. Among them, MEMCAD (http://www.memcad.com) from Microcosm Technologies, Inc. is an integrated package for mask layout, fabrication process description, geometric modeling, electromechanical simulation, and results visualization. It incorporates custom tools for mask layout, and for capacitance calculation using a boundary element method (BEM) code (called FASTCAP). Standard commercial packages are used for geometric modeling (SDRC's IDEAS) and structural analysis (ABAQUS). It also has CoSolve-EM for self-consistent coupled-domain electromechanical analysis [5.1]. Some work based on MEMCAD has already been reported recently [5.2], [5.3]. Another commercially available package is IntelliCAD from IntelliSense Corporation (http://www.intellis.com), which includes both commercial and custom tools and databases [5.4]. IntelliSense software products are also directed at providing MEMS modeling and simulation capability. However, these commercial CAD systems applicable to MEMS are primarily aimed at simulating and fabrication processes and electromechanical behavior of a

given design. Parametric optimization of a design for specified requirements is very difficult to do but with the help of any search technique combined with Bond Graph this can be done easily. Basically the ability of Bond Graph of consideration of physical system rather than extensive mathematical modeling makes it the best choice where the system is already reduced to a lower order model.

Transient dynamic problems with very large numbers of degrees of freedom in microelectromechanical systems (MEMS) are nowadays solvable in a feasible computational time due to the tremendous improvement of computers. However, the continual and pressing demands for simulating a better dynamical responses of more complicated multiphysical MEMS systems have needed increasingly large and complex models, which consequently lead to much higher computational cost. In order to alleviate this difficulty, Bond Graph is one of the best solutions because of its model order reduction technique.

Model order reduction of linear large-scale dynamic systems is a rapidly developing area of mathematics [5.7]. The reduced-order modeling methods play an indispensable role by providing an efficient computational prototyping tool to replace a large-scale model with an approximate smaller model, which is still capable of capturing dynamical behavior and preserving essential properties of the original model.

5.1 Design of a Comb Drive:

Comb drive actuators consist of two interdigitated finger structures, where one comb is fixed and the other is connected to a suspension designed to comply in the direction of displacement and stiff in the orthogonal direction [5.8]. Applying a voltage difference between the comb structures will result in a

deflection of the movable comb structure by electrostatic forces, which varies directly with the square of the applied voltage.

Variations of driving forces and displacement of different comb drive designs with the applied voltage has already been modeled by a robust finite element method and solved within multi physics environment in a commercial finite element package ANSYS [5.9].

The authors in this paper introduce the implementation of BGM by constructing a Bond graph model to get the variation of electrostatic force and displacement of comb drive with voltage. The model acquired is directly solved and simulated on 20-SIM, commercially available BGM software. BGM provides an easy way to investigate the system behavior with the variation of different parameters directly, without changing the basic design of system. It is a special ability of BGM which enhances the robustness of parametric study of multi physics system with reliability and repeatability.

5.2 Mathematical Expressions

The driving principle of electrostatic Comb-Drive actuator is based on electrostatic characteristics [5.8]. When voltage is applied to the fixed electrode (or fingers) while the movable electrodes (or fingers) are potential grounded, a potential difference results across the electrodes and they become electrically charged. This action will induce a certain capacitance in the charged electrodes. Thus, an electrostatic force is generated causing a displacement in the x direction. The driving force F created in the Comb can be expressed as:

$$F = \partial U / \partial g = nt\varepsilon_o\varepsilon_r V^2 / 2g \qquad (I)$$

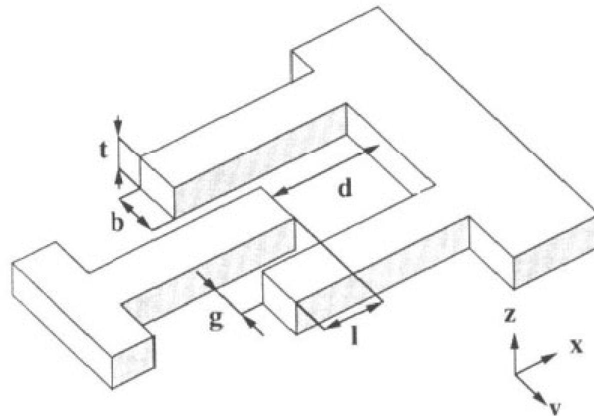

Fig. 1: *Design of the comb structure.*

where U is the energy associated with the applied electric potential V, ε_r is the relative permittivity of the dielectric material between the two electrodes, ε_o is the permittivity in the free space and equal to 8.85 pF/m, n is the number of the pairs of electrodes, t is the thickness of the electrodes and g is the gap between two fingers as in Fig 1.

This shows schematic details of one movable finger between two fixed fingers. All geometric dimensions used for the analytical calculations are indicated. The following numeric values were employed:

If the movable electrode is displaced following Hook's law, the reaction force F_s induced and the displacement can be calculated from the following equation:

$$F_s = K_x x \qquad \text{(II)}$$

where, K_x is the spring stiffness in the x-direction (i.e. actuation direction) and x is the displacement. Formulae used to drive the spring stiffness are shown in Jaecklin et al. [5.10] and Rob et al. [5.11]. In equilibrium position, the forces F_s and F have to be equal, where the displacement x can then be expressed

as a function of the driving voltage (V), the gap (g), the thickness (t), the number of electrodes (n) and the stiffness (K_x) as:

$$x = nt\varepsilon_o\varepsilon_r V^2 / 2K_x g \qquad \text{(III)}$$

Equation (III) shows that the relation between the actuator displacement and the applied driving voltage is not quite linear and as the applied voltage increases the displacement increases, normally this relation is known as the voltage-stroke relation of the Comb-Drive.

5.3 Mixed Domain Physical Structure

A microresonator fabricated in MUMPs was first described and analyzed by Tang [5.12] and is commonly used as for MEMS process characterization. The resonator components are made entirely from the homogeneous, conducting, 2 μm thick polysilicon film. The spacer gap of 2 μm above the substrate is set by this thickness. The movable microstructure (in the center of the micrograph) is fixed to the substrate at only two points. Simplified layout and schematic views of the device are shown in Fig. 2 and 3. The resonator is a mechanical mass-spring-damper system consisting of a central shuttle mass that is suspended by two folded beam

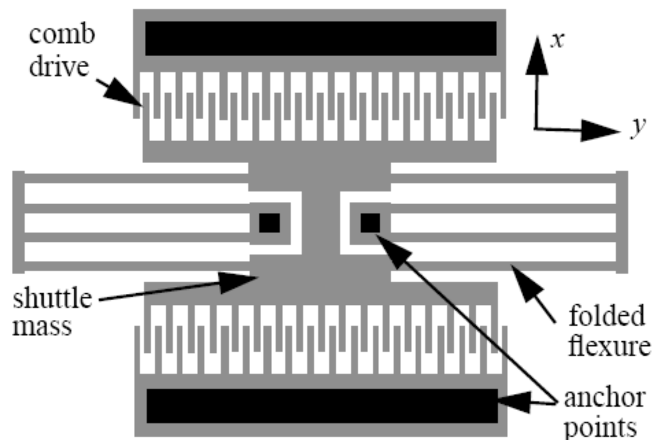

Fig. 2: *Shows the original comb-drive actuator with a folded-flexure suspension. This is a traditional actuator design with symmetry about x- and y-axis.[5.13]*

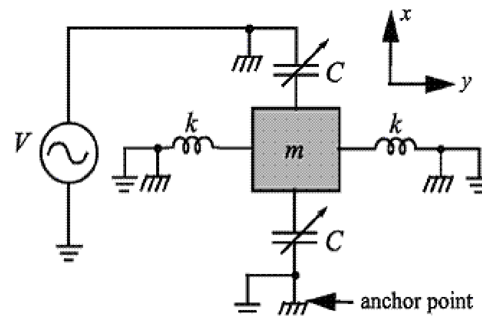

Fig. 3: *A Mixed domain structure view of comb drive with a voltage source V.[5.8]*

flexures. The folded flexure is a popular design choice because it is insensitive to buckling arising from residual stress in the polysilicon film. Instead of buckling, the beams expand outward to relieve the stress in the film. The resonator is driven in the preferred (*x*) direction by electrostatic actuators that are symmetrically placed on the sides of the shuttle. Each actuator, commonly called a 'comb drive, are made from a set of interdigitated comb fingers. When a voltage is applied across the comb fingers, an electrostatic force is generated which, to first order, does not depend on *x*. The suspension is designed to be compliant in the *x* direction of motion and to be stiff in the orthogonal direction (*y*) to keep the comb fingers aligned.

5.4 <u>Bond Graph Development</u>

A bond graph of system is constructed to relate the state variables of voltage and displacement. It can be further modified to relate other variables like gap, no of fingers, thickness, height and length of combs etc. which are not considered here.

So this simplest bond graph results a state space development to study frequency and time response through which a controller can be designed.

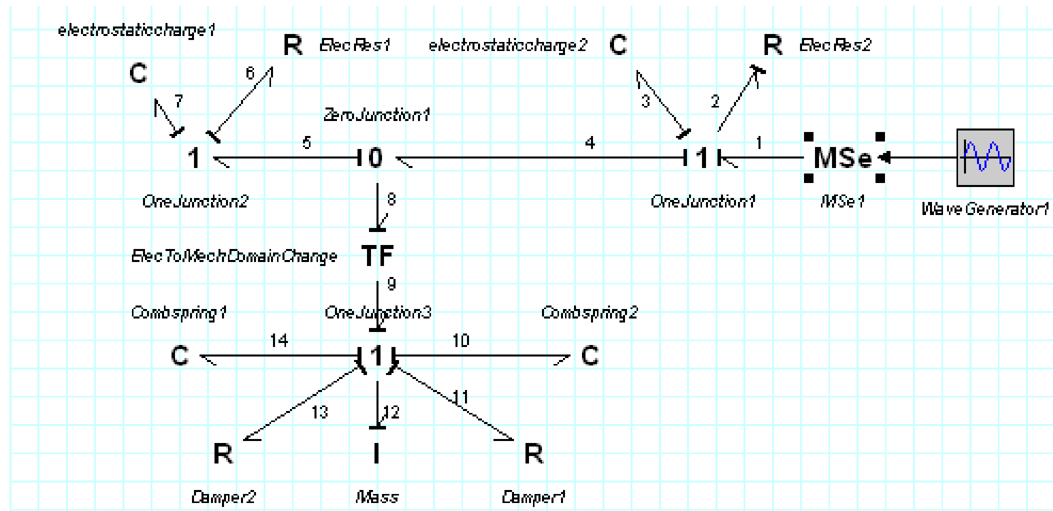

Fig. 4: *Bond Graph Model of electrostatic comb-drive.*

Here in our Bond Graph Model we have two clear domains which are electrical and mechanical. None of these has dominancy. In electrical domain we have taken a wave generator (Wave Generator1) to give alternate voltage signals to the system. This signal enters in the system through a modulated voltage source (MSe). Now system has taken AC voltage of 40 volt through MSe. Then we placed a serial connection element that is one junction through which a resistor (R) and a capacitor (C) are connected. Resistor represent sum of all electrical resistances of the electrical domain and capacitor represents all the capacitances of fixed electrodes of comb drive. Same one junction is placed on the other side for the representation of moving electrode. All elements are connected with each other through power ports. These two 1-juntion elements are then connected in series (represented as 0-juntion.) with each other.

The electrical circuit is then connected to mechanical domain through a transformer. We used transformer here because we need to convert electrical effort (Voltage) into mechanical effort.

In mechanical system mechanical damping, stiffness of flexible comb structure and proof mass are attached all together through a 1-junction. We

have only modeled a pair of electrodes as shown in structural description of the physical system.

The design is then successfully simulated and all results have been compared with mathematical and other software results of comb drive actuation.

5.5 State Space Formulation through Bond Graph Method:

5.5.1 State Variables

There are five energy storage devices in the system which implies five state variable in which only three are independent.

1 $\frac{d}{dt} q_3$

2 $\frac{d}{dt} q_7$

3 $\frac{d}{dt} x_{10}$

4 $\frac{d}{dt} x_{13}$

5 $\frac{d}{dt} p_{14}$

5.5.2 Consecutive equations

The are the constitutive equations of bond graph, through which a state space have been developed, for each element of different domain are as follows

5.5.3 Mechanical Domain

5.5.3.1 I-Junction

.$\frac{d}{dt}x_{10}=\frac{d}{dt}x13=V14=V12=V11+V9$

.$f9=f12+f10+f13+f11+\frac{d}{dt}P_{14}$

5.5.3.2 Capacitors

$v_3=1/c\ q3$ $v7=1/c7\ q7$

5.5.3.3 Spring

$F_{10}=k_{10}x_{10}$ $f_{13}=k_{13}x_{13}$

5.5.3.4 Mass

.$v_{14}=1/I_{14}\ p_{14}$

5.5.4 Electrical Domain

5.5.4.1 1-Junction

$i2=\frac{d}{dt}q_3=i_4=i_1$

$v_1=v_2=v_3=v_4$

5.5.4.2 O-Junction

.$v_4=v8=v5$

$i4=i5+i8$

5.5.4.3 1-Junction

$i5=i6=\frac{d}{dt}q7$

$.v5=v7+v6$

5.5.4.4 Transformer

$.f9=u(v8)$

$.i8=u(V9$

5.5.5 Equations of the system

$$\frac{d}{dt}q_{3=}-x_{13}/R_2*(1/C_{13}+1/R_{16}C_{13}-1/C_5-R_{10})+x_{10}(1/C_4R_2 - +R_{11}) - -(1/C_3-1/C_3R_2)Q_3/R_2+1/R_2R_6C_7*Q_7+V_1(t)*(1/R^2{}_2-1/R_2)+(R_{12}+R_{11})/I_{14}R_2*P_{14}$$

$$\frac{d}{dt}q_7=1/R_6C_7*Q_7-1/R_6C_{13}*Q_{13}$$

$$\frac{d}{dt}x_{10}=V_1(t)/R_{12}-1/C_3R_2*Q_3-1/C_{10}R_2*x_{10}-1/R_6C_7*Q_7-1/R_6C_{13}*x_{13}$$

$$\frac{d}{dt}x_{10}=x_{13}$$

$$\frac{d}{dt}p_{14}=V_1(t)/R_2-(1/C_{10}R_{12}+1/C_{10}+R_{11})X_{10}-1/C_3R_2*Q_3-(1/C_{13}+R_{10}-1/R_6C_{13})X_{13}$$

5.5.6 Developed State Space

Hence after solving these mathematical models we will get the state space as given below

$$\dot{X} = AX + BU$$

$\dot{X}$ =

$$\begin{bmatrix} -\frac{1}{\mathrm{C3R2}}+\frac{1}{\mathrm{C3}} & \frac{1}{\mathrm{R2R6C7}} & \frac{1}{\mathrm{R2(R2C4)}}+\frac{R11}{R2} & \frac{-1}{R6C13R2}+\frac{R10}{R2} & \frac{R12+R11}{R2I14} \\ 0 & \frac{1}{R6C7} & 0 & -\frac{1}{R6C13} & 0 \\ -\frac{1}{C3R2} & -\frac{1}{R6C7} & -\frac{1}{C10R2} & -\frac{1}{R6C13} & 0 \\ -\frac{1}{C3R2} & -\frac{1}{R6C7} & -\frac{1}{C10R2} & -\frac{1}{R6C13} & 0 \\ -\frac{1}{C3R2} & 0 & -\left(\frac{1}{C10R2}+\frac{1}{C10}+R11\right) & -\left(\frac{1}{C5}+R10+\frac{1}{R6C13}\right) & 0 \end{bmatrix} \begin{bmatrix} Q3 \\ Q7 \\ Q10 \\ Q13 \\ P14 \end{bmatrix}$$

$$+\begin{bmatrix} \left(\frac{1}{R12(R12)}-\frac{1}{R2}\right) \\ 0 \\ \frac{1}{R12} \\ \frac{1}{R12} \\ \frac{1}{R12} \end{bmatrix} V_1(t)$$

The design, modeling and simulation of a comb drive is basically an original work. I didn't find any paper on this application of Bond Graph yet.

6

Results and discussions

A Comb-Drive actuator is a basic actuation device of MEMS. The development of large-range, high speed electrostatic actuators have been possible since the emergence of latest fabrication techniques. However, this development required the optimization of several aspects of Comb-Drive. Here required a modern approach to physical system modeling by using energy-based method. The reason clearly results the requirement of a systematic, unified treatment, which scales up from simple to very complex interactions, including nonlinear one.

6.1 Bond Graph a Method of Choice:

The starting ideas for system modeling in this fashion is to enable the use of interconnected elements. It should be noted that the number of elements in the model does not necessarily coincide with the number of identifiable physical parts in the system.

The primary advantages of bond graph modeling are:

- well developed models already exists (circuit models, linear graphs, bond graph models). This means that the knowledge accumulated into one field is easily transported to any other. There are templates for design and analysis in this method.
- finite order of the differential equations describing the system
- the treatment of the intercoupling between domains is done uniformly, starting from a single scalar function (forces as spatial derivatives of potential energy), rather than defining local expressions for the interactions
- the resulting models have given a good fit with the experimental results in many cases

Of course, the simplifications made along the path brought disadvantages as well:

- restricted validity of the model (discrete elements are used to model a physical continuum, where the physical laws are rather in terms of partial differential equations). This means that the most mixed element models are generally accurate only for the relatively low-frequency range.
- there are structures in which the continuous nature of the medium plays a major role in determining system's behavior. In consequence, their structure is not well modelled by interconnecting primitive elements blocks

Choosing whether a bond graph representation is suitable or not was dependent of the context. Verification with finite analysis simulations or experimental results was the required step. Nevertheless, the strong physical insight which results from such a modeling approach is an important benefit to be exploited in the design phase.

Microelectronics and MEMS fields, even if both deal with systems at the microscale level, present different features which sometimes lead to different modeling methodologies. A short comparative list is given below:

Microelectronics

- few elementary structures
- complex system topologies and topographies
- huge number of interconnected simple electrical components
- electrical signal dominant

MEMS

- growing number of elementary structures
- generally simple topologies
- few components, but of high individual complexity
- different energy domains, with no dominance

As a result of these differences, MEMS modeling techniques should concentrate on an unified perspective over the representation of various systems, regard-less of the energy-domain to which they belong. The coupling between energy-domains becomes more and more important as the dimensions are scaled-down.

Energetic Coupling Modeling:

An energetic coupling modeling offers several formalisms. The main goal is to show that by applying the energetic modeling approach, based on the use of complementary power variables, one bridges the gap between system modeling, analysis and design in MEMS, and borrow successful techniques from one field to the other. For a mechanical engineer, a block diagram or flow signal flow like representation of an electrical system can immediately give a qualitative/ quantitative insight over the functioning and the main control parameters. Efficient techniques for signal processing developed in the electrical domain can be mapped immediately to other domains, by just making a different correspondence between the electrical scheme representation and the physical field to be considered. Alternatively, borrowing the techniques from the mechanical domain related to different characterization of constrained motions could prove very successful when

applied in the electrical domain, especially in the case of nonlinear systems. Of course, the challenge remains to go smoothly between different levels of abstractions, where each level takes different types of details into account:

• information processing level - representation by means of block or state-flow diagrams, or directly as abstract mathematical equations (methods used in programming languages as Matlab/Simulink, Mathematica, Macsy-ma, etc.)
• network topology representations - like in different ware of electrical domain, or more recently, in VHDL-AMS and Modelica languages
• geometry level - used for instance when a finite element analysis is per-formed (Ansys, Nastran, ProEngineer etc.)

The purpose of this thesis is not to tackle these aspects, but rather to use the methodologies in a consistent manner for deriving qualitative or/and quantitative analytical models and compare them with numerical models and experimental results. These kind of work can be lead to the optimized design of MEMS system. The advantage of having an analytical model at hand is essential for a designer in MEMS field. Even if it is not too perfect, but a qualitative analytical model can offer directions of improvements and explorations in a more direct manner than pure FEM analysis. The problem with numerical modeling is the huge dimension of the parameters exploration space. This high dimensionality of the problem often hides the essential aspects and control parameters - "one cannot see the forest because of the trees". This is mainly the role of an analytical model, even at the conceptual level. It reduces the number of essential parameters to a small number, and offers a prototype device in the design phase. The FEM analysis comes in a second step, when the hints about the main degrees of freedom were already given by the analytical model. The numerical, detailed modeling, at the geometry level, has the role to confirm the conceptual model, and to refine it by taking into account second-order effects, or to perform optimizations in a reduced-order space

6.2 Simulation through Bond Graph

Simulation work focuses on investigating the control parameters of lateral electrostatic comb-drive actuators. We used Bond Graph Method for this purpose. It is the very first time that bond graph method is applied on the comb drive simulation. Multi-physics approach and cross-domain reach of Bond Graph Method made the work easily implement able and its fast performance made the work comfortable. For the purpose of simulation firstly a bond graph model is developed. From this model the state space is extracted. State space equation were only required to make a mathematical model and not used in the simulation. the model developed Bond Graph Method is then given parameters and directly simulated on 20-SIM Then a computer software, 20-SIM utilizing the power of bond graph method is used to simulate the constructed robust comb drive model and solve its multi-physics interaction problem. Investigation of System Response was the study of variation of displacement of combs and electrostatic force against the driving voltage. The calculated comb displacement and the electrostatic force generated are known to be directly proportional to the square of the driving voltage.

6.3 20-SIM Results; Displacement and Electrostatic Force vs. Driving Voltage

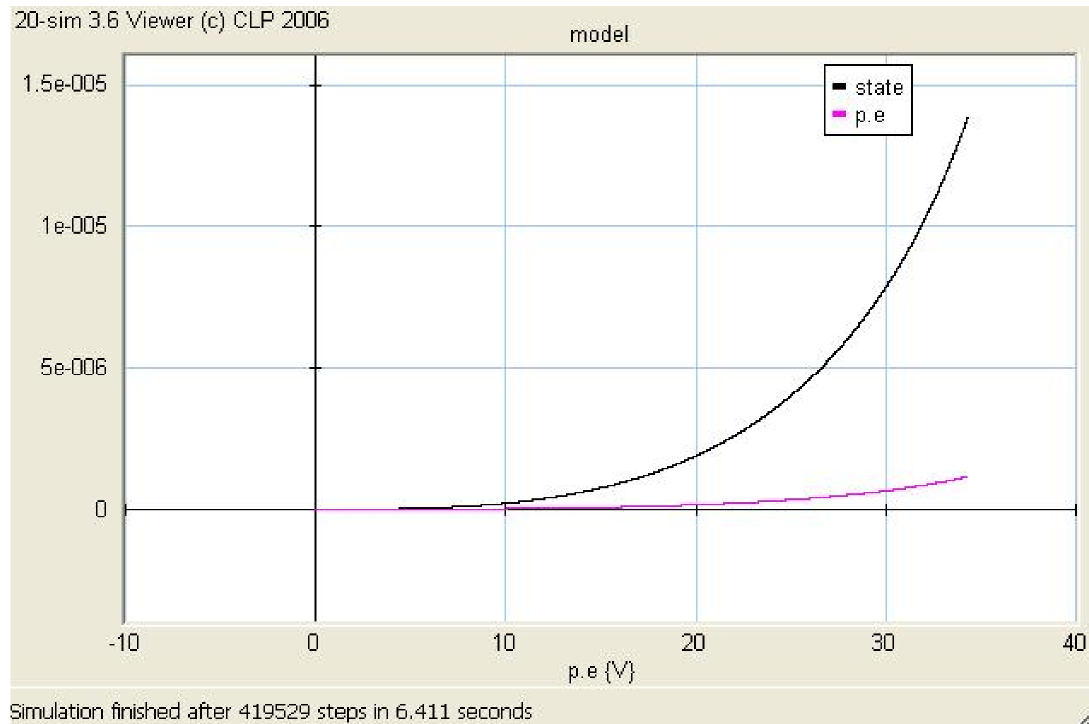

Fig1: Simulation of Comb Drive displacement and electrostatic force against driving voltage

In the current study, the Bond Graph Method is applied to the simple electrostatic Comb-Drive model, where the effects of this Comb's design parameters on the actuation performance are explored in figs. 1-9. Fig. 1 shows the variation of the Comb displacement and generated electrostatic force with the driving voltage of 40 volts. In this figure, the calculated Comb displacement and generated electrostatic force are shown to be linearly proportional to the squire of driving voltage for constant spring stiffness and other parameters.

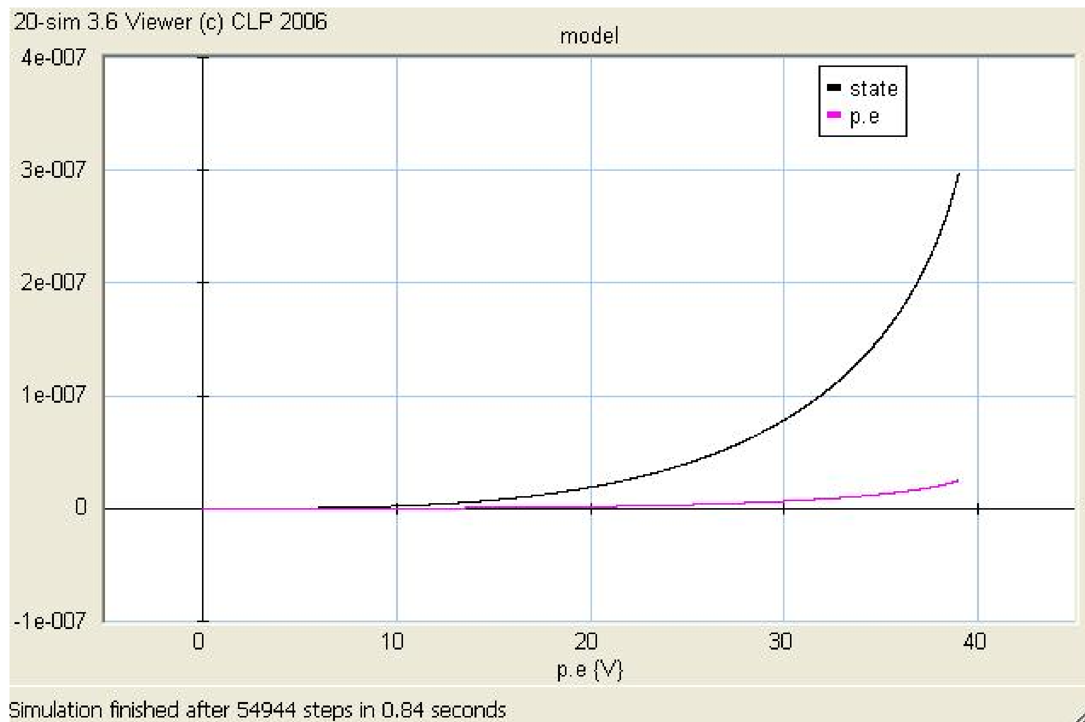

Fig2: Frequency Increased

The natural frequency for the free undamped vibration of a uniform cantilever is a function of its cross-sectional properties, length, and boundary conditions, and will effect the displacement. Trend of natural frequency with the displacement of combs is observed in Fig. 2. This dependence of displacement and force on natural frequency has been simulated at 40V and the results are displayed which shows that the displacement of the system decreases with the increase in natural frequency, as expected.

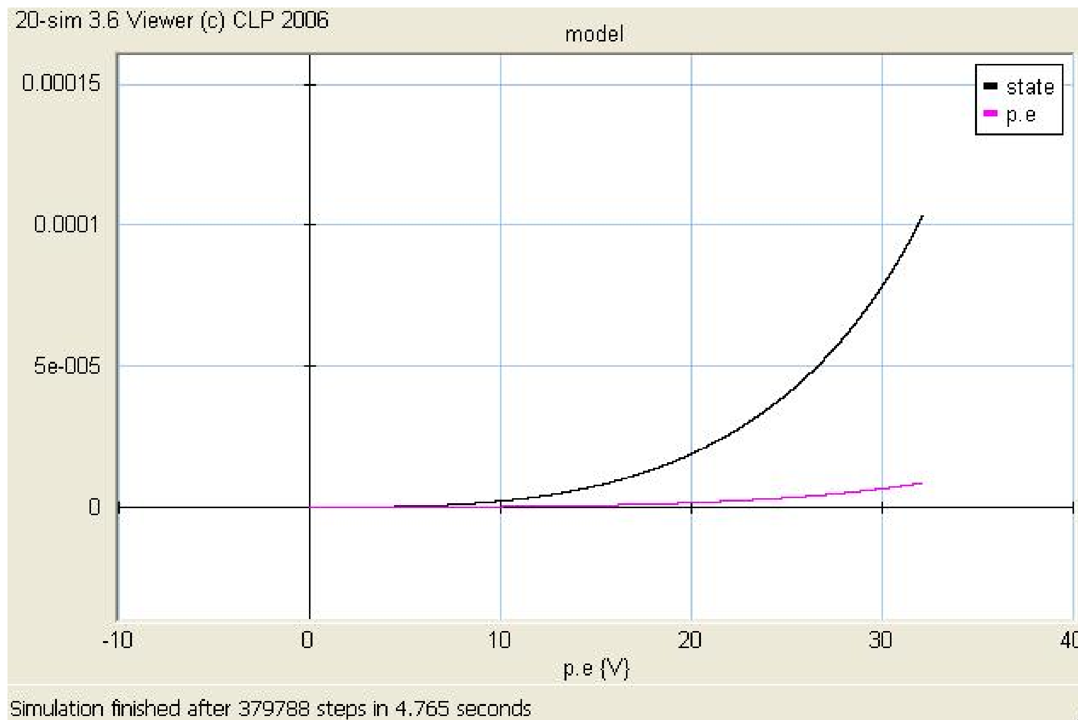

Fig3: Mass Increased

The results shown in Fig. 3 indicate that for a driving voltage of 40 volts, as the value of proof mass is increased, the inertia of the drive increased and so is the induced Comb displacement. This effect of the Comb is also expected.

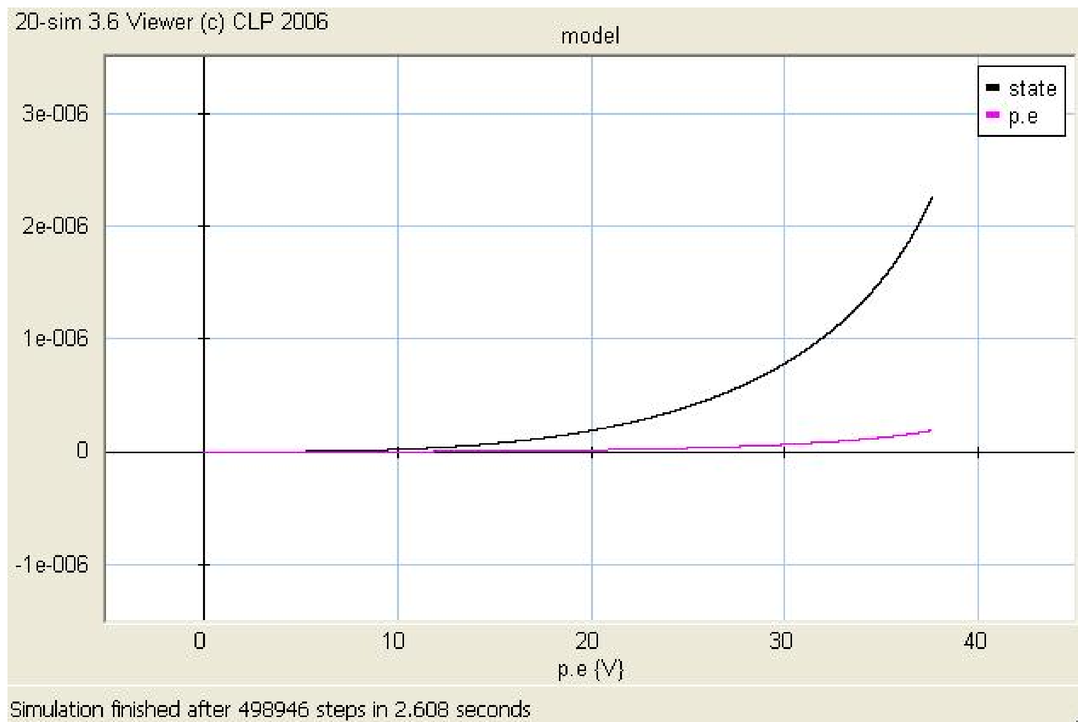

Fig. 4: Mass decreased

The displacement variation rate is shown to decrease with the decrease of the proof mass (m) as well . This effect verifies the above result. It is simulated in fig.4

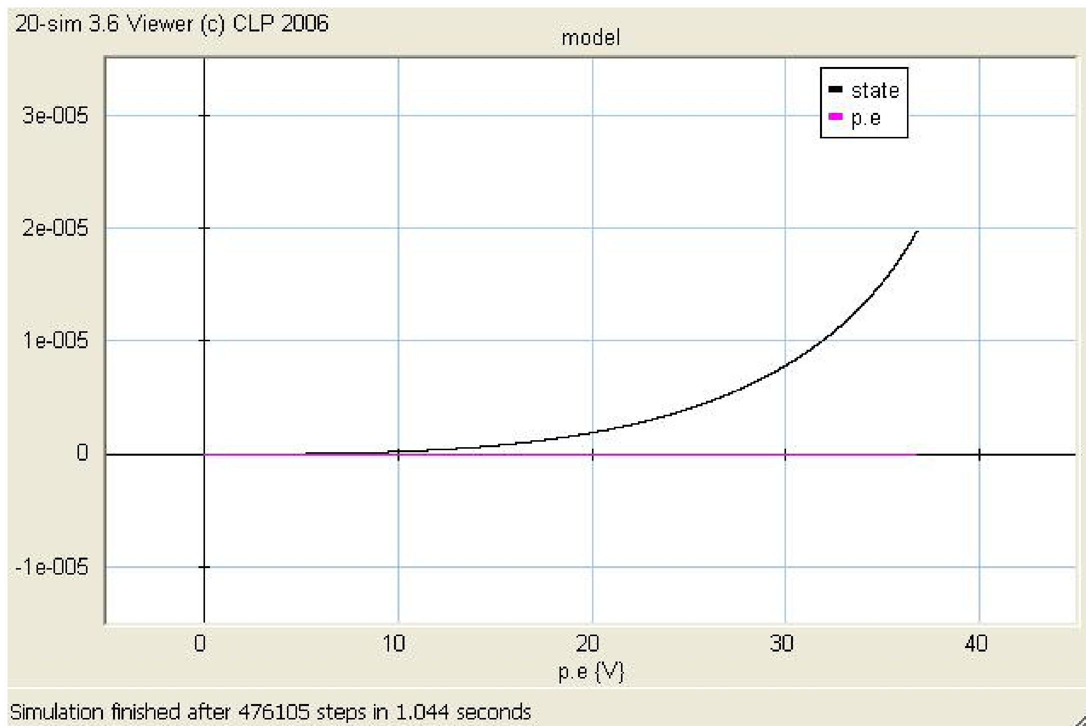

Fig. 5: Stiffness Decreased

On the other hand, decreasing the value of stiffness is proven to increase the Comb displacement. This relation between the Comb displacement and the stiffness is demonstrated in Fig. 5 for a driving voltage of 40 volts and keeping all other parameter same as case of fig.1.

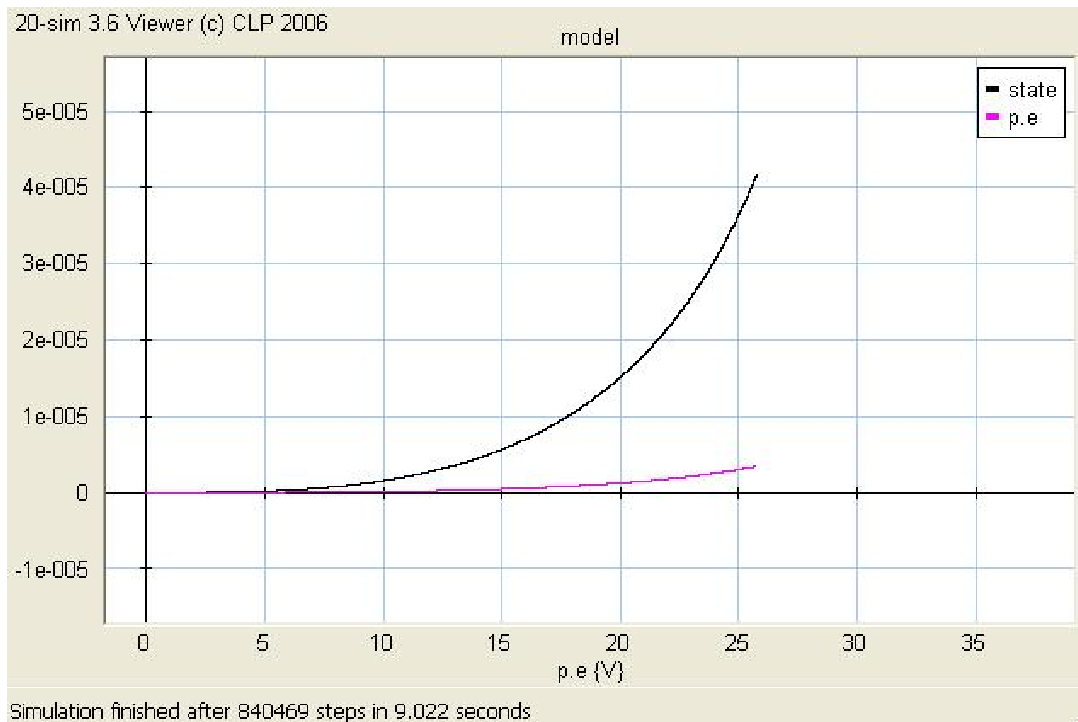

Fig. 6: 30V

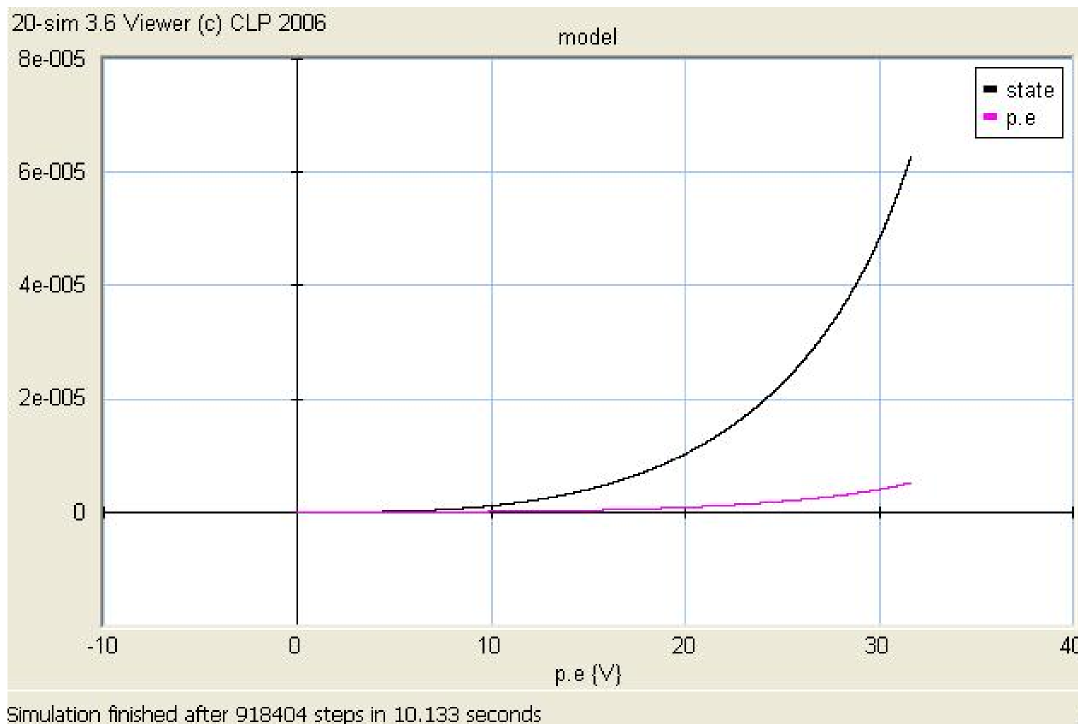

Fig. 7: 35V

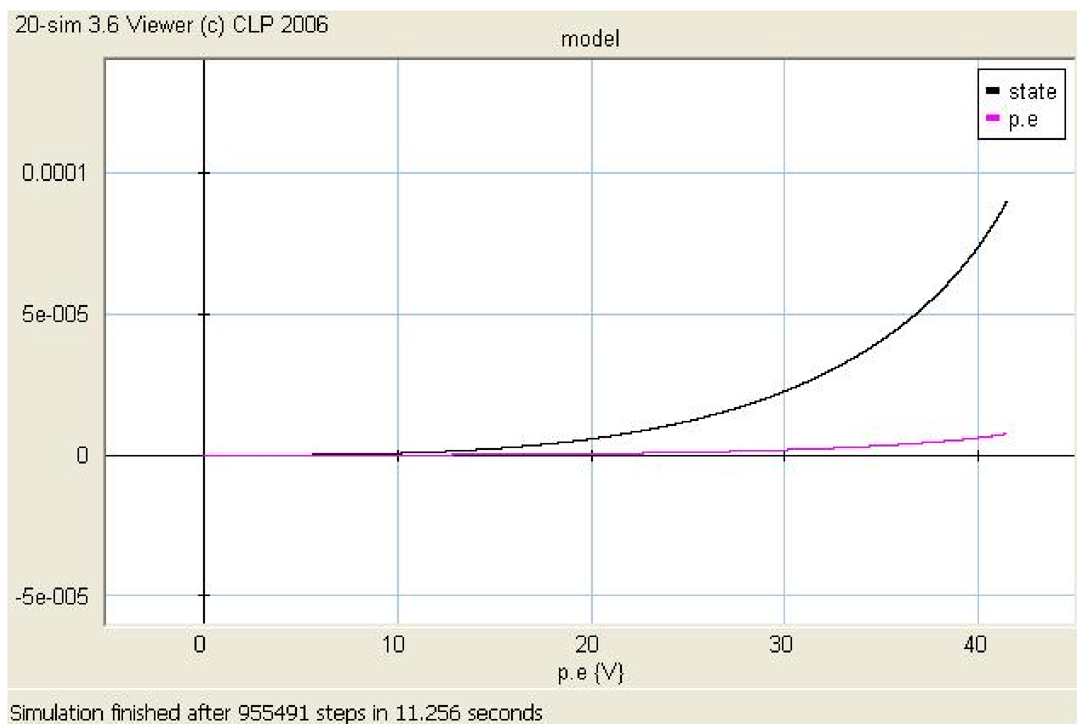

Fig. 8: 45V

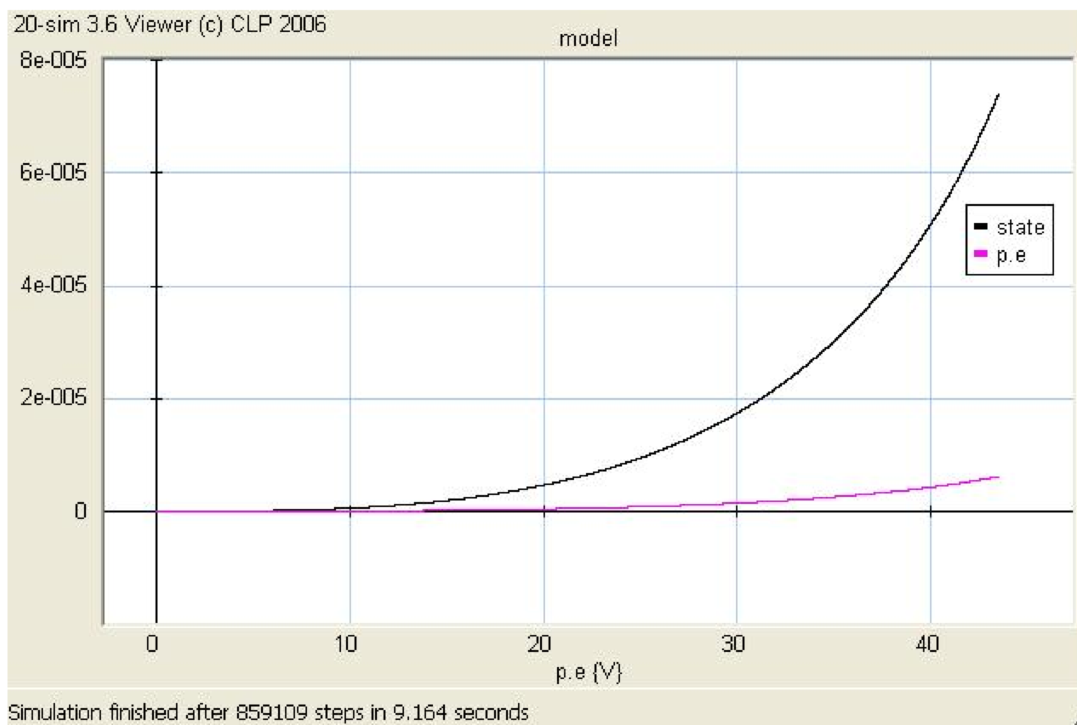

Fig. 9: 50

When supplied voltage decreased as in fig. 6-7 the displacement of the comb drive will also decrease. On the other hand, when the supplied voltage is increased, the comb displacement is shown in fig. 8-9 to increase for the taken comb design. In these figures, the displacement variation rate is shown to change with the driving voltage.

To facilitate the use of the current study results in optimizing the design of linear comb drives, an effort is made in the current work to condense these results into a compact non-dimensional form that correlates the studied geometric parameters of the modeled comb-drive with its displacement. utilizing the method of Runge-Kutta Dormand Prince 8, built-in with 20-SIM it is found that the displacement values presented in Figs. 2 to 7 are well described by the equations of chapter 5 and results of FE and Mixed domain method presented below also confirms the trends of these simulations.

6.4 ANSYS Results[1]

6.4.1 Displacement vs. Driving Voltage

Here we are presenting the result regarding the variation of displacement against voltage which shows same trends as our results shown.

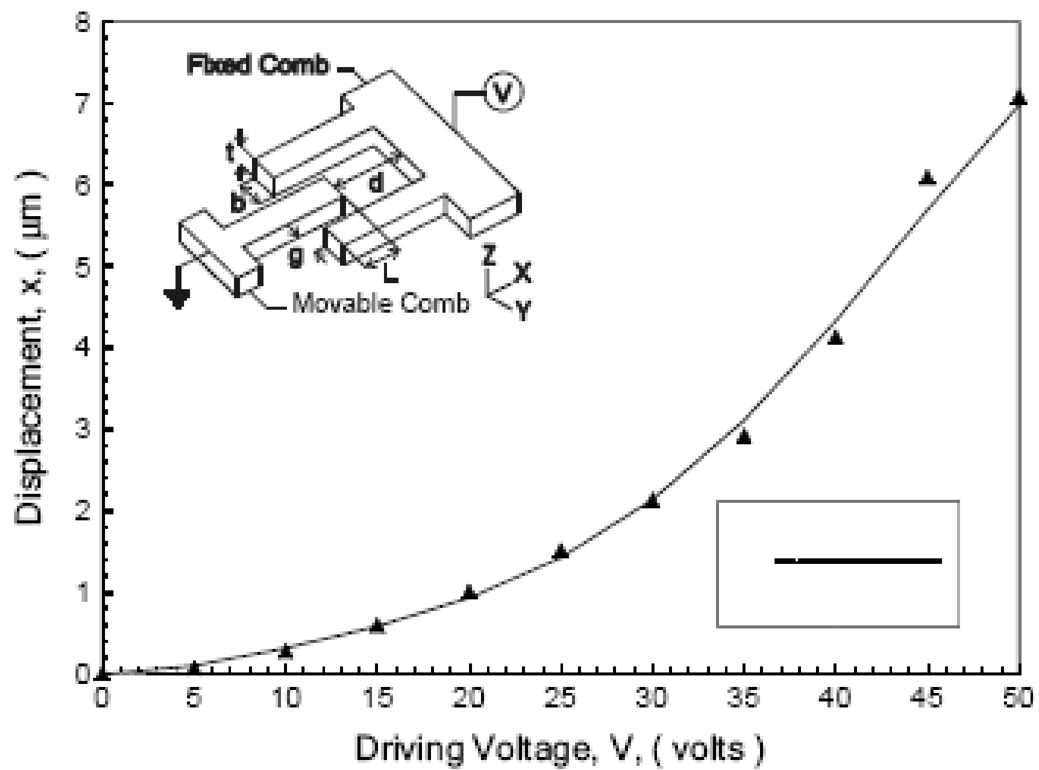

Fig. 10: Results of Ansys; displacement of comb finger vs. driving voltage.

6.4.2 Electrostatic Force vs. Driving Voltage

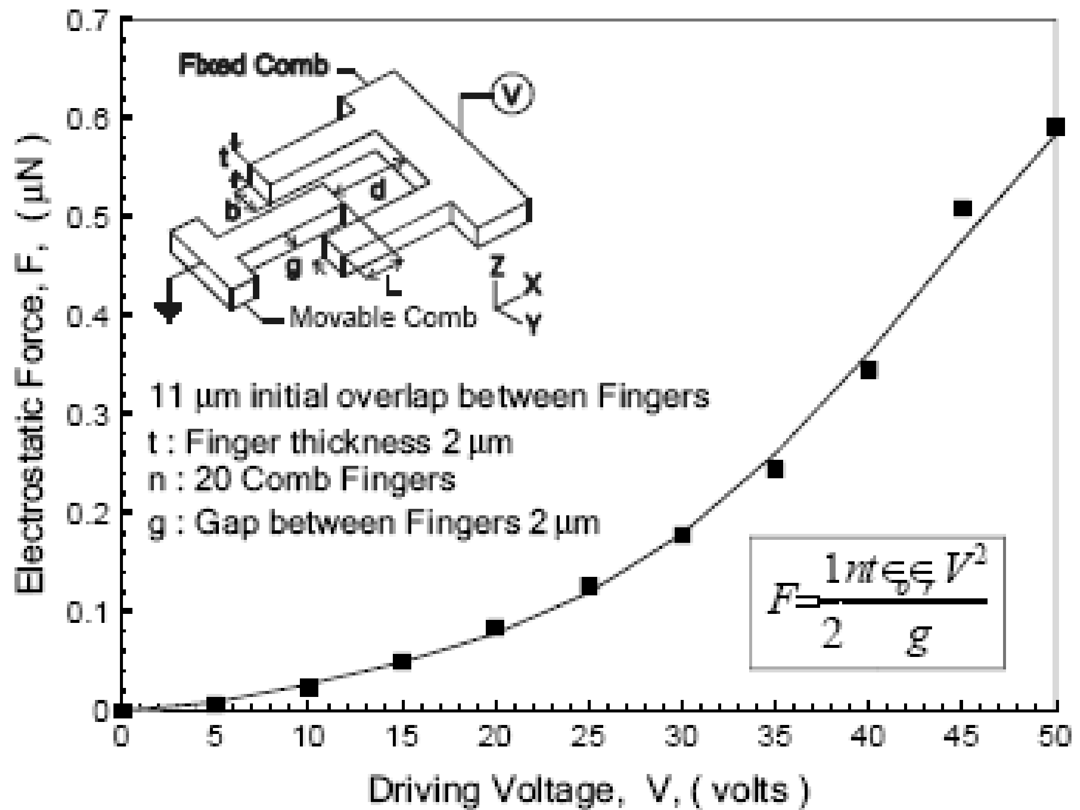

Fig. 11: Results of Ansys; displacement of comb finger vs. driving voltage.

6.5 PolyPUMPS Results[2]

Displacement vs. Driving Voltage

For the comparison of these result simulated through 20-SIM we got the results of Comb Drive designed in mixed domains. In this technique they used MATLAB for mathematical modeling of the system and structural modeling is done with PolyPUMP a designated MEMS design software.

The trends shown in fig 12 also maches with the simulation of 20-SIM.

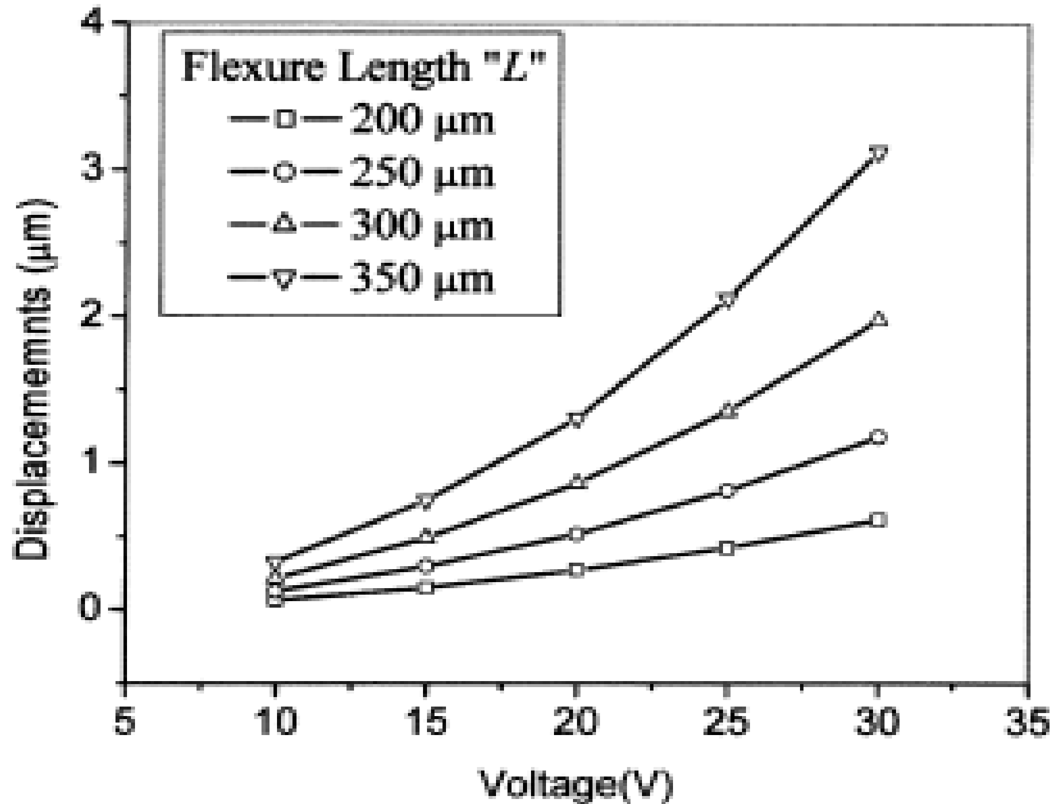

Fig. 12: Results of modeling through PolyPUMP

Results and discussion

The effect of comb-drive design parameters on actuation performance is explored. Equations (i) and (iii) of section 5.2 shows that the displacement of combs and the force generated is directly proportional to the square of applied voltage. The same results are indicated by the results of FEM and PolyPUMP. The relationship of our developed physical model follows the trend represented in these results.

In this research coupled domain mechanical and electrostatic analysis of MEMS Comb-Drive has been carried out by bond graph method. Mostly this kind of multidomain designing requires more then one analyzing schemes like numerical simulations using Finite Element Method for Mechanical Analysis

and Boundary Element Method for Electrostatic Analysis. but through bond graph method we did it at once. Various design parameters of a Comb-Drive like finger overlap, folded flexure spring length and applied voltage were considered and their effect on performance variables like mass, natural frequency and displacement of comb were studied using simulation on 20-SIM a commercial software on bond graph method. Simulations were performed using a standard Comb-Drive with 2 movable fingers in the comb and folded flexure spring. The results showed that the comb finger displacement increases with decreasing stiffness and the displacement of combs also increase with the increase in the proof mass. A relationship between Comb-Drive displacement and the natural frequency of the structure with folded flexure spring is also comprehensively covered in this study.

We are planning to model a Comb-Drive based on this research using different design to verify the model.

Conclusions

The bond graph method is successfully applied to the MEMS system to study the variations of considered variables with change of parameters and the variation follows the expected trends of comb drive actuation

By considering the actual parameters of comb drive, an optimized design of this kind of a system can be developed without indulging into an extensive mathematical modeling but achieved through correct physical Bond Graph Model of the system.

The thesis examines an important method of MEMS modeling, simulation and design that is, The use of Bond Graph Method with its power of simulation. All simulation results maps with the expected trends of design variables.

This research shows that bond graph method can be used as a better choice to design a MEMS comb drive and even a Gyro with less computational efforts. The reduced model through bond graph provides us an opportunity of better design in short time.

Future Work and Recommendations

An optimized comb drive based gyroscope is to be designed with Bond Graph Method, its simulation and verification of results, is my proposed PhD research work

Any kind of MEMS device can be design by taking Bond Graph Method as a method of Modeling and Simulation

REFERENCES

[1.1] Soderkvist “Micromachined Gyroscopes” Sensors and Actuators A,43, 65-71 (1994)

[1.2] N. Yazdi, F. Ayazi and K. Najafi “ Micromachined Inertial Sensors,”, Proc. IEEE, 86, 1640-59 (1998)

[1.3] R, Voss, K. Bauer, W. Ficker, T. Gleissner, W. Kupke, M. Rose, S. Sassen, J Schalk, H. Seidel and E. Stenzel, “ Silicon Angular rate Sensor for Automotive Applications with Piezoelectric Drive and Piezoresistive Read-out,” Transducers ’97, pp 879-82, Chicago, UISA, June 16-19, 1997

[1.4] S. Huang, X. Li, Y. Wang, J Jiao, X. Ge, D. Lu, L. Che, K, Zhang and B. Xiong “ A piezoresistive accelerometer with axially stressed tiny beams for both much increased sensitivity and much broadened frequency bandwidth,” Transducers ’03, pp. 91-94, Boston, USA, June 8-12, 2003.

[2.1] Dr. Albert Pisano*, in presentation material distributed by the* United States Defense Advanced Research Program Agency (DARPA), available at *http://web-ext2.darpa.mil.*

[2.2] G. T. A. Kovacs, *Micromachined Transducers Sourcebook.* Boston: WCB/McGraw-Hill, 1998.

[2.3] S. Gheorghe, *Circuite integrate digitale.* Bucharest: Den ix, 1993.

[3.1] Tang W C, Nguyen T C H and Howe R T 1989 Laterally driven polysilicon resonant microstructures *Sensors Actuators* **20** 25–32

[3.2] Tang W C, Nguyen T C H, Judy M W and Howe R T 1990 Electrostatic comb drive of lateral polysilicon resonators *Sensors Actuators* A **21–23** 328–31

[3.3] Furuhata T, Hirano T, Gabriel K J and Fujita H 1991 Sub-micron gaps without sub-micron etching *Tech Digest, IEEE Micro Electro Mechanical Systems Workshop (Nara, Japan, January 30–February 2, 1991)* (New York: IEEE) pp 57–62

[3.4] Hirano T, Furuhata T, Gabriel K J and Fujita H 1991 Operation of sub-micron electrostatic comb-drive actuators *Proc. 6th Int. Conf. on Solid State Sensors and Actuators (San Francisco, CA, June 23–27, 1991)* pp 1–4

[3.5] Jaecklin V P, Linder C, de Rooij N F and Moret J M 1992 Micromechanical comb actuators with low driving voltage *J. Micromech. Microeng.* **2** 250–5

[3.6] Zhang Z L and MacDonald N C 1992 A RIE process for submicron silicon electromechanical structures *J. Micromech. Microeng.* **2** 31–8

[3.7] Shaw K A, Zhang Z L and MacDonald N C 1994 SCREAM I: a single-mask, single-crystal silicon, reactive ion etching process for microelectromechanical structures *Sensors Actuators* A **40** 63–70

[3.8] Gianchandani Y B and Najafi K 1992 A bulk silicon dissolved wafer process for micro-electromechanical devices *J. Microelectromech. Syst.* **1** 77–85

[3.9] Syms R R A, Hardcastle B M and Lawes R A 1997 Bulk micromachined silicon comb-drive electrostatic actuators with diode isolation *Sensors Actuators* A **63** 61–7

[3.10] Selvakumar A and Najafi K 1994 High density vertical comb array microactuators fabricated using a novel bulk/poly-silicon trench refill technology *Tech. Digest, Solid State Sensors and Actuators Workshop (Hilton Head, SC)* (New York: IEEE) pp 138–41

[3.11] Hirano T, Kobayashi D, Furuhata T and Fujita H 1994 Electroplated and dry-released metallic microstructures for a lateral tunneling unit *Japan. J. Appl. Phys.* **33** 1202–8

[3.12] Frazier A B, Chong H A and Allen M G 1994 Development of micromachined devices using polyimide-based process *Sensors Actuators* A **45** 47–55

[3.13] Lee A P and Pisano A P 1992 Polysilicon angular vibromotors *J. Microelectromech. Syst.* **1** 70–6

[3.14] Daneman M J, Tien N C, Olgaard O, Pisano A P, Lau K Y and Muller R S 1996 Linear vibromotor for positioning optical components *J. Microelectromech. Syst.* **5** 159–65

[3.15] Garcia E J and Sniegowski J J 1995 Surface micromachined microengine *Sensors Actuators* A **48** 203–14

[3.16] Uenishi Y, Honma K and Nagaoka S 1996 Tunable laser diode using a nickel micromachined external mirror *Elect. Lett.* **32** 1207–8

[3.17] Kiang M-H, Solgaard O, Lau K Y and Muller R S 1998 Electrostatic combdrive-actuated micromirrors for laser-beam scanning and positioning *J. Microelectromech. Syst.* **7** 27–37

[3.18] Tanaka K, Mochida Y, Sugimoto M, Moriya K, Hasegawa T, Atsuchi K and Ohwada K 1995 A micromachined vibrating gyroscope *Sensors Actuators* A **50** 111–15

[3.19] Welham C J, Gardner J W and Greenwood J 1996 A laterally driven micromachined resonant pressure sensor *Sensors Actuators* A **52** 86–91

[3.20] Lin L, Howe R T and Pisano A P 1998 Microelectromechanical filters for signal processing *J. Microelectromech. Syst.* **7** 286–94

[3.21] Yao J J, Arney S C and MacDonald N C 1992 Fabrication of high frequency two-dimensional nanoactuators for scanned probe devices *Microelectromech. Syst.* **1** 14–22

[3.22] Jaecklin V P, Linder C, de Rooij N F, Moret J M, Bischof R and Rudolf F 1992 Novel polysilicon comb actuators for *xy*-stages *Micro Electro Mechanical Syst. (MEMS '92) (Travem¨unde, Germany, Feb. 4–7 1992)* (New York:IEEE) pp 147–9

[3.23] Inderm¨uhle P-F, Linder C, Brugger J, Jaecklin V P and de Rooj N F 1994 Design and fabrication of an overhanging *xy*-microactuator with integrated tip for scanning surface profiling *Sensors Actuators* A **43** 346–50

[3.24] Inderm¨uhle P-F, Jaecklin V P, Brugger J, Linder C, de Rooij N F and Binggeli M 1995 AFM imaging with an *xy*-micropositioner with integrated tip *Sensors Actuators* A **46–47** 562–5

[3.25] McNie M E, King D O, Ward M C L, Blackstone S, Quinn C and Burdess J 1997 Deep reactive ion etching of SOI for silicon micromachined structures *Proc. Digest, Intl. SOI Conference (Yosemite, October 1997)* pp 60–1

[3.26] Geiger W, Folkmer B, Sobe U, Sandmaier H and Lang W 1998 New design of micromachined vibrating rate gyroscope with decoupled oscillation modes *Sensors Actuators* A **66** 118–24

[3.27] Benitez A, Esteve J and Bausells J 1995 Bulk silicon microelectromechanical devices fabricated from commercial bonded and etched-back silicon-on-insulator substrates *Sensors Actuators* A **50** 99–103

[3.28] Klaassen E H, Petersen K, Noworolski J M, Logan J, Maluf N I, Brown J, Storment C, McCulley W and Kovacs T A 1996 Silicon fusion bonding and deep reactive ion etching: a new technology for microstructures *Sensors Actuators* A **52** 132–9

[3.29] Bhardwaj J and Ashraf H 1995 Innovative silicon trench process proves a winner *Surface Technology Systems Newsletter* July [30] Kong S, Minami K and Esashi M 1997 Fabrication of reactive ion etching systems for deep silicon machining *Trans. Inst. Electr. Eng. Japan.* E **117** 10–14

[3.31] Fan L S,Woodman S J and Crawforth L 1995 Integrated high aspect ratio milliactuators *Sensors Actuators* A **48** 221–7

[3.32] de Graaf G, Wolffenbuttel M R and Wolfenbuttel R F 1993 A measurement system for the visual analysis of integrated micromechanical systems *Sensors Actuators* A **37–38** 772–8

[3.33] Zook J D, Burns D W, Guckel H, Sniegowski J J, Engelstad R L and Feng Z 1992 Characteristics of polysilicon resonant microbeams *Sensors Actuators* A **35** 51–9

[3.34] Pember A, Smith J and Kemhadjian H 1995 Long-term stability of silicon bridge oscillators fabricated using the boron etch stop *Sensors Actuators* A **46–47** 51–7

[3.35] Adams S G, Bertsch F and MacDonald N C 1998 Independent tuning of linear and nonlinear stiffness coefficients *J. Microelectromech. Syst.* **7** 172–80

[3.36] Adams S G, Bertsch F, Shaw K A, Hartwell P G, Moon F C and McDonald N C 1998 Capacitance based tunable resonators *J. Micromech. Microeng* **8** 15–23

[3.37] Hosaka H, Itao K and Kuroda S 1994 Evaluation of energy dissipation mechanisms in vibrational microactuators *IEEE Micro Electro Mechanical Systems Workshop (MEMS'94) (January 25–28, 1994)* pp 193–8

[3.38] Zhang H and Tang W C 1994 Viscous air damping in laterally driven microresonators *IEEE Micro Electro Mechanical Systems Workshop (MEMS'94) (January 25–28, 1994)* pp 199–204

[3.39] Cho Y-H, Pisano A P and Howe R T 1994 Viscous damping model for laterally oscillating microstructures *J. Microelectromech. Syst.* **3** 81–6

[3.40] Tang W C, Lim M G and Howe R T 1992 Electrostatic comb drive levitation and control method *J. Microelectromech. Syst.* **1** 170–8

[3.41] Johnson W A and Warne L K 1995 Electrophysics of micromechanical comb actuators *J. Microelectromech. Syst.* **4** 49–59

[3.42] H. Lefevre, The Fiber-Optic Gyroscope. Norwood, MA: Artech House, 1993.

[3.43] A. Lawrence, Modern Inertial Technology: Navigation, Guidance, and Control, New York: Springer-Verlag, 1993.

[3.44] M. W. Putty and K. Najafi, "A micromachined vibrating ring gyroscope," in Tech. Dig. Solid-State Sensor and Actuator Workshop, Hilton Head Island, SC, June 1994, pp. 213–220.

[3.45] R. R. Ragan and D. D. Lynch, "Inertial technology for the future, Part X: Hemispherical resonator gyro," IEEE Trans. Aerosp. Electron. Syst., vol. AES-20, p. 432, July 1984.

[3.46] Ki-Hun Jeong and Luke P Lee 2005 A novel microfabrication of a self-aligned vertical comb drive on a single SOI wafer for optical MEMS applications *J. Micromech. Microeng.* **15** 277–281

[3.47] Robert D. white 1999 Effects of impact and Vibration on the performance of a micromachined Tunning fork Gyroscope *Thesis for Msc in Mech Enginnering MIT.*

[3.48] Jaecklin V P, Linder C, de Rooij N F, Moret J M"Micromechanical comb actuators with low driving voltage" Journal of Micro-mechanics and Microengineering. Vol. 2, (1992) p 250-255

[3.49] T. Y. Harness and Richard R A Syms "Characteristic modes of Electrostatic Comb-Drive X-Y Microactuators", J. Micro-mech. Microeng. 10 (2000), pp. 7-14

[3.50] M. H. Kiang, O. Solgaard, K. Y. Lau and R. S. Muller "Electrostatic Comb-Drive-Actuated Micromirros for laser-Beam Scanning and Positioning", J. Microelectromech. Syst. Vol.7 n.1, pp. 27-37, March 1998

[3.51] Sandia National Laboratories "Sandia Lab News", Vol.53 n.13, June 29 ,2001

[3.52] W. C. Tang, T. Cuong H. Nguyen, and R. T. Howe "Laterally Driven Polysilicon Resonant Microstructures", Proc. 1989 IEEE Micro Electro Mechanical Systems, pp. 53-59, February 1989

[3.53] R. Legtenberg, A. W. Groeneveld and M. Elwenspoek "Comb-Drive actuators for large displacements", J. Micromech. Microeng. 6 (1996), pp. 320-329.

[3.54] S . Groothuis, "Analyzing Microminiature Devices", ANSYS Solutions, Vol. 1, No. 1, Spring 1999.

[3.55] D . Ostergaard, "Tooling-Up for MicroElectroMechanical Systems (MEMS)", ANSYS Solutions, Vol. 1, No. 3, Winter 1999.

[3.56] R, Voss, K. Bauer, W. Ficker, T. Gleissner, W. Kupke, M. Rose, S. Sassen, J Schalk, H. Seidel and E. Stenzel, " Silicon Angular rate Sensor for Automotive Applications with Piezoelectric Drive and Piezoresistive Read-out," Transducers '97, pp 879-82, Chicago, UISA, June 16-19, 1997

[3.57] J. Bernstein, S. Cho, A. T. King, A. Kourepenis, P. Maciel, and M. Weinberg, "A micromachined comb-drive tuning fork rate gyroscope," in Proc. IEEE Micro Electro Mechanical Systems Workshop (MEMS'93), Fort Lauderdale, FL, Feb. 1993, pp. 143–148.

[3.58] M. Hashimoto, C. Cabuz, K. Minami, and M. Esashi, "Silicon resonant angular rate sensor using electromagnetic excitation and capacitive detection," J. Micromech. Microeng., pp.219–225, 1995.

[3.59] M. Lutz, W. Golderer, J. Gerstenmeier, J. Marek, B. Maihofer, S. Mahler, H. Munzel, and U. Bischof, "A precision yaw rate sensor in silicon micromachining," in Tech. Dig. 9th Int. Conf. Solid-State Sensors and Actuators (Transducers'97), Chicago, IL, June 1997, pp. 847–850.

[3.60] K. Maenaka and T. Shiozawa, "A study of silicon angular rate sensors using anisotropic etching technology," Sensors Actuators A, vol. 43, pp. 72–77, 1994

[3.61] J. Soderkvist, "Design of a solid-state gyroscopic sensor made of quartz," Sensors Actuators, vol. A21/A23, pp. 293–296, 1990.

[3.62] , "Micromachined gyroscopes," Sensors Actuators A, vol. 43, pp. 65–71, 1994.

[3.63] S. D. Orlosky and H. D. Morris, "Quartz rotation (rate) sensor," in Proc. Sensor Expo, Cleveland, OH, 1994, pp. 171–177.

[3.64] P. Greiff, B. Boxenhorn, T. King, and L. Niles, "Silicon monolithic micromechanical gyroscope," in Tech. Dig. 6th Int. Conf. Solid-State Sensors and Actuators (Transducers'91), San Francisco, CA, June 1991, pp. 966–968.

[3.65] Y. Gianchandani and K. Najafi, “A bulk silicon dissolved wafer process for microelectromechanical systems,” J. Microelectromech. Syst., pp. 77–85, June 1992.

[3.66] W. C. Tang, M. G. Lin, and R. T. Howe, “Electrostatically balanced comb drive for controlled levitation,” in Tech. Dig. Solid-State Sensor and Actuator Workshop, Hilton Head Island, SC, June 1990, pp. 23–27.

[3.67] M. Weinberg, J. Bernstein, S. Cho, A. T. King, A. Kourepenis, P. Ward, and J. Sohn, “A micromachined comb-drive tuning fork gyroscope for commercial applications,” in Proc. Sensor Expo, Cleveland, OH, 1994, pp. 187–193.

[3.68] F. Paoletti, M. A. Gretillat, and N. F. de Rooij, “A silicon micromachined vibrating gyroscope with piezoresistive detection and electromagnetic excitation,” in Proc. IEEE Micro Electro Mechanical Systems Workshop (MEMS’96), San Diego, CA, 1996, pp. 162–167.

[3.69] J. Soderkvist, “Micromachined vibrating gyroscopes,” in Proc. SPIE 1996 Symp. Micromachining and Microfabrication, Austin, TX, 1996, pp. 152–160.

[3.70] K. Maenaka, T. Fujita, Y. Konishi, and M. Maeda, “Analysis of a highly sensitive silicon gyroscope with cantilever beam as vibrating mass,” Sensors Actuators A, vol. 54, pp. 568–573, 1996.

[3.71] D. Wood, G. Cooper, J. Burdess, A. Harris, and J. Cruickshank, “A silicon membrane gyroscope with electrostatic actuation and sensing,” in Proc. SPIE 1995 Symp. Micromachining and Microfabrication, Austin, TX, 1995, pp. 74–83.

[3.72] H. Kuisma, T. Ryhanen, J. Lahdenpera, E. Punkka, S. Ruotsalainen, T. Sillanpaa, and H. Seppa, “A bulk micromachined silicon angular rate sensor,” in Tech. Dig. 9th Int. Conf. Solid-State Sensors and Actuators (Transducers’97), Chicago, IL, June 1997, pp. 875–878.

[3.73] W. A. Clark, R. T. Howe, and R. Horowitz, “Surface micromachined x-axis vibratory rate gyroscope,” in Tech. Dig. Solid-State Sensor and Actuator Workshop, Hilton Head Island, SC, June 1996, pp. 283–287.

[3.74] T. Juneau and A. P. Pisano, “Micromachined dual input axis angular rate sensor,” in Tech. Dig. Solid-State Sensor & Actuator Workshop, Hilton Head Island, SC, June 1996, pp. 299– 302.

[3.75] Y. Oh, B. Lee, S. Baek, H. Kim, J. Kim, S. Kang, and C. Song, “A surface-micromachined tunable vibratory gyroscope,” in Proc. IEEE Micro Electro Mechanical Systems Workshop (MEMS’97), Japan, 1997, pp. 272–277.

[3.76] K. Y. Park, C. W. Lee, Y. S. Oh, and Y. H. Cho, “Laterally oscillated and force-balanced micro vibratory rate gyroscope supported by fish hook shape springs,” in Proc. IEEE Micro Electro Mechanical Systems Workshop (MEMS’97), Japan, 1997, pp. 494–499.

[3.77] S. An, Y. S. Oh, B. L. Lee, K. Y. Park, S. J. Kang, S. O. Choi, Y. I. Go, and C. M. Song, “Dual-axis microgyroscope with closed-loop detection,” in Proc. IEEE Micro

Electro Mechanical Systems Workshop (MEMS'98), Heidelberg, Germany,Feb. 1998, pp. 328–333.

[3.78] K. Tanaka, Y. Mochida, M. Sugimoto, K. Moriya, T. Hasegawa, K. Atsuchi, and K. Ohwada, "A micromachined vibrating gyroscope," Sensors Actuators A, vol. 50, pp. 111–115, 1995.

[3.79] T. Juneau, A. P. Pisano, and J. H. Smith, "Dual axis operation of a micromachined rate gyroscope," in Tech. Dig. 9th Int. Conf. Solid-State Sensors and Actuators (Transducers'97), Chicago, IL, June 1997, pp. 883–886.

[3.80] T. Fujita, T. Mizuno, R. Kenny, M. Maenaka, and M. Maeda, "Two-dimensional micromachined gyroscope," in Tech. Dig. 9th Int. Conf. Solid-State Sensors and Actuators (Transducers'97), Chicago, IL, June 1997, pp. 887–890.

[3.81] T. K. Tang, R. C. Gutierrez, J. Z. Wilcox, C. Stell, V. Vorperian, R. Calvet, W. J Li, I. Charkaborty, R. Bartman, and W. J. Kaiser, "Silicon bulk micromachined vibratory gyroscope," in Tech. Dig. Solid-State Sensor and Actuator Workshop, Hilton Head Island, SC, June 1996, pp. 288–293.

[3.82] T. K. Tang, R. C. Gutierrez, C. B. Stell, V. Vorperian, G. A. Arakaki, J. T. Rice, W. J. Li, I. Chakraborty, K. Shcheglov, J. Z. Wilcox, and W. J. Kaiser, "A packaged silicon MEMS vibratory gyroscope for microspacecraft," in Proc. IEEE Micro Electro Mechanical Systems Workshop (MEMS'97), Japan, 1997, pp. 500–505.

[3.83] W. Geiger, B. Folkmer, J. Merz, H. Sandmaier, and W. Lang, "A new silicon rate gyroscope," in Proc. IEEE Micro Electro Mechanical Systems Workshop (MEMS'98), Heidelberg, Germany, Feb. 1998, pp. 615–620.

[3.84] M. W. Putty, "A micromachined vibrating ring gyroscope," Ph.D. dissertation, Univ. Michigan, Ann Arbor, Mar. 1995.

[3.85] D. R. Sparks, S. R. Zarabadi, J. D. Johnson, Q. Jiang, M. Chia, O. Larsen, W. Higdon, and P. Castillo-Borelley, "A CMOS integrated surface micromachined angular rate sensor: It's automotive applications," in Tech. Dig. 9th Int. Conf. Solid-State Sensors and Actuators (Transducers'97), Chicago, IL,
June 1997, pp. 851–854.

[3.86] F. Ayazi and K. Najafi, "Design and fabrication of a highperformance polysilicon vibrating ring gyroscope," in Proc. IEEE Micro Electro Mechanical Systems Workshop (MEMS'98), Heidelberg, Germany, Feb. 1998, pp. 621–626.

[3.87] A. Selvakumar and K. Najafi, "High density vertical comb array microactuators fabricated using a novel bulk/poly-silicon trench refill technology," in Tech. Dig. Solid-State Sensor and Actuator Workshop, Hilton Head Island, SC, USA, 1994, pp. 138–141.

[3.88] I. Hopkin, "Performance and design of a silicon micromachined gyro," in Proc. Symp. Gyro Technology, Stuttgart, Germany, 1997, pp. 1.0–1.10.

[3.89] R. Torti, V. Gondhalekar, H. Tran, B. Selfors, S. Bart, and B. Maxwell, “Electrostatically suspended and sensed micromechanical rate gyroscope,” in Proc. SPIE 1994 Symp. On Micromachining and Microfabrication, Austin, TX, 1994, pp. 27–31.

[3.90] C. Shearwood, C. B. Williams, P. H. Mellor, R. B. Yates, M. R. J. Gibbs, and A. D. Mattingley, “Levitation of a micromachined rotor for application in a rotating gyroscope,” Electron. Lett., vol. 31, no. 21, p. 1845, Oct. 1995.

[3.91] John D. Grade, Kevin Y. Yasumura, and Hal Jerman YEAR a drie comb-drive actuator with large, stable deflection range for use as an optical shutter JOURNAL NAME

[3.92] Liwei Lin, Roger T. Howe 1998 Microelectromechanical Filters for Signal Processing *J. Microelectromech.Syst.* **7** 286–9

[3.93] Caglar Ataman and Hakan Urey 2006 Modeling and characterization of comb-actuated resonant microscanners *J. Micromech. Microeng.***16** 9-16

[3.94] Wibool Piyawattanametha, Pamela R. Patterson, Dooyoung Hah, Hiroshi Toshiyoshi, and Ming C. Wu 2005 *J. Microelectromech. Syst.* **14** 1329-10

[3.95] Yoomin Ahn, Takahito Ono and Masayoshi Esashi 2005 *. J. Micromech. Microeng.***15** 1224-1229

[3.96] Chunrong Peng, Xianxiang Chen, Cao Ye, Hu Tao, Guoping Cui, Qiang Bai1, Shaofeng Chen and Shanhong Xia1 2006 Design and testing of a micromechanical resonant electrostatic field sensor *J. Micromech. Microeng.* **16** 914–919

[3.97] Peter Y. Kwok, Marc S. Weinberg and Kenneth S. Breuer 2005 Fluid Effects in Vibrating Micromachined Structures *J. Microelectromech.Syst.* **14** 770–781

[3.98] Tsung-Lin Chen, Kenn Oldham, Yunfeng Li, Roberto Horowitz YEAR suspension vibration compensation using a mems microactuator in hard disk drives.

[3.99] Isabelle P.F. Harouche, C. Shafai 2005 Simulation of shaped comb drive as a stepped actuator for microtweezers application *Sensors and Actuators A 1-7*

[3.100] Chunchieh Huang, Christophoros Christophorou, Khalil Najafi, Ahmed Naguib, and Hassan M. Nagib 2002 An Electrostatic Microactuator System for Application in High-Speed Jets *J. Microelectromech Syst.* **2** 222–14

[3.101] MEMS Booklet on the research projects conducted in A * STAR’s research institutes, the national university of the Singapore and Nanyang Technical University

[4.1] D. Karnopp and R. Rosenberg, *System Dynamics: a Unified Approach. New* York: John Wiley & Sons, 1975.

[4.2] F. A. Firestone, "A new analogy between mechanical and elec-trical systems," *Journal of the Acoustic Society of America,* no. 3, pp. 249-267, 1933.

[4.3] M. H. Trent, "Isomorphisms between oriented linear graphs and lumped physical systems," *Journal of the Acoustic Society of America,* no. 27, pp. 500-527, 1955.

[4.4] H. M. Paynter, *Analysis and Design of Engineering Systems.* Cambridge, Massachusetts: M.I.T. Press, 1961.

[4.5] S. H. Crandall, D. C. Karnopp, E. F. J. Kurtz, and D. C. Prid-more-Brown, *Dynamics of Mechanical and Electromechanical Systems.* New York: McGraw-Hill, 1968.

[4.6] J. Meisel, *Principles of Electromechanical-Energy Conversion.* New York: McGraw-Hill, 1966.

[5.1] S. D. Senturia, "*CAD for microelectromechanical systems*," in *Proc. 8th Int. Conf. Solid-State Sensors and Actuators, and Eurosensors IX*, Stockholm, Sweden, vol. 2, 1995, pp. 5–8.

[5.2] J. R. Gilbert, R. Legtenberg, and S. D. Senturia, "*3D coupled electromechanics for MEMS: Applications of CoSolve-EM*," in *Proc. IEEE Workshop on MEMS*, Amsterdam, The Netherlands, 1995, pp. 122–127.

[5.3] J. R. Gilbert, G. K. Ananthasuresh, and S. D. Senturia, "*3D modeling of contact problems and hysteresis in coupled electro-mechanics*," in *Proc. IEEE 9th Annu. Int. Workshop on Micro Electro Mechanical Syst.*, 1996, pp. 127–132.

[5.4] Y. He, R. Harris, G. Napadenski, and F. Maseeh, "*A virtual prototype manufacturing software system for MEMS*," in *Proc. IEEE 9th Annu. Int. Workshop on Micro Electro Mechanical Syst.*, 1996, pp. 122–126.

[5.5] Rudnyi E B and Korvink J G 2002 *Automatic model reduction for transient simulation of MEMS-based devices Sensors Update* 11 3–33

[5.6] Bai Z J 2002 Krylov *subspace techniques for reduced-order modeling of large-scale dynamical systems Appl. Numer. Math.* 43 9–44

[5.7] Freund R W 2000 Krylov-*subspace methods for reduced-order modeling in circuit simulation J. Comput. Appl. Math.* 123 395–421

[5.8] Gary K. Fedder and Tamal Mukherjee "*Physical design for surface-micromachined MEMS*", 5th ACM/SIGDA Physical Design Workshop, Reston, VA USA, April 15-17, 1996, pp. 53-60

[5.9]Walied A Moussa, Hesham Ahmed,Wael Badawy, Medhat Moussa, *"Investigating the Reliability of Electrostatic Comb-Drive Actuators Utilized in Microfluidic and Space systems Using Finite Element Analysis*"

[5.10] Jaecklin V P, Linder C, de Rooij N F, Moret J M "*Micromechanical comb actuators with low driving voltage*" Journal of Micromechanics and Microengineering. Vol. 2, (1992) p 250-255

[5.11] R. Legtenberg, A. W. Groeneveld and M. Elwenspoek "*Comb-Drive actuators for large displacements*", J. Micromech. Microeng. 6 (1996), pp. 320-329.

[5.12] W. C. Tang, T.-C. H. Nguyen, M. W. Judy, and R. T. Howe, "Electrostatic Comb Drive of Lateral Polysilicon Resonators," *Sensors and Actuators A*, vol.21, no.1-3, pp. 328-31, Feb. 1990.

[5.13] John D. Grade, Hal Jerman, and Thomas W. Kenny, "Design of Large Deflection Electrostatic Actuators", Journal Of Microelectromechanical Systems, Vol. 12, No. 3, June 2003

[6.1] Rana I. Shakoor, Imran R. Chughtai, Shafaat A. Bazaz, Muhammad J. Hyder, Masood-ul-Hassan *Numerical Simulations of MEMS Comb-Drive Using Coupled Mechanical and Electrostatic Analyses* 2005 IEEE

[6.2] Walied A. Moussa1, Hesham2 Ahmed, Wael Badawy3, Medhat Moussa4 *Investigating the Reliability of Electrostatic Comb-Drive Actuators Utilized in Microfluidic and Space systems Using Finite Element Analysis*